Scientific Drilling

Reports on Deep Earth Sampling and Monitoring

Editorial Preface

Dear Reader:

Volcanoes have many stories to tell, and their activity profoundly impacts human life and Earth's environment. In this issue of *Scientific Drilling*, a report on the Hawaii Drilling Project highlights "hot spot" volcanism (p. 4). A decade of planning and drilling on the island of Hawaii resulted in 3500 m of drillcores from lava flows piled up by the Mauna Loa and Mauna Kea volcanic systems. Detailed analyses tell an intriguing story about the Earth's mantle down to 3000 km depth, and how the volcanoes, rising 10 km from the seabed, formed over time and host an unexpected hydrogeological system. Planned drilling in Kamchatka (p. 54) will address the source of energy and water driving hydrothermal systems in volcanoes typical of the Pacific Ring of Fire. And, a report on the potential for ocean drilling to address volcanic, seismogenic, and other geohazards is presented on p. 15.

Climate and environmental change are at the top of global research initiatives. The environment in which life flourished 3.2 billion years ago is the target for drilling in northwestern Australia (p. 34). Drilling into a lake in southeastern Europe holds the potential to recover much more recent records of environmental evolution linked to an amazing biological speciation (p. 51). The quest for drilling cores at high latitudes significantly depends on the ability to image targets seismically (p. 40) and the ability to cope with challenging logistics (p. 38). Gas hydrates are important components in the global carbon cycle and a potentially giant hydrocarbon resource. Technology to sample the icy gas under *in situ* conditions is reported on p. 44. Lastly, the global science community will be greatly supported by the concentration of ocean drilling cores (p. 31) in three fully accessible international core repositories.

Taken together, the fundamental contributions by scientific drilling projects to understanding Earth's environment and its immense natural variability over geological time should leave no doubt about their importance. Unfortunately, delays in drilling platform refurbishment and repair, and unavailability of mission-specific platforms—all related to an overheated offshore and shipyard market—have caused an almost three-year-long drilling hiatus during IODP's initial five years. Light now appears at the end of the tunnel. The Japanese riser drilling platform *Chikyu*, the U.S.-supplied *JOIDES Resolution* (following complete refurbishment of vessel, drilling equipment, and laboratory), and mission-specific platforms for shallow-water coring will all be active in 2009 (see schedule on back cover). This schedule will set a new high mark for scientific ocean drilling activity and provide a welcome backdrop for preparations for IODP renewal in 2013, which will start in 2009 with a major, community-wide conference (p. 66) addressing the scientific challenges and opportunities for ocean drilling after 2013. The constructive interaction with ICDP and other drilling programs, observatory science, and environmental modeling efforts will no doubt form the context of this major conference.

Hans Christian Larsen
Editor-in-Chief
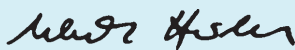
Ulrich Harms
Editor

Front Cover: Formation of pahoehoe lava, Kilauea volcano, big island of Hawaii. Photo: Katharine Cashman, University of Oregon. See article on p. 4.
Left inset: Assembling drill core pieces after recovery and preparations for the initial core marking, description and optical scanning at the HSDP field laboratory in Hilo. (See page 4.)

Contents

Deep Drilling into a Mantle Plume Volcano: The Hawaii Scientific Drilling Project

by Edward M. Stolper, Donald J. DePaolo, and Donald M. Thomas

Introduction

Oceanic volcanoes formed by mantle plumes, such as those of Hawaii and Iceland, strongly influence our views about the deep Earth (Morgan, 1971; Sleep, 2006). These volcanoes are the principal geochemical probe into the deep mantle, a testing ground for understanding mantle convection, plate tectonics and volcanism, and an archive of information on Earth's magnetic field and lithosphere dynamics. Study of the petrology, geochemistry, and structure of oceanic volcanoes has contributed immensely to our present understanding of deep Earth processes, but virtually all of this study has been concentrated on rocks available at the surface. In favorable circumstances, surface exposures penetrate to a depth of a few hundred meters, which is a small fraction of the 10- to 15-kilometer height of Hawaiian volcanoes above the depressed seafloor (Moore, 1987; Watts, 2001).

The shield volcanoes of Hawaii are enormous in comparison to most other types of volcanoes. The average Hawaiian volcano has a volume of 30,000–50,000 km^3 (DePaolo and Stolper, 1996; Robinson and Eakins, 2006). By comparison, stratovolcanoes like Mt. Shasta in California,

Figure 1. Map showing the boundaries of the major volcanoes of the island of Hawaii and the locations of the HSDP pilot hole drilled in 1993, and the deep hole drilled in 1999 and 2004–2007. The red line shows the approximate location of the shoreline of Mauna Kea when it reached its maximum extent above sea level, at the end of the shield-building stage about 150,000 years ago (see Fig. 6). Subsequently, subsidence has moved the shoreline 10–20 km closer to the volcano summit.

or Mt. Fuji in Japan, have volumes of only 50–500 km^3. Hawaiian volcanoes grow upward from the ocean floor by systematically covering their roughly conical surfaces with new lava flows. In their main growth phase, they increase in height at an average rate of 10–30 meters per thousand years (DePaolo and Stolper, 1996), and their surfaces are completely covered with new lava about every thousand years (Holcomb, 1987). The lava flows of these large volcanoes dip gently away from the summits at angles of about 5–15 degrees relative to horizontal (Mark and Moore, 1987). The subhorizontal orientation of the flows, and the fact that they accumulate systematically with time just like sediments, means that the flanks of a volcano contain an ordered history of the volcanism that can be accessed efficiently by drilling.

The particular interest in drilling Hawaiian volcanoes is that as they grow, they are slowly carried to the northwest by the moving Pacific plate. Each individual volcano "sweeps" across the top of the Hawaiian mantle plume as it forms. The magma-producing region of the plume is roughly 100 km wide (Ribe and Christensen, 1999), so with the plate moving at 9–10 cm yr^1, it takes a little over one million years for a volcano to cross the magma production region. During this time the volcano goes through its major growth phases, starting as a steep-sided cone on the ocean floor, growing until it breaches the sea surface and becomes a small island, and then continuing to grow, expand, and subside until it becomes a massive, 100-km-wide pancake of lava and volcanic sediment with intrusive rocks at its core. As a volcano forms, the magma supply comes first from one side of the plume, then the middle, and then the other side, so sampling a stack of Hawaiian lavas provides a cross-section through the plume. The plume itself brings up rock material that comes from the deepest layers of the mantle (Farnetani et al., 2002; Bryce et al., 2005; Sleep, 2006). Thus, by drilling a few kilometers into a Hawaiian volcano, one can in theory look 2900 km down into the Earth and (if current models are correct) gather information about the bottom 100 kilometers of the mantle. No other place on Earth that we know of affords the possibly of doing this with quite the regularity that is inherent to Hawaiian volcanoes.

In recognition of the opportunities afforded by drilling in Hawaiian volcanoes, the Hawaii Scientific Drilling Project (HSDP) was conceived in the mid-1980s to core continuously to a depth of several kilometers in the flank of a Hawaiian volcano. The Mauna Kea volcano, which makes up the north-
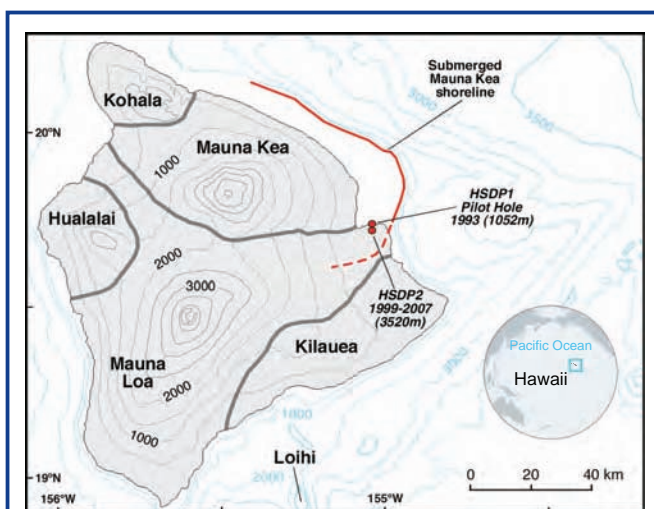
eastern part of the island of Hawaii, was chosen as the target (Fig. 1). The drill sites are located within the city of Hilo at elevations just a few meters above sea level. The project proceeded in three phases of drilling. What we refer to as "HSDP1" involved coring a pilot hole to a depth of 1052 meters below sea level (mbsl) in 1993 (Stolper et al., 1996; DePaolo et al., 1996). The deep drilling project, referred to as HSDP2, took place in two phases. In the first phase a hole was core drilled in 1999 to a depth of 3098 mbsl (3110 m total depth; DePaolo et al., 2001b). In the second phase the hole was cased (2003) and then deepened in 2004–2007 to a final depth of 3508 mbsl (3520 m total depth). After each phase of coring, an integrated set of investigations characterized the petrology, geochemistry, geochronology, and the magnetic and hydrological properties of the cored lavas. Most of the funding for this long-term project was provided by the National Science Foundation (U.S.A.) through its Continental Dynamics program, but critical support for drilling was received for the 1999 and 2004–2007 phases from the ICDP. We summarize here the results of the HSDP1 and HSDP2-Phase 1 drilling and preliminary results of ongoing studies from the HSDP2-Phase 2 drilling.

Hawaii Scientific Drilling Project

A Hole Design

B Downhole Temperature

Figure 2. [A] Diagram showing the casing diameter in the HSDP2 hole, and the dates when coring and hole opening were done. Presently the hole is cased to a depth of 2997 mbsl, and is open below that. [B] Temperature measured in the hole and the inferred relationships to subsurface hydrological features. Freshwater is shown as light blue, seawater as light green, and brackish waters as intermediate colors. Temperature survey (red line), done while the hole was flowing and still uncased below 1820 mbsl, suggests that water is entering the hole below ~2800 mbsl, and additional entry levels are at 2370 and 2050 mbsl. Circulation of cold seawater through the section below 600 mbsl is rapid enough to cool the rocks to temperatures 15°C–20°C below a normal geothermal gradient.

Site Location

An abandoned quarry on the grounds of Hilo International Airport was chosen as the site for HSDP2. The HSDP1 pilot hole was located 2 km to the NNW, north of the airport, within fifty meters of the shoreline of Hilo Bay (Fig. 1; Stolper et al., 1996; DePaolo et al., 1996). Although the Mauna Kea volcanic section was the primary target, the HSDP sites in Hilo required drilling through a veneer of Holocene Mauna Loa flows. The Mauna Kea lavas are encountered at depths of 280–245 m. Because the volcanoes are younger to the southeast, and overlap with subsurface boundaries sloping to the southeast (Moore, 1987), it was expected that once Mauna

Kea lavas were entered, the hole would remain in Mauna Kea to total depth. The drill sites were chosen to be (1) far from volcanic rift zones to avoid intrusive rocks, alteration, and high-temperature fluids; (2) close to the coastline to minimize the thickness of subaerial lavas that would need to be penetrated to reach the older, submarine parts of the volcano; and (3) in an industrial area to minimize environmental and community impacts.

Drilling and Downhole Logging

The main phase of HSDP2 drilling in 1999 consisted primarily of successive periods of coring to predetermined depths, followed by rotary drilling to open the hole for installation of progressively narrower casing strings (Fig. 2). No commercially available system could satisfy both the coring and rotary drilling requirements, so a hybrid coring system (HCS) was designed and fabricated. The HCS employed a rotating head and feed cylinder to drive the coring string, and it was attached to the traveling block of a standard rotary

Figure 3. Lithologic column of the HSDP2 drill cores. Boundary between Mauna Loa (ML) and Mauna Kea (MK) lavas is shown, as well as the subaerial-submarine transition, and depths at which the first pillow lava and the first intrusive rocks were encountered. Patterns represent different lithologies as indicated. The total depth of the hole is measured from a reference level 11.7 meters above sea level; the depth scale used here is in meters below sea level (mbsl).

time, but two additional factors contributed. In the thinly bedded pillow lavas, the core tended to fragment as it was cut from the formation, thus blocking the core barrel and resulting in short core runs. Broken core fragments also tended to drop into the drill string as the core tube was brought to the surface. These fragments needed to be cleared from the drill string before sending a new core tube down, and this process typically added nearly an hour to the core retrieval process. Higher rates of bit wear also required more frequent trips to change the bit. In spite of these challenges, an average penetration rate of ~21 m d^{-1} was maintained down to 2986 mbsl, where a zone was encountered in which the basalts were thoroughly broken and unstable. This broken zone triggered some deviation of the hole from vertical and presented additional problems with rubble caving into the hole and threatening to jam the bottom hole assembly (BHA). The drillers tried various strategies to deal with the caving, but they achieved only a small amount of additional progress before the decision was made to terminate coring operations at a depth of 3098 mbsl and run downhole logs. The hole was then left filled with heavy mud.

The HSDP Phase 2 drilling commenced in March to August 2003, by first enlarging the diameter of the hole below the 7-inch casing from 3.85-inches to 6.5-inches , and then installing a 5-inch casing to bottom (Fig. 2). Because the casing weight was beyond the capacity of any Hawaii-based drill rigs, a rotary rig was acquired for the project. This "hole-opening" phase proved difficult due largely to unexpected high formation fluid pressures. Before the start of hole opening, the well produced artesian water at a modest rate from depths of 2605 mbsl, 2370 mbsl, and 2059 mbsl. However, soon after the hole was widened, strong water flow began. As depth increased, formation pressures increased. The peak wellhead pressure was measured at ~11 bar, and water flow rates reached as high as 250 L s^{-1}. Initial efforts at controlling flow with increased mud weight were only partially successful, as was an alternative cementing strategy. As a result, progress for most of the hole opening was difficult, dangerous, and slow. Eventually, after the hole had been opened down to about 2732 mbsl, a decision was made to allow the hole to flow freely, with periodic mud "sweeps" conducted to ensure that cuttings were fully cleared from the hole. This strategy was successful and the penetration rate increased from <20 m d^{-1} to nearly 100 m d^{-1}. Hole opening then continued down to 2997 mbsl, where caving problems were again encountered. After several attempts at drilling through the problematic zone, each resulting in a temporarily stuck BHA, the decision was made to terminate hole opening and to begin casing.

Challenges during the hole-opening phase continued when improper lifting tools were used, and late in the process a 2347-m string of 5-inch casing was dropped into the hole. After the condition of the dropped casing was checked, it was left in the hole. The casing was completed by threading an additional 610-m string onto the top of the dropped casing;

rig to allow core and rotary drilling from the same platform. Core penetration rates averaged 48 m d^{-1} through the subaerial section, but slowed upon entering the submarine section, where poorly consolidated hyaloclastites (Fig. 3) led to short bit life and poor core recovery. A 3.5-inch tricone bit, driven by the coring unit, was used to penetrate the most difficult portion of this interval, the only significant depth interval where core was not recovered. Progressive induration of the hyaloclastites with depth enabled an average penetration rate of ~25 m d^{-1} down to the first occurrence of pillow basalts (1980 mbsl; Fig. 3). The opening of the hole and setting of the casing also progressed well; the rotary drilling penetration rate down to 1820 mbsl averaged ~46 m d^{-1}.

After casing was set to 1820 mbsl, coring through the alternating intervals of pillow and hyaloclastite progressed at a slower rate than in the upper section of hole. Reduced rates of penetration were expected due to the longer trip

the bottom of the casing was at a depth of 2997 mbsl. As the follow-on coring work began in late 2004, we discovered that the bottom joint of the dropped casing string had been damaged. It was necessary, using special tools, to cut a window through the side of the bent casing to extend the hole. After rubble was cleared from the hole down to 3098 mbsl, coring proceeded in two stages (December 2004 to February 2005, and December 2006 to February 2007) to a total depth of 3508 mbsl. The first coring effort averaged only 6 m d^{-1} and reached 3326 mbsl. At that point the rotary rig was sold, and a leased coring rig was used. The coring done in early 2007 achieved about 8 m d^{-1}, but problems with the leased rig and exhaustion of project funds resulted in only 180 m of additional core.

At the conclusion of HSDP2-Phase 2 drilling, the 5-inch casing was perforated, cement was pumped into the annulus at depth, and at 2031 mbsl, the casing was cut at 1635 mbsl and the top section removed from the hole. The final depth of the HSDP core hole is about 914 m less than was originally planned in 1996, but it is still nearly twice as deep as the next deepest core hole drilled in Hawaii (SOH-2 to 2073 m on the Kilauea East Rift Zone; Novak and Evans, 1991).

Hydrology

Although the primary purpose of the borehole was to document the geochemical evolution of an oceanic volcano, a significant finding was the unexpected hydrology. The traditional view of ocean island subsurface hydrology is one of a freshwater lens (fed by rainfall recharge) "floating" atop saltwater-saturated rocks that extend to the island's base. Circulation of seawater within the basement rocks is presumed to occur to the extent made possible by permeability and thermal conditions. The HSDP boreholes showed that the hydrology of the island of Hawaii is considerably more complicated and interesting. Whereas it has been assumed that the youth of the island of Hawaii meant that artesian aquifers, such as those arising from the buried cap rocks on Oahu, would be absent, the borehole encountered multiple artesian aquifers (Fig. 2). Estimated groundwater flow through the first of these, at a depth of only 300 m, may represent as much as a third of the rainfall recharge to the windward mid-level slopes of Mauna Kea. The deeper artesian aquifers have equally unexpected implications. Some of the groundwater produced by the deep aquifers was hypersaline, with chloride concentrations about 20% higher than seawater. These aquifers must be isolated from ocean water, and they may have lost 25% of their water to hydration reactions with basalt glass. Other fluids produced by the borehole had salinities less than half those of seawater, indicating that a connection exists between these deep confined pillow aquifers and the basal fresh groundwater system. Evidence for freshwater in the formation fluids was found in the borehole to as deep as 3000 mbsl, implying that the volume of freshwater within Mauna Kea may be ten times greater than previously estimated.

Thermal Profile

The downhole temperature profile for the HSDP2 corehole (Fig. 2) yields additional information about the subsurface hydrology of Hawaii. Within the first 200 m of the borehole, the thermal conditions were consistent with the expected basal freshwater lens underlain by rocks saturated with freely circulating saline water. However, at ~300 m a temperature reversal occurs that was later demonstrated to be the result of a ~150-m-thick freshwater aquifer confined by multiple soil and ash layers present at the interface between Mauna Loa lavas and late-stage Mauna Kea flows (Thomas et al., 1996). Below the artesian fresh aquifer, the temperature falls rapidly to ~9°C, reflecting the presence of an actively circulating saltwater system that draws deep, cold sea water in through the submerged slopes of Mauna Kea. Circulation within this system is rapid enough to maintain a very weak temperature gradient (~7°C km^{-1}) down to a depth of ~1600 mbsl where the gradient begins a progressive rise to ~19°C km^{-1} at 2000 mbsl. This value is to be expected for a conductive thermal gradient (Büttner and Huenges, 2002). Temperature measurements made below 2000 mbsl under static conditions (no internal well flow) show a nearly constant 19°C km^{-1} gradient to total depth. Downhole temperature measurements made during and soon after well flow show sharper temperature gradients that are interpreted to reflect flow into or out of the formation during drilling or production, respectively. The positive temperature steps at permeable formations indicate entry of warm fluids from deep within Mauna Kea's core.

Lithologic Column

A major effort was made to characterize and catalogue the rock core on-site. This nearly-real-time logging allowed us to monitor the volcano structure, which helped with drilling and allowed us to immediately start systematic sampling. On-site activities included hand-specimen petrographic description and photographic documentation of the recovered core. There were 389 distinguishable lithological units identified (e.g., separate flow units, sediments, soils). A simplified version of the lithological column is shown in Fig. 3. A diagrammatic representation of the internal structure of the Mauna Kea volcano in the vicinity of the drill site (Fig. 4) helps explain the significance of the volcanic stratigraphy.

The core was split longitudinally into a working portion (two-thirds) to be used for analysis and an archival portion (one-third) to be reserved for future study. A reference suite of samples for geochemical analyses, chosen to be representative and to cover the depth of the core at specified intervals, was taken on-site and sent to participating scientists. A key feature of the sampling is that a complete suite of petrological and geochemical analyses was conducted on these reference samples, allowing for a high level of comparability among complementary textural, chemical,

and isotopic measurements. All of the data collected on-site can be accessed at http://www.icdp-online.org/contenido/icdp/front_content.php?idcat=714,; the data include digital photographs of each box containing the working and archival splits, high-resolution scans of the working split, a detailed lithological column, and detailed descriptions of the entire recovered core. A summary of the lithologic column from the HSDP2 drilling follows.

Subaerial Mauna Loa lavas (surface to 246 mbsl): The lava flows from the surface to 246 mbsl are all subaerial Mauna Loa (ML) tholeiites, as determined by major and trace element analyses. These flows range from aphyric to 30% (by volume) olivine phenocrysts; the average phenocryst abundance is ~11%. Thirty-two flow units with an average thickness of ~8 m were identified in this depth range; and pahoehoe flows are approximately equally abundant. A total thickness of 2–3 m of ash, soil, and volcanic sandstone occurs interspersed with the ML lavas. The contact between the ML lavas and underlying subaerial Mauna Kea (MK) lavas occurs at 246 mbsl. Lavas from the two volcanoes are sufficiently different in chemical and isotopic compositions that it is easy to demonstrate that there is no interfingering of lavas from the two volcanoes, which is consistent with subsurface structural analysis based on the age and growth-rate relations between Mauna Kea and Mauna Loa (DePaolo and Stolper, 1996). Although the drill site was near that of the pilot hole, and the depths of the ML-MK transition (275 mbsl in the pilot hole) are similar at the two sites, the shallow carbonates and beach deposits observed in the pilot hole (DePaolo et al., 1996) are not present in the HSDP2 core.
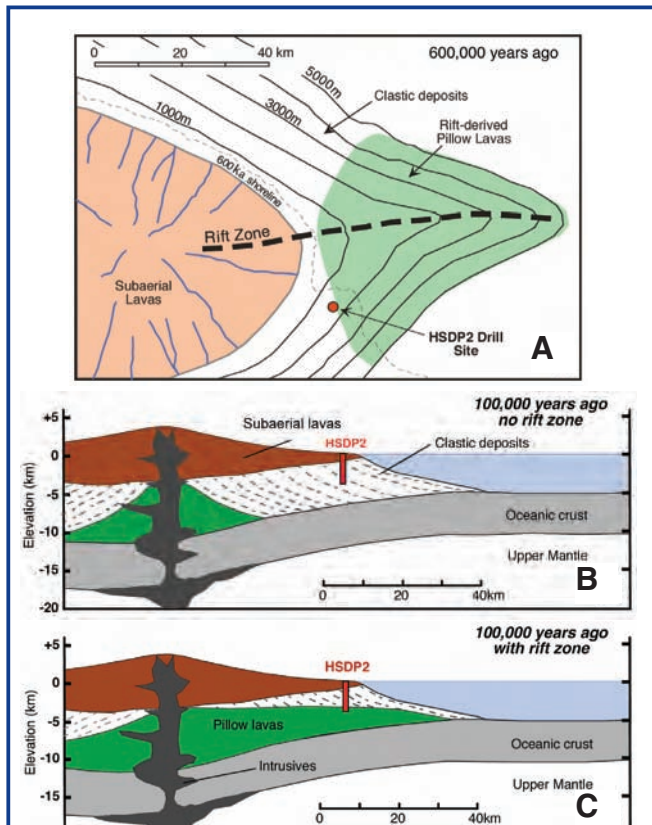
Figure 4. [A] Reconstruction of the Mauna Kea east rift and shoreline at about 600 ka. The shoreline was about 12–15 km NW of the drill site, and the surface at the drill site location was at about 1500 m water depth. Prior to the time depicted, the drill site location would have been receiving submarine lavas from the (hypothesized) Mauna Kea east rift. Subsequently, it was receiving mainly clastic material derived from the shoreline. Since 600 ka there has been about 1500 m of subsidence, so the depth in the HSDP drillcore corresponding to this map is about 3000 mbsl. Below this depth, the rocks encountered in the drillcore should be exclusively submarine pillow lava. The distribution of submarine pillow lava is based on the interpretation of Kilauea's east rift zone bathymetry by Moore (1996). [B] Schematic cross section from the Mauna Kea summit through the HSDP2 drill site (in red), model for 100 ka ago: assuming that there is no rift zone. [C] In this model the HSDP2 core hole should not have intersected any pillow lava, assuming the presence of a rift zone, which fits the observations better.
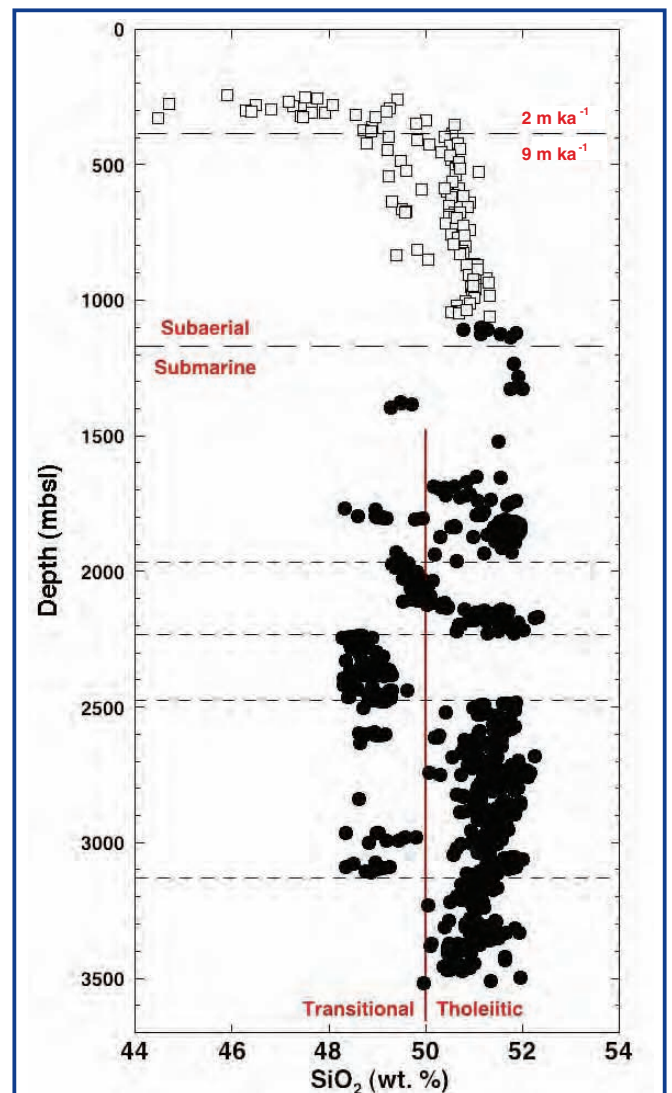
Figure 5. SiO2 contents of Mauna Kea lavas and hyaloclastites plotted versus depth below sea level in the HSDP core. Solid symbols are glass samples, open symbols are whole rock measurements adjusted for crystal fractionation and accumulation to MgO content of 7% by weight. Below 1350 mbsl there is a bimodal distribution of SiO2 concentrations indicative of two distinct magma types. Short horizontal dashed lines separate subsections of the core where one or the other lava type predominates. In the uppermost subaerial portion of the core a systematic decrease in the SiO2 concentration, representing the tholeiitic to alkaline transition, is also associated with a pronounced decrease in the local lava accumulate rate from 9 m ka[-1] to 2 m ka[-1] (see Figs. 6 and 7). Data from Rhodes and Vollinger (2004), Stolper et al. (2004), and unpublished data.

Moreover, although the number of ML flow units identified in the HSDP2 core is similar to that in the pilot hole (thirty), there is no one-to-one correspondence of units in the two cores below the first few near-surface flows. Dating of the ML section of the pilot hole core suggests that it extends back to about 100 ka (Lipman and Moore, 1996). During this time trace element and isotopic geochemistry show significant changes; most of the samples from the core are quite different from sub-aerially exposed lavas of Mauna Loa (DePaolo et al., 2001a).

Subaerial Mauna Kea lavas (246–1079 mbsl): The upper 834 m of the MK section comprises primarily ~120 subaerial flows of 7 m average thickness; about twenty-five percent of these flows are pahoehoe. A total thickness of ~2 m of ash and soil occurs within and between many flow units. Chemical analyses (Fig. 5) demonstrate that the uppermost ~50 m of the MK section contains interbedded nepheline-normative (low SiO_2) and hypersthene-normative lavas, marking the end of the shield-building phase of MK's volcanic cycle (Rhodes and Vollinger, 2004). Deeper subaerial MK lavas are tholeiitic with variable olivine phenoscryst content (0–35 volume %).

Submarine Mauna Kea — dominantly hyaloclastite debris flows (1079–1984 mbsl): An abrupt transition to the submarine part of the MK section occurs at a depth of 1079 mbsl, marked by the occurrence of volcaniclastic sediments and glassy lavas significantly denser than those above the transition. Based on radiometric ages of the lavas at the base of the nearby pilot hole, the estimated age of the subaerial-submarine transition is ~400 ka (Sharp and Renne, 2004; Sharp et al., 1996; Fig. 6). The estimated average subsidence rate at the drill site over this interval, ~2.5 mm y^{-1} (corrected for sea level variations), is similar to the current subsidence rate in Hilo measured by tide gauges; to the average subsidence rate for the past several tens of thousands of years based on sediments in the pilot hole (Beeson et al., 1996); and to the average values over 100–200 ka at several near-shore sites around Hawaii based on the ages of drowned coral reefs (Moore et al., 1996).

The upper 60 m of the submarine section (1079–1140 mbsl) is different from the rest of the submarine section. This near-shore facies is an alternation of massive basalts (2–3 m average thickness) and clastic sediments (~3 m average thickness; dominantly basaltic hyaloclastite). These occur in roughly equal amounts. The vesicularity of the massive basalts in this depth range is variable but mostly lower than the 10%–20% typical of the subaerial lavas; when combined with the low water and sulfur contents of most glasses from these basalts, this suggests that these massive basalts are subaerial flows that continued past the shoreline as submarine flows. The hyaloclastites consist of a matrix rich in glassy fragments plus basaltic lithic clasts from <1 cm up to several tens of centimeters in size. These clasts are similar lithologically to the massive basaltic units, although they

are usually more vesicular. The basalts in this depth range are highly fractured, and the hyaloclastites are poorly indurated, leading to the poor drilling conditions described above.

The interval from 1220 mbsl to 1984 mbsl consists of ~90% well-indurated basaltic hyaloclastite, interspersed with ~10% massive submarine basalts (Fig. 3). The basalts are divided into twenty-six units with an average thickness of 3–4 m. They are olivine phyric, and point counts and chemical analyses indicate a systematic decrease in olivine abundance with depth in this interval from >20% at the top to <10% at the bottom. The vesicularity of the massive basalts in this interval is typically <1%. Although some of these massive basalts could be intrusives or large lithic clasts, most have been interpreted as subaerial flows that continued past the shoreline as submarine flows. As at the top of the submarine section, the hyaloclastites in this deeper interval comprise a matrix often rich in fresh glass fragments plus variably olivine-phyric, variably vesicular basaltic lithic clasts. In some intervals, where these volcaniclastic sediments are bedded and/or poor in lithic clasts, they are described as sandstones or siltstones. Analyses of water and sulfur contents of glassy fragments in the hyaloclastites demonstrate that they have been degassed subaerially. This composition, plus the often highly vesicular nature of the basaltic clasts and the presence of charcoal in at least one hyaloclastite, suggests that this thick interval of hyaloclastite represents material transported downslope (probably by slumping from oversteepened near-shore environments) as the shoreline moved outward during the subaerial phase of growth of the Mauna Kea volcano (Moore and Chadwick, 1995; Fig. 4).
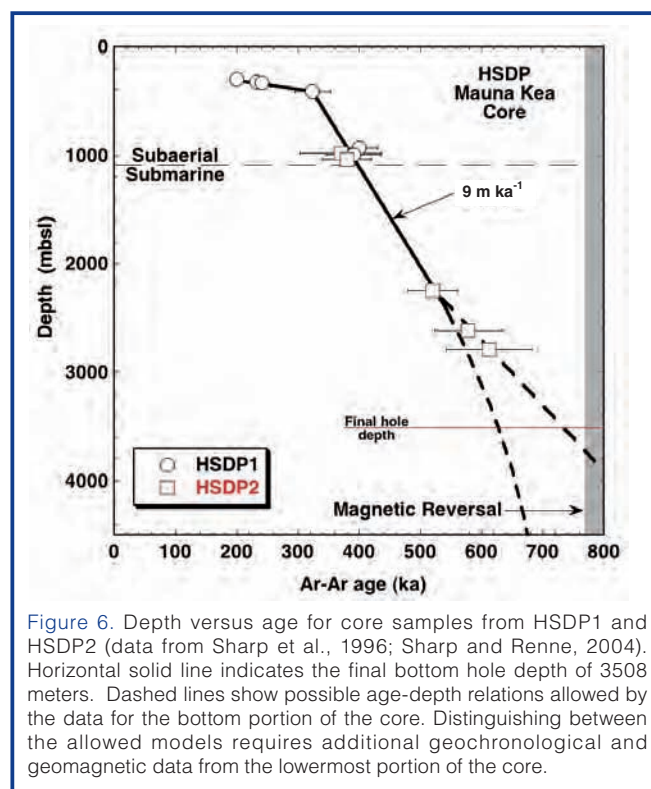
Figure 6. Depth versus age for core samples from HSDP1 and HSDP2 (data from Sharp et al., 1996; Sharp and Renne, 2004). Horizontal solid line indicates the final bottom hole depth of 3508 meters. Dashed lines show possible age-depth relations allowed by the data for the bottom portion of the core. Distinguishing between the allowed models requires additional geochronological and geomagnetic data from the lowermost portion of the core.

Submarine Mauna Kea — dominantly pillow lavas (1984–3098 mbsl): From a depth of 1984 mbsl to the to the depth reached in the 1999 phase of drilling, the section is ~60% pillow basalt, with less abundant intercalated volcaniclastic sediment (Fig. 3). Several thick intervals (up to ~100 m each) composed nearly entirely of sediment are also present. The sediments are primarily hyaloclastite, and they were probably transported from near-shore environments. The pillows typically have fresh glassy margins; the average olivine content is ~6% by volume, much lower than the average for the subaerial MK flows. Vesicularities range up to 10%, but the average is 1%–2%. Water contents of the glassy pillow margins are ~0.08 wt % at 1984–2140 mbsl (consistent with subaerial degassing), but most pillow margins from depths >2200 mbsl have water contents of 0.2–0.8 wt %. The water-rich, deeper lavas were never degassed under subaerial conditions and are interpreted as submarine eruptions. The deepest ~180 m of this interval contains no hyaloclastite. Before drilling the final 422 m (see below) it was hypothesized, based on the presence of the 180-meter hyaloclastite-free section, that pillow lavas would dominate the deeper sections of the core.

Submarine Mauna Kea – the final phase of drilling (3098–3508 mbsl): Although the final phase of drilling was at times challenging as described above, core recovery was close to 100%. All rocks from the final phase of drilling were deposited below sea level; based on chemical analyses currently available of whole rocks and glass, they have been determined to be from the Mauna Kea volcano, On-site core logging led to the identification of forty-four distinguishable units (the main phase of drilling had identified 345 units). Five lithologies were identified: pillows (~60%); pillow breccias (~10%); massive lavas (~12%); hyaloclastites (~17%); intrusives (~1%; these are mostly multiple, thin (down to cm-scale) fingers of magma with identical lithologies occurring over narrow depth intervals; see next section). As with the shallower portions of the drill core, the rocks are primarily tholeiitic, ranging from aphyric to highly olivine-phyric lavas (up to ~25% olivine phenocrysts). Although they are variably altered (clays, zeolites), considerable fresh glass and olivine are present throughout this part of the core. Forty whole-rock samples were collected as a reference suite, processed (including the cutting of thin sections), and sent to multiple investigators for study. Additionally, glass was collected at roughly 3-m intervals for electron microprobe analysis.

Although samples were continuous and consistent with the shallower rocks from the previous phases of coring, there are several noteworthy features of the deepest 422 m of core. (1) Glasses from the shallower core were characterized by bimodal silica contents (Fig. 5, a low SiO_2 group (48–49 wt %), and a high SiO_2 group (51–52 wt %). Glasses from the deepest section are essentially all in the high SiO_2 group and are somewhat more evolved (5.1–7.6 wt % MgO compared to 5.1–10.8 wt % for the glasses from the shallower portion of the core). (2) The overall expected sequence of lithologies with depth in the core is subaerial lava flows, hyaloclastite (formed by debris flows carrying glass and lithic fragments from the shoreline down the submarine flanks of the volcano), and finally pillow lava (Fig. 4). This sequence was generally observed in the earlier phases of drilling, and it appeared that the deepest rocks from the 1999 phase of drilling were essentially all formed from pillow lavas (i.e., there were no more hyaloclastites). However, thick hyaloclastites reflecting long distance transport from the ancient shoreline reappear in the bottom ~100 m of the drill hole. Although it may be coincidence, pillow breccias occur in the shallower parts of the core from the final phase of drilling, but not in the deeper parts in which the hyaloclastites reappear. (3) There are three units classified as "massive" including one relatively thick (~40 m), featureless (no internal boundaries, no evidence of mixing or internal differentiation) moderately olivine-phyric basalt. Their origin is unclear.

Intrusive units: Intrusive basalts are present in the deepest portions of the core, but they are abundant nowhere; between their first occurrence at 1880 mbsl and the bottom of the core, they make up several percent of the core. They are most abundant in the 2500–3100 mbsl interval, where they constitute 7% of the core (Fig. 3). Intrusive rocks make up a lower fraction (~1 %) of samples from the final phase of coring than in the deeper parts of the section from the 1999 phase of drilling. It had been suggested that intrusives might become more common the deeper the drilling, but this is not the case at depths down to 3500 m. Individual intrusive units typically occur as multiple, thin (up to a few centimeters long) splays or fingers. The average olivine phenocryst content is 4%–5%, and their vesicularities are all ≤1%. The relationship of the intrusives to the lavas and sediments they intrude is not firmly established, but the lobate shapes of some of the intrusive contacts with the hyaloclastites suggest that the latter were still soft when they were intruded.

Alteration and faulting: Basalts in the subaerial and submarine parts of the section are relatively fresh (unweathered), based on the presence of fresh glass and olivine. Although secondary minerals (e.g., gypsum, zeolites, clays) are common below 1000 mbsl, they tend to be localized in vesicles or lining fractures (Walton and Shiffman, 2003; Walton, 2008). Olivines are often partially altered, and in some of the subaerial lavas the matrix is clayey. The overall fresh nature of the rocks is consistent with their low vesicularity and the low downhole temperatures (Fig. 2). The hydrology of the drill site may also contribute to this, in that less reactive, freshwater is present to great depth. Near the base of the core, there is some suggestion of an increased abundance of secondary minerals and alteration based on hand-specimen descriptions. An interesting aspect of the alteration is a blue coating on most fragments starting near the depth of the subaerial-submarine transition that becomes less apparent after several hundred meters. Another distinctive feature is a bright blue-green alteration zone extending

up to ~30 cm into hyaloclastites from intrusive contacts; although striking when the core came out of the ground, it faded and was difficult to distinguish within a few weeks. No significant fault displacements were observed in the core, but slickensides (though rare) are found throughout the section, demonstrating that at least local relative motions occurred in the section.

Key Petrologic, Geochemical, and Volcanological Results

Although only preliminary results are available for the final phase of drilling, considerable work has been completed on the samples recovered in the two previous phases of drilling. We summarize them briefly here, with references to the primary publications.

Age and growth rates of Hawaiian volcanoes: Much of what we can infer from the studies of the chemical and isotopic composition of the lavas depends on their age. What we have learned about the age of lavas is summarized in Fig. 6. The deepest dated sample (at 2789 mbsl) has an age of 683±82 ka (Sharp and Renne, 2004). Comparison with previous age and growth rate estimates for the Hawaiian volcanoes (Moore and Clague, 1992) indicates that the volcano lifetimes are apparently almost four times longer than was inferred from surface data (although very close to our predictions as laid out in the 1991 NSF proposal). Reconciling the age data from the core with the surface observations is a challenge still to be undertaken, but one of the implications is that we have been able to sample a long time period and hence have a long record of the magma output from the Hawaiian plume. Figures 4a and 7 show the island geography roughly 600,000
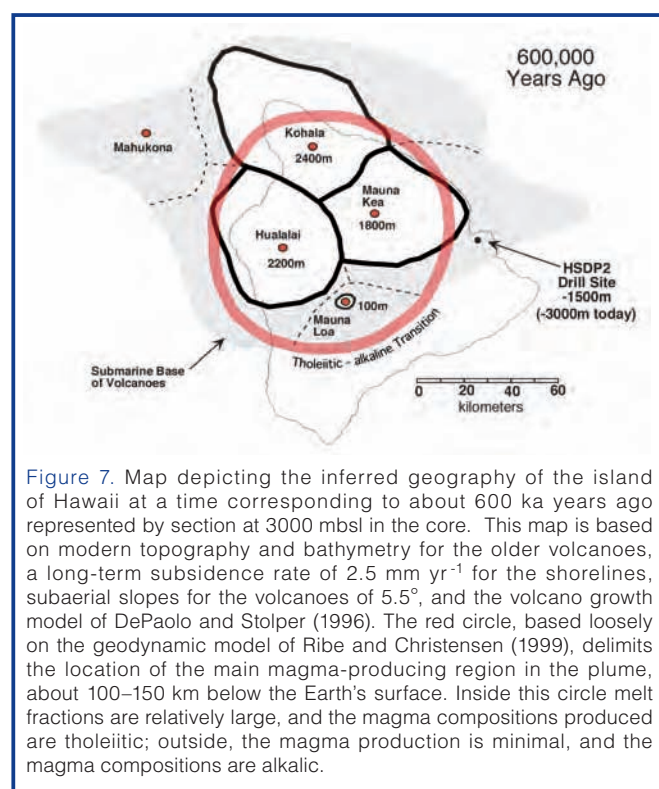

Figure 7. Map depicting the inferred geography of the island of Hawaii at a time corresponding to about 600 ka years ago represented by section at 3000 mbsl in the core. This map is based on modern topography and bathymetry for the older volcanoes, a long-term subsidence rate of 2.5 mm yr^{-1} for the shorelines, subaerial slopes for the volcanoes of 5.5°, and the volcano growth model of DePaolo and Stolper (1996). The red circle, based loosely on the geodynamic model of Ribe and Christensen (1999), delimits the location of the main magma-producing region in the plume, about 100–150 km below the Earth's surface. Inside this circle melt fractions are relatively large, and the magma compositions produced are tholeiitic; outside, the magma production is minimal, and the magma compositions are alkalic.

years ago as reconstructed from the HSDP age data and the models of DePaolo and Stolper (1996). To date, we have had difficulty in reconciling the growth history of the volcanoes with what is known of the Pacific plate velocity over the plume, both its speed and direction (DePaolo et al., 2001a). Based on the ages of the older islands and seamounts in the Hawaiian chain, the long-term inferred velocity of the plate is about 8.6 cm yr^{-1}. Modern GPS measurements suggest a present-day plate velocity of 7 cm yr^{-1}. Moore and Clague (1992), on the basis of their growth model, suggested that the volcanoes on the island of Hawaii were moving over the plume at a velocity of 13 cm yr^{-1} or more! So far, we have been able to make a reasonable fit to the age data with a velocity of 10 cm yr^{-1}, but this model can probably only be tested by drilling in other volcanoes.

Lava stratigraphy and volcano evolution: Excluding the abrupt change from the Mauna Loa lavas at the top of the core to the Mauna Kea lavas that extend over most of the length of the core, there is considerable evidence of chemical and isotopic heterogeneity in the recovered lavas (Figs. 5 and 8). The data provide critical insights into plume structure and the time dependence of magma generation over much of the lifetime of the Mauna Kea volcano. Two key results are described here. (1) The coring captured in detail the termination of the shield-building phase of the Mauna Kea volcano at about 150–300 ka, which is characterized by a shift from tholeiitic to alkaline magmas and a drastic slowing of eruption rate (Figs. 5 and 6). These changes reflect a shift in degree and depth of melting as the volcano passed from the center to the exterior of the melt-producing region of the mantle plume (Fig. 7). (2) The Mauna Kea section is characterized by a bimodal distribution of SiO$_2$ contents in the lavas of the main, shield-building phase of the volcano, with both abrupt and continuous transitions between the two magma types occurring in the section (Fig. 5). The bimodal compositional distribution has never previously been observed in Hawaii, and since these major element characteristics are correlated with isotopic ratios, they indicate a bimodal distribution of source components. In a potentially major paradigm shift, these results may suggest that the mantle source materials in the Hawaiian plume are not peridotite (i.e., olivine-rich) as generally thought, but rather pyroxene-rich lithologies that straddle a thermal divide.

Geochemical structure of the Hawaiian mantle plume: The HSDP geochemical data can be interpreted in terms of the geochemical structure of the Hawaiian plume. The continuous nature of the HSDP core, with the implied continuous monitoring of the lava output from the volcanoes, has dictated that we develop models for the plume behavior just below the lithosphere and for how magma is collected from the plume melting region and supplied to an individual volcano. These models can be constrained by the volume and volume-age structure of the Hawaiian volcanoes and by available geodynamic models for the Hawaiian plume (DePaolo and

Stolper, 1996; DePaolo et al., 1996; Ribe and Christensen, 1999; DePaolo et al., 2001a; Bryce et al., 2005). Systematic variability in Hawaiian lavas with depth (age) in the drillcore can be attributed to structure in the plume, and one of the interesting results is that there is such structure even though melting within the plume represents only the innermost third or so of the plume radius (Fig. 8). The data show that there is radial geochemical zoning of the melting region of the plume in terms of He, Pb, Nd, Sr and Hf isotopes (Blichert-Toft et al., 2003; Eisele et al., 2003; Kurz et al., 2004; Bryce et al., 2005). This geochemical structure represents the hot core of the plume and does not reflect entrainment of ambient lower or upper mantle. The radial component of the geochemical structure of the plume represents the vertical structure at the thermal boundary layer from which the plume originates (Fig. 9). In the case of Hawaii, all of the

lavas are derived from melting of mantle that originates from within 20–50 km of the base of the mantle (Farnetani et al., 2002). One of the most striking characteristics of the HSDP data is that a high $^3He/^4He$ anomaly (R/Ra > 16) is nested within the core of the melting region of the plume and is much larger in amplitude and much smaller in diameter than the Nd, Sr and Hf anomalies (Fig. 8). A ^3He anomaly apparently has a different origin than the other anomalies and is restricted to the lowermost 10–20 km of the mantle plume source. The helium signal is therefore likely to come either directly from the Earth's core via leakage across the core-mantle boundary, or from a dense layer separating the main mantle from the outer core (Bryce et al., 2005).

Thermal history, hydrology, lithification, and alteration geochemistry: As noted above, one of the unexpected features of the HSDP drill site is the low temperature at depth (Fig. 2). The temperature profile requires that cold seawater (or deeply penetrating basal groundwater) be circulating through the volcanic pile even at depth greater than 3 km. Moreover, as emphasized above, there are pressurized aquifers near the bottom of the hole.

Studies of alteration minerals in the hyaloclastites have so far indicated that the mineral phases represent low temperatures of alteration less than 50°C, which is consistent with
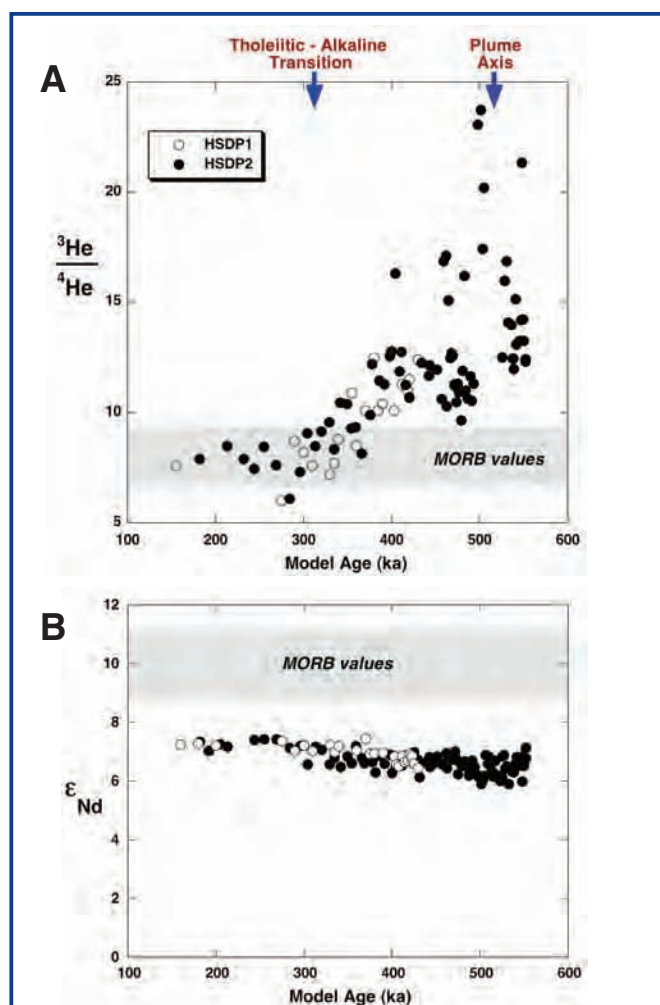
Figure 8. Isotopic composition of [A] He and [B] Nd in HSDP lavas plotted versus age. The ages were assigned using the model of DePaolo and Stolper (1996) and are consistent with the measured ages (Fig. 6). During the period of time represented by the core samples (ca. 600 ka to 150 ka), the summit of the Mauna Kea volcano moved from a position close to the center of the plume melting region (depicted in Fig. 7) to a position close to the edge of the melting region. The systematic shift of isotopic ratios shows that there is radial structure within the plume. The isotopic variations are more dramatic; near the center of the plume they are much different from mid-ocean ridge basalt (MORB) values and indistinguishable from them at the edge of the melting region (data from Kurz et al., 1996, 2003). The Nd isotopic variations are subtle but consistently different from MORB values (data from Bryce et al., 2005).
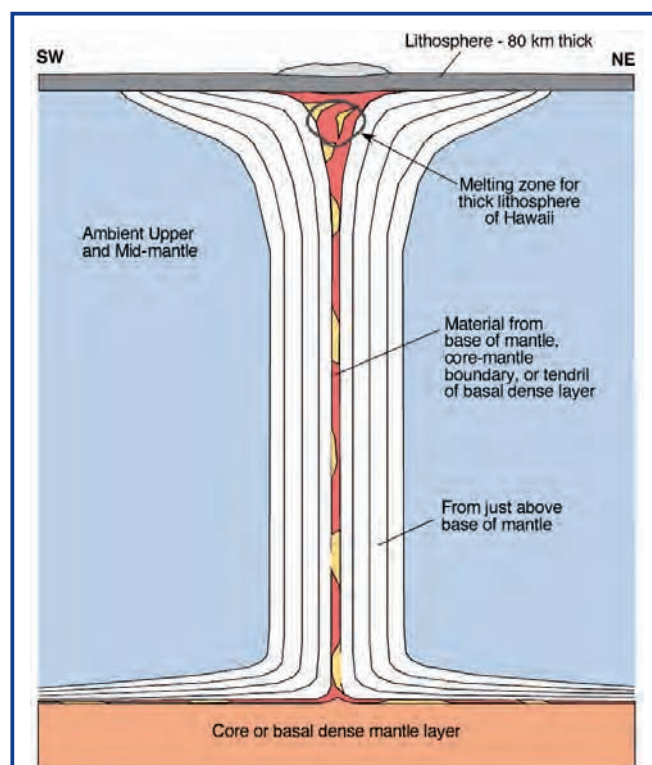
Figure 9. Schematic drawing showing the relationship between the central axis of a cylindrical mantle plume and the base of the mantle (from Bryce et al., 2005). The He and Nd isotopic ratio versus age data shown in Fig. 8 may represent a detailed vertical section through the lowermost 20–50 km of the mantle. In this interpretation, the high-3He signal is confined to the extreme base of the mantle and suggests that the ^3He signal may be associated with a basal, high-density mantle layer, or the outer core. The figure also depicts heterogeneities within the axial region of the plume.

the measured temperature profile (Walton and Shiffman, 2003). Hence the temperatures in this section have always been low. The alteration mineralogy of glass in pillow rinds and pillow breccias is similar to that of hyaloclastites. A unique aspect of studying alteration of the HSDP core is that the age and stratigraphic position of the samples are known, and the temperature measurements can be used to reconstruct the thermal history. By systematically sampling down the core it is possible to reconstruct the time and temperature of both the alteration of the rocks and the microbial activity (Walton, 2008). Most other situations require study of samples with unknown temperature history or do not preserve the stages of progressive alteration and infection that can be observed in the HSDP core. The alteration process may be significant in understanding the reactions and compositional exchange between seawater and basalt glass at low temperatures, thereby providing an analogue system for the early history of fluids that circulate through mid-ocean hydrothermal systems. Signs of microbial involvement in the alteration process are evident as filamentous channels in glass, but only within a restricted portion of the core between about 1080 mbsl and 1460 mbsl (Walton and Schiffman, 2003; Walton, 2008; Fisk et al., 2003). This re-striction suggests that microbes infected the hyaloclastites early in their history but are not very active at present.

Summary

The Hawaii Scientific Drilling Project drilled and cored two holes in Hilo, Hawaii, the deeper reaching a depth of 3508 mbsl, and it retrieved a total of 4600 meters of rock core (525 meters from the Mauna Loa volcano and the remainder from the Mauna Kea volcano). The Mauna Loa core extends the continuous lava stratigraphy of that volcano back to 100 ka and reveals major changes in lava geochemistry over that time period. The Mauna Kea core spans an age range from about 200 ka to perhaps 700 ka, and when combined with surface outcrops, it provides a 700-kyr record of the lava output from a single volcano. During the time covered by the lavas from the core, the volcano drifted some 60–80 km across the melting region of the Hawaiian mantle plume, and therefore the HSDP rock core provides the first systematic cross-sectional sampling of a deep mantle plume. The geochemical characterization of the core, which involved an international team of forty scientists over a period of fifteen years provides information about mantle plume structure and ultimately about the deepest parts of the Earth's mantle. The study of the lava core (which still continues) has provided unprecedented information about the internal structure of a large oceanic volcano and the time scale over which volcanoes grow. The hole also provides an intriguing glimpse of a complex subsurface hydrological regime that differs greatly from the generalized view of ocean island hydrology.

Drilling conditions were favorable in the subaerial parts of the volcanic section, where coring was generally fast and efficient. The submarine part of the lava section, made up primarily of volcanogenic sediments and pillow lavas, proved considerably more difficult to drill. Some of the difficulties and considerable additional expense were due to pressurized aquifers at depth and a few critical mistakes made while setting casing. Even with the more difficult conditions, the project retrieved about 2400 meters of nearly continuous core from the submarine section of Mauna Kea. Overall, the HSDP project was highly successful even though the original target depth was about 20% deeper than the final hole depth. As expected, the project results answer several important questions about oceanic volcanoes, mantle plumes, and ocean island water resources, but they raise many more that might be addressed with further moderate-depth drilling in other Hawaiian volcanoes.

Acknowledgements

References

Beeson, M.H., Clague, D.A., and Lockwood, J.P., 1996. Origin and depositional environment of clastic deposits in the Hilo drill hole, Hawaii. *J. Geophys. Res.*, 101(B5):11617–11629, doi:10.1029/95JB03703.

Blichert-Toft, J., Weis, D., Maerschalk, C., Agranier, A., and Albarède, F., 2003. Hawaiian hot spot dynamics as inferred from the Hf and Pb isotope evolution of Mauna Kea volcano. *Geochem. Geophys. Geosyst.*, 4(2): 8704, doi:10.1029/2002GC000340.

Bryce, J., DePaolo, D.J., and Lassiter, J., 2005. Geochemical structure of the Hawaiian plume: Sr, Nd and Os isotopes in the 2.84 km HSDP-2 core of Mauna Kea volcano. *Geochem. Geophys. Geosyst.*, 6: Q09G18, doi:10.1029/2004GC000809.

Büttner, G., and Huenges, E., 2002. The heat transfer in the region of the Mauna Kea (Hawaii)—constraints from borehole temperature measurements and coupled thermo-hydraulic modelling. *Tectonophysics,* 371:23–40, doi:10.1016/S0040-1951(03)00197-5.

DePaolo, D.J., and Stolper, E.M., 1996. Models of Hawaiian volcano growth and plume structure: Implications of results from the Hawaii Scientific Drilling Project. *J. Geophys. Res.*, 101:11643–11654, doi:10.1029/96JB00070.

DePaolo, D.J., Bryce, J.G., Dodson, A., Shuster, D.L., and Kennedy, B.M., 2001a. Isotopic evolution of Mauna Loa and the chemical structure of the Hawaiian Plume. *Geochem. Geophys. Geosyst.,* 2(7):41–43.

DePaolo, D.J., Stolper, E.M., and Thomas, D.M., 1996. The Hawaii Scientific Drilling Project: Summary of preliminary results.

GSA Today, 6(8):1–8.

DePaolo, D.J., Stolper, E.M., and Thomas, D.M., 2001b. Deep drilling into a Hawaiian volcano. *EOS, Trans. Am. Geophys. Union*., 82(149):154–155.

Eisele, J., Abouchami, W., Galer, S.J.G., and Hofmann, A.W., 2003. The 320 kyr Pb isotope evolution of Mauna Kea lavas recorded in the HSDP-2 drill core. *Geochem. Geophys. Geosyst.*, 4(5): 8710, doi:10.1029/2002GC000339.

Farnetani, C., Legras, G.B., and Tackley, P.J., 2002. Mixing and deformation in mantle plumes. *Earth Planet. Sci. Lett.*, 196:1–15, doi:10.1016/S0012-821X(01)00597-0.

Fisk, M.R., Storrie-Lombardi, M.C., Douglas, S., Popa, R., McDonald, G., and Di Meo-Savoie, C., 2003. Evidence of biological activity in Hawaiian subsurface basalts. *Geochem. Geophys. Geosyst.*, 5:1103, doi.10.1029/2002GC000387.

Holcomb, R.T., 1987. Eruptive history and long-term behavior of Kilauea Volcano. *U.S. Geol. Surv. Prof. Pap.*, 1350:261–350.

Kurz, M.D., Curtice, J., Lott III, D. E., and Solow, A., 2004. Rapid helium isotopic variability in Mauna Kea shield lavas from the Hawaiian Scientific Drilling Project. *Geochem. Geophys. Geosyst.*, 5:Q04G14, doi:10.1029/2002GC000439.

Lipman, P.W., and Moore, J.G., 1996. Mauna Loa lava accumulation rates at the Hilo drill site: Formation of lava deltas during a period of declining overall volcanic growth. *J. Geophys. Res.*, 101(B5):11631–11641, doi:10.1029/95JB03214.

Mark, R.K., and Moore, J.G., 1987. Slopes of the Hawaiian Ridge. *U.S. Geol. Surv. Prof. Pap.*, 1350:101–107.

Moore, J.G., 1987. Subsidence of the Hawaiian Ridge. *U.S. Geol. Surv. Prof. Pap.*, 1350:85–100.

Moore, J.G., and Chadwick, W.W., Jr. 1995. Offshore geology of Mauna Loa and adjacent areas, Hawaii. *In* Rhodes, J.M., and Lockwood, J.P. (Eds.), *Mauna Loa Revealed: Structure, Composition, History, and Hazards*, Washington, D.C. (American Geophysical Union), 21–44.

Moore, J.G., and Clague, D.A., 1992. Volcano growth and evolution of the island of Hawaii. *Geol. Soc. Amer. Bull.* 104: 1471–1484, doi:10.1130/0016-7606(1992)104<1471:VGAEOT>2.3.CO;2.

Moore, J.G., Ingram, B.L., Ludwig, K.R., and Clague, D.A., 1996. Coral ages and island subsidence, Hilo drill hole. *J. Geophys. Res.*, 101:11599–11605, doi:10.1029/95JB03215.

Morgan, W.J., 1971. Convection plumes in the lower mantle. *Nature,* 230:42–43, doi:10.1038/230042a0.

Novak, E.A., and Evans, S.R., 1991. Preliminary results from two scientific observation holes on the Kilauea East Rift Zone. *Geotherm. Resour. Counc. Trans.*, 15:187–192.

Rhodes, J. M., and Vollinger, M.J., 2004. Composition of basaltic lavas sampled by phase-2 of the Hawaii Scientific Drilling Project: Geochemical stratigraphy and magma types. *Geochem. Geophys. Geosyst.,* 5:Q03G13, doi:10.1029/2002GC000434.

Ribe, N.M., and Christensen, U.R., 1999. The dynamical origin of Hawaiian volcanism. *Earth Planet. Sci. Lett.*, 171:517–531, doi:10.1016/S0012-821X(99)00179-X.

Robinson, J.E., and Eakins, B.W., 2006. Calculated volumes of individual shield volcanoes at the young end of the Hawaiian Ridge. *J. Volc. Geotherm. Res.*, 151:309–317, doi:10.1016/j.jvolgeores.2005.07.033.

Sharp, W.D., and Renne, P.R., 2004. The ^{40}Ar/^{39}Ar dating of core recovered by the Hawaii Scientific Drilling Project (phase 2), Hilo, Hawaii. *Geochem. Geophys. Geosyst.*, 6(4):Q04G17, doi:10.1029/2004GC000846.

Sharp, W.D., Turrin, B.D., Renne, P.R., and Lanphere, M.A., 1996. The ^{40}Ar/^{39}Ar and K/Ar dating of lavas from the Hilo 1-km core hole, Hawaii Scientific Drilling Project. *J. Geophys. Res.*, 101:11607–11616.

Sleep, N.M., 2006. Mantle plumes from top to bottom. *Earth-Sci. Rev.*, 77:231–271, doi:10.1016/j.earscirev.2006.03.007.

Stolper, E.M., DePaolo, D.J., and Thomas, D.M., 1996. The Hawaii Scientific Drilling Project: Introduction to the special section. *J. Geophys. Res.*, 101:11593–11598, doi:10.1029/96JB00332.

Stolper, E.M., Sherman, S., Garcia, M., Baker, M., and Seaman, C., 2004. Glass in the submarine section of the HSDP2 drill core, Hilo, Hawaii. *Geochem. Geophys. Geosyst.*, 5: Q07G15, doi:10.1029/2003GC000553.

Thomas, D.M., Paillet, F., and Conrad, M., 1996. Hydrogeology of the Hawaii Scientific Drilling Project borehole KP-1: 2. Groundwater geochemistry and regional flow patterns. *J. Geophys. Res.*, 101:11683–11694, doi:10.1029/95JB03845.

Walton, A.W., 2008. Microtubules in basalt glass from Hawaii Scientific Drilling Project #2 phase 1 core and Hilina slope, Hawaii: evidence of the occurrence and behavior of endolithic microorganisms. *Geobiology*, 6:351–364, doi:10.1111/j.1472-4669.2008.00149.x.

Walton, A.W., and Schiffman, P., 2003. Alteration of hyaloclastites in the HSDP2 Phase 1 drill core: 1. Description and paragenesis. *Geochem. Geophys. Geosyst.*, 5:8709, doi.10.1029/2002GC000368.

Watts, A.B., 2001. *Isostasy and Flexure of the Lithosphere*. Cambridge, UK (Cambridge University Press), 458p.

Authors

Edward M. Stolper, Division of Geological and Planetary Sciences, California Institute of Technology, Pasadena, Calif., 91125, U.S.A., email: ems@caltech.edu

Donald J. DePaolo, Department of Earth and Planetary Science, University of California, Berkeley, and Earth Sciences Division, Lawrence Berkeley National Laboratory, Berkeley, Calif., 94720, U.S.A.

Donald M. Thomas, Center for Study of Active Volcanoes, University of Hawaii at Hilo, 200 West Kawili Street, Hilo, Hawaii, 96720, U.S.A.

Web Links

http://hawaii.icdp-online.org
http://www.icdp-online.org/contenido/icdp/front_content.php?idcat=714

Addressing Geohazards Through Ocean Drilling

by Julia K. Morgan, Eli Silver, Angelo Camerlenghi, Brandon Dugan, Stephen Kirby, Craig Shipp, and Kiyoshi Suyehiro
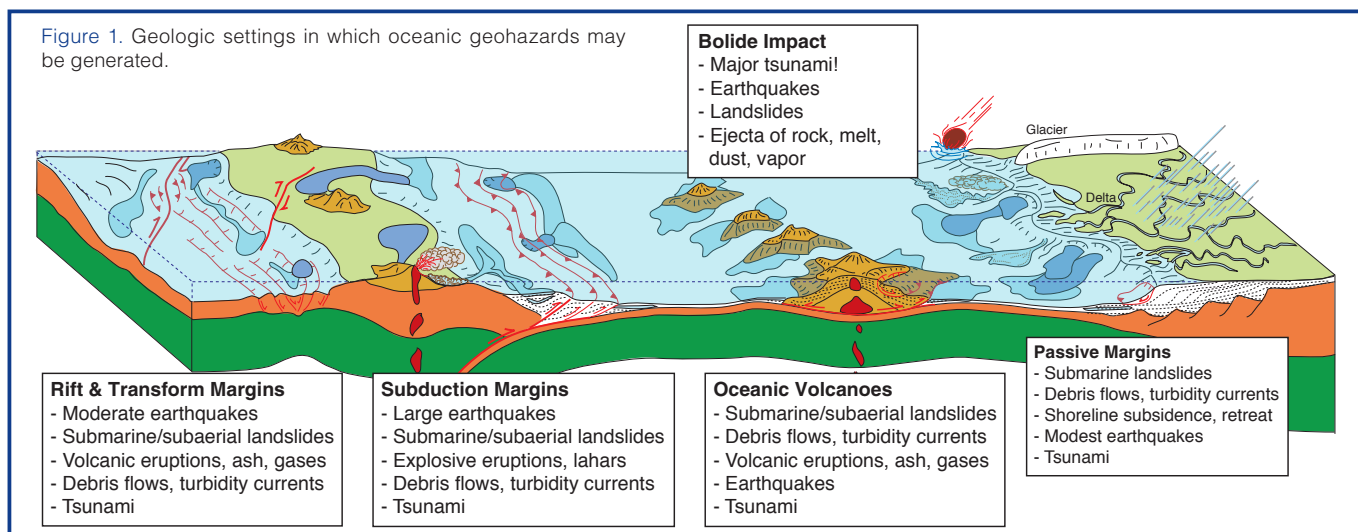
Introduction

Natural geohazards, such as earthquakes, volcanic eruptions, landslides, and volcanic collapse, are of immediate societal concern. In an oceanic setting (Fig. 1), all are capable of generating tsunami that threaten coastal zones at distances of many thousands of kilometers. This power and its effects were forcefully shown by the giant earthquake (M_w 9.2) and tsunami of 26 December 2004 off the coast of northern Sumatra. Smaller magnitude submarine earthquakes and landslides occur with shorter recurrence intervals and the capability of tsunami generation, creating hazards for local coastal communities as well as for offshore industry and infrastructure. At the other end of the scale, the geologic record suggests that less common, large-volume volcanic collapses and extraterrestrial meteorite and comet impacts in ocean basins have the potential to initiate tsunami of extraordinary power that can threaten huge sections of coastlines with growing populations. These events also disperse enormous volumes of ash, steam, and ejecta into the atmosphere, with short- and long-term consequences, including climate change. All of these processes, which have operated throughout the Earth's history, are instrumental in shaping the Earth system today. However, they are characteristically difficult to predict, and viable risk assessment and hazard mitigation depend on a clearer understanding of the causes, distributions, and consequences of such natural events.

Understanding the spatial and temporal variability of submarine geohazards, their physical controls, and their societal effects requires a diverse array of observational techniques. Ocean drilling can be a key element in understanding oceanic geohazards, given that the submarine geologic record preserves structures and past evidence for earthquakes, landslides, volcanic collapse, and even bolide impacts. This record can be read and interpreted through drilling, coring, *in situ* characterization, observatory studies, monitoring, and laboratory studies to provide insight into future hazards and associated risks to society.

With these concerns and opportunities in mind, an Integrated Ocean Drilling Program (IODP) workshop on oceanic geohazards was held at McMenamins Edgefield, outside Portland, Oregon (U.S.A.) on 27–30 August 2007. A primary objective of the workshop was to document how scientific oceanic drilling could provide fundamental information on the frequency and magnitudes of these destructive events, as well as provide scientific insights into their variability and underlying physics. The workshop was attended by eighty-nine scientists from eighteen countries, who were charged with the following goals: (1) establish the state of knowledge regarding conditions and distribution of catastrophic geohazards; (2) define key unresolved scientific questions relating to geohazards; (3) formulate realistic science plans to answer them; (4) evaluate the tools and technologies available for geohazards study; (5) identify potential drilling targets for specific hazardous phenomena; and (6) enhance international collaborations and stimulate proponent teams to develop competitive IODP proposals. Participants contributed to the workshop through oral and poster presentations, white paper preparation, proposal and

Figure 1. Geologic settings in which oceanic geohazards may be generated.

Bolide Impact
- Major tsunami!
- Earthquakes
- Landslides
- Ejecta of rock, melt, dust, vapor

Rift & Transform Margins
- Moderate earthquakes
- Submarine/subaerial landslides
- Volcanic eruptions, ash, gases
- Debris flows, turbidity currents
- Tsunami

Subduction Margins
- Large earthquakes
- Submarine/subaerial landslides
- Explosive eruptions, lahars
- Debris flows, turbidity currents
- Tsunami

Oceanic Volcanoes
- Submarine/subaerial landslides
- Debris flows, turbidity currents
- Volcanic eruptions, ash, gases
- Earthquakes
- Tsunami

Passive Margins
- Submarine landslides
- Debris flows, turbidity currents
- Shoreline subsidence, retreat
- Modest earthquakes
- Tsunami

"concept" presentations, focused breakout discussions, and open plenary discussions.

Submarine Landslides

Submarine landslides occur at a wide range of scales and settings. They often comprise distinctive mass transport deposits recognized on the seafloor or in seismic reflection profiles (Fig. 2). Small-scale submarine landslides are relatively frequent. They have displaced oil rigs, damaged pipelines, broken deep-sea communication cables (Piper et al., 1999), and, in a few cases, damaged segments of coastline (Longva et al., 2003; Sultan et al., 2004). Large and small events along coastal zones also create local, destructive tsunamis (Lee et al., 2003; Tappin et al., 2001).

A range of conditions and triggers has been implicated in the initiation of submarine landslides; these depend on geologic setting, slope evolution, and tectonic and volcanic activity. Earthquake triggering of landslides is well-known;

they can produce tsunami much larger than predicted for the earthquake. As a dramatic reminder, more than 1600 people died in 1998, when the M 7.0 Sissano earthquake in Papua New Guinea triggered a massive submarine landslide, generating a tsunami that inundated a small stretch of coastline (Synolakis et al., 2002). In North America, a large earthquake in eastern Canada in 1929 triggered the Grand Banks landslide, turbidity flow, and tsunami that resulted in twenty-nine deaths and substantial coastal damage (Whelan, 1994). The possible role of co-seismic landsliding in generating a local tsunami in Hawaii in 1975 is still debated (Lander and Lockridge, 1989; Ma et al., 1999). Some of the largest submarine landslides, however, have occurred on relatively aseismic passive margins. The best known example is the Storegga slide on the mid-Norwegian margin (Fig. 3), which disrupted 90,000 km^2 of the continental slope about 8100 years ago (Solheim et al., 2005). Although the cause of this slide is still debated, it is thought to have produced tsunami inundations in Norway, Iceland, and the British Isles (Bondevik et al., 1997). Hypothesized triggers include local fluid overpressures, groundwater seepage forces, and storm-induced wave-action. Sea level or sea temperatures may also cause slope failure through gas hydrate dissociation or dissolution, which can release free gas to the atmosphere (Bünz et al., 2005; Mienert et al., 2005). This process fits into the more general "Clathrate Gun Hypothesis", relating methane release and global climate change (Kennett et al., 2000).

To date, there are no known examples of medium- to large-sized submarine mass movements where the geometry, *in situ* stresses and pressures have been characterized prior to, during, and after the failure. Thus, it is still unclear how and why failures initiate where and when they do, and what governs their subsequent flow behaviors. For example, some landslides disintegrate rapidly, transitioning into debris flows, avalanches, and turbidity currents, whereas others remain cohesive, undergoing incremental down-slope creep and deformation, with impacts on their tsunamigenic behavior. The Storegga landslide is one of the best-characterized examples (Solheim et al., 2005); borings and *in situ* measurements have been col-lected inside and outside of the landslide body which, along with geophysical surveys and seabed characterization, have served to define

Figure 2. [A] Schematic diagram of a mass transport deposit. [B] Seismic cross-section showing stacked submarine slides/slumps within the Ursa region of the northern Gulf of Mexico. Some of the failures show low-amplitude, discontinuous reflections; others show distinct dipping reflectors suggesting block rotation. [C] Interpreted cross-section identifying key lithologic units and features. Blue Unit is a sand-prone layer. B and C modified from Flemings et al. (2006).

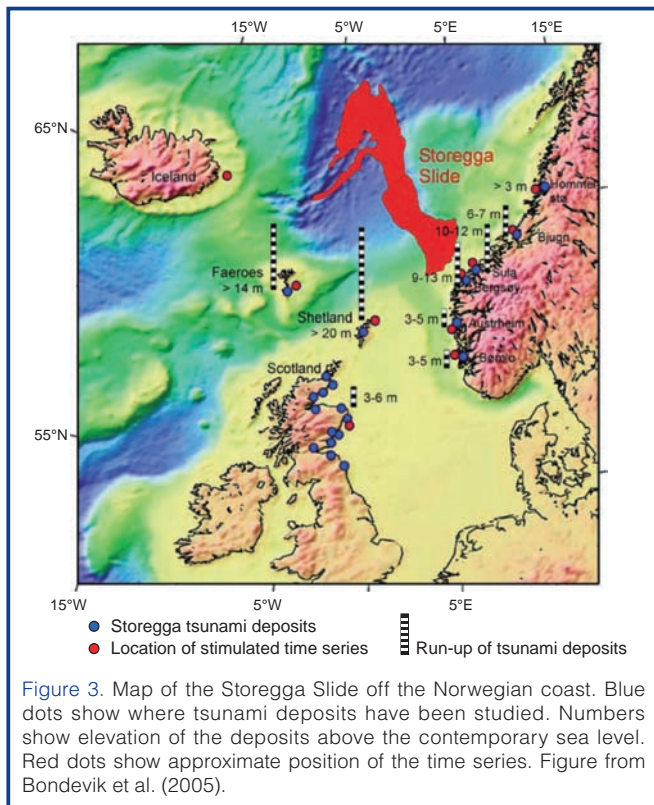Figure 3. Map of the Storegga Slide off the Norwegian coast. Blue dots show where tsunami deposits have been studied. Numbers show elevation of the deposits above the contemporary sea level. Red dots show approximate position of the time series. Figure from Bondevik et al. (2005).

and constrain geotechnical parameters, their lateral variability, and slope failure potential. Similar approaches can be used in other settings to further evaluate specific hypotheses and models (Fig. 4). Some specific questions are outlined below.

Does flow focusing cause lateral pressure variations and failure? Two-dimensional modeling of the New Jersey continental slope suggests that lateral fluid flow in permeable beds under differential overburden stress produces fluid pressures that approach lithostatic stress where overburden is thin (Dugan and Flemings, 2000). This transfer of pressure may drive slope failure at the base of the continental slope, demonstrating that permeability, depositional history, and fluid flow are important controls on slope stability. IODP Expedition 308 (Fig. 2) tested this hydrogeologic model in a
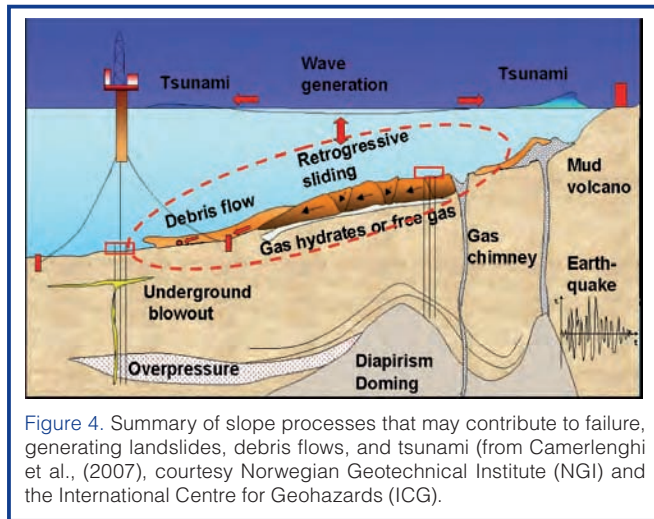

Figure 4. Summary of slope processes that may contribute to failure, generating landslides, debris flows, and tsunami (from Camerlenghi et al., (2007), courtesy Norwegian Geotechnical Institute (NGI) and the International Centre for Geohazards (ICG).

region subject to overpressure and slope failure (Flemings et al., 2006). Similar fluid flow and failure processes might occur due to glacial loading of permeable sediments or in temperate passive margins with high volumes of terrigenous sediment. As the setting for such failures is robust, it is critical that this model be further tested and validated to investigate for which margin architectures and stratigraphic settings it is applicable.

How important are strong ground motions for triggering landslides compared with pre-conditioning or other mechanisms? Earthquakes can increase pore pressure within slope sediments, locally accelerate sediment, or create oversteepened surfaces ultimately driving failure. Although the mechanisms relating earthquakes and slope failure are conceptually understood, drilling is necessary to measure sediment properties to understand how they will respond to strong ground motions. Drilling can provide insights into the most likely modes of failure, the regions most prone to failure, and the potential for slope failure to create a tsunami.

How do methane emissions relate to submarine landslides during rapid climatic changes? Methane emissions from gas hydrate dissociation induced by bottom water warming are thought to occur primarily via submarine slides (Bünz et al., 2005, Mienert et al., 2005). Carbon isotope chemistry, assemblages of benthic calcareous foraminifera, or other (micro)biological indicators living close to paleo-slide heads could be used as a local proxy for massive paleo-methane seeps (Panieri, 2003; Sen Gupta et al., 1997). Such proxies need to be tested by drilling where the history of oceanographic changes is well known and there is a record of submarine slope failure.

Can deep sea megaturbidites and shallower marine deposits be produced by tsunami? Megaturbidites in deep-sea basins have been explained as the result of submarine landslides and particle resuspension due to tsunami-induced bottom shear stress in deep and shallow water (Cita and Aloisi, 2000; Hieke, 2000; Pareschi et al., 2006a). The study of megaturbidites through ocean drilling, especially those deposited in historical times, will permit their correlation with known earthquakes and tsunami and resolve the cause-effect relationships.

Subduction Zones

Subduction zones rank at the top of all classes of plate boundaries in the destructive power of shallow offshore and near-shore earthquakes, explosive eruptions of arc volcanoes, and the tsunami that such events spawn. As seafloor displacements and tsunami generation scale with shallow moment release, shallow interplate earthquakes have the highest capacity to produce damaging regional and ocean-crossing tsunami. Drilling in subduction systems can have multi-hazard payoffs, as the marine sedimentary record also reveals slumps and turbidites caused by large earthquakes
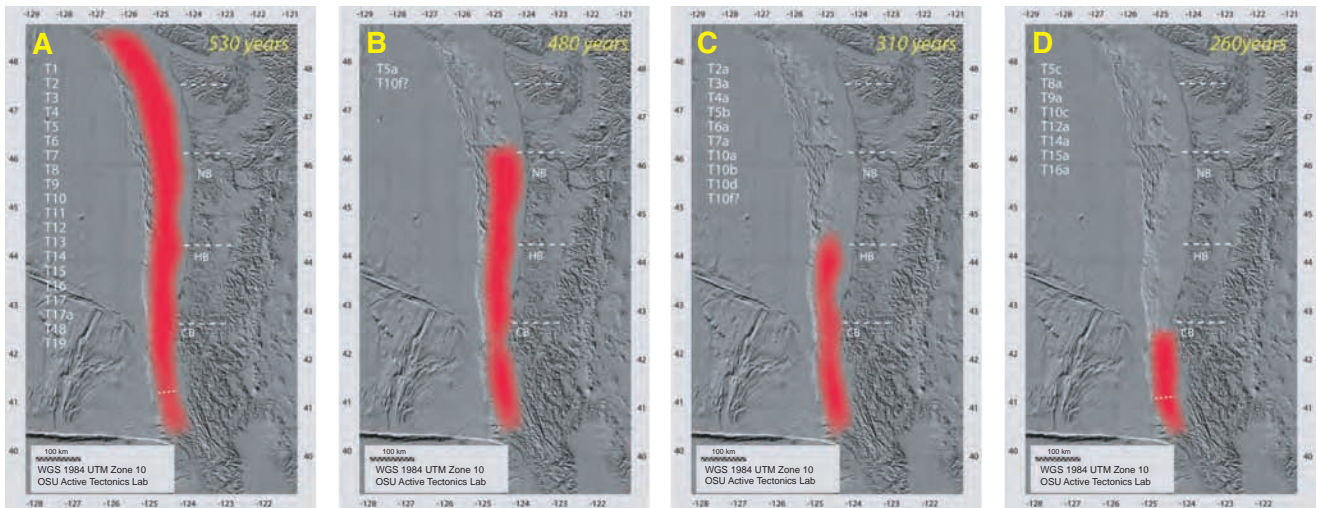
Figure 5. Holocene rupture lengths of Cascadia great earthquakes from marine and onshore paleoseismology. Four panels showing rupture modes inferred from turbidite correlation, supported by onshore radiocarbon data: [A] full rupture, represented at all sites by twenty turbidites; [B] mid-southern rupture, represented by three events; [C] southern rupture from central Oregon southward represented by eight events; [D] southern Oregon/northern California five events. Southern rupture limits vary, as indicated by white dashed lines. Recurrence intervals for each segment are shown, and include all full margin events as well as those exclusive to that segment. Rupture terminations are approximately located at three forearc structural uplifts: Nehalem Bank (NB), Heceta Bank (HB), and Coquille Bank (CB). Paleoseismic segmentation is also compatible with latitudinal boundaries of episodic tremor and slip events (Brudzinski and Allen, 2007), shown by white dashed lines (adapted from Goldfinger et al., 2008).

that may augment tsunami run-ups. Moreover, tephra deposits from explosive eruptions provide a record for dating earthquake-triggered turbidites and reflect eruptive histories of dangerous explosive arc volcanoes that are vital for volcano hazard appraisal.

With the exceptions of subduction zones in Japan (Ando, 1975), and perhaps those in the Mediterranean Sea, the historical record of subduction earthquakes, explosive volcanic eruptions, and tsunami is too short to be truly useful in quantitative earthquake and tsunami hazard assessment. Onshore geological investigations of the Holocene record of coastal uplift and subsidence, shoreline tsunami deposits, liquefaction effects, and terrestrial landslides have extended the historical record for tsunamigenic earthquakes for some subduction systems. A prime example is the Pacific Northwest of the U.S. and southwestern Canada, where paleoseismic investigations confirmed the giant earthquake of 26

January 1700 recorded by its tsunami in Japan (Atwater et al., 2005; Satake et al., 1996), and they also identified other late-Holocene earthquakes (Atwater, 1987). However, the onshore record of such earthquakes is limited by removal of these deposits through coastal and near-coastal erosion. Shallow piston coring of turbidites in submarine canyon levees and trench deposits have identified additional Holocene events (Fig. 5; Goldfinger et al., 2003, 2008), permitting a statistical record of earthquake size and history that has been used for probabilistic earthquake hazard assessment by the U.S. Geological Survey. More complete IODP drilling of deeper turbidite deposits could extend this record into the Pleistocene or earlier.

Characterizing the behavior of subduction zones throughout the seismic cycle is fundamental to understanding seismic hazards and earthquake mechanics. This effort ties in well with ongoing seismogenic zone investigations, and in particular, NanTroSEIZE (Fig. 6), which represents a phased drilling program with an ultimate goal of sampling the seismogenic zone directly (Kinoshita et al., 2008; Tobin and Konishita, 2007). Seismicity, ground deformation, and geochemical and fluid fluxes appear to vary throughout the seismic cycle in response to stress and strain evolution, and they can be monitored through borehole installations (Brown et al., 2005). If earthquake recur-
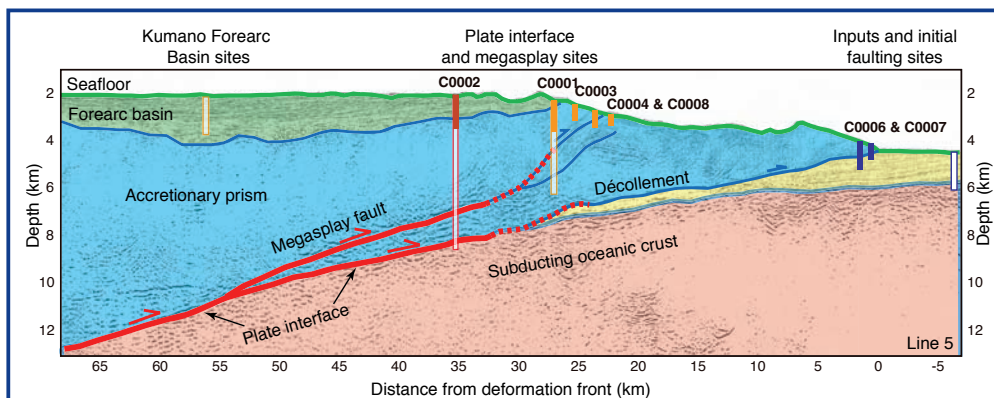

Figure 6. IODP NanTroSEIZE drill sites defining a "distributed observatory" to study the seismogenic zone. Sites drilled during 2007–2008 Stage 1A are shown in solid colors, and are preparatory to much deeper planned drilling that will sample the splay faults and plate boundary seismogenic zone. Modified from Kinoshita et al. (2008); seismic data from Park et al. (2002).

rence intervals are long, it is unreasonable to monitor the entire seismic cycle in one location. However, observations along comparable margins at different points within their seismic cycles could be integrated to reconstruct processes active throughout a generic seismic cycle, and extrapolated to predict the behavior of specific margins. Comparative studies (Kanamori, 1972) along margins like the Nicaragua margin that produce tsunami earthquakes—and even those margins that do not—can test whether precursory behaviors differ in these settings and are indicative of their tsunamigenic behavior.

Four key questions associated with subduction zone geohazards that can be addressed by ocean drilling relate to characterizing and quantifying earthquake magnitude, frequency, and tsunamigenic potential.

What is the long-term record of the size, distribution, and frequency of plate-boundary earthquakes in a subduction zone? Dating turbidite deposits obtained by drilling can provide information about the chronology of triggering earthquakes, as well as information about event sizes and distributions. Thus, drilling can provide a much longer record than historical and instrumental data have to date. Potentially, such records contain fundamental information about seismicity rate, maximum event magnitude, and primary parameters needed to assess the probabilistic earthquake hazard in a given subduction zone. Moreover, seismic moment release tends to be heterogeneous, and in some well-characterized systems such as northeast Japan, earthquake slip recurs on consistent segments of the subduction boundary over decades to centuries. As the underlying physics behind locations and sizes of such "asperities" is not known, quantitative probabilistic earthquake hazard analysis is more appropriately based on resolving the spatial and temporal record of subduction events, a task that requires ocean drilling.

What factors control the global variability in seismicity rate and maximum earthquake magnitudes? The existence and rate of backarc spreading, the thickness of the incoming sediment layer, plate convergence rate, dip of the subducting plate, width of the seismogenic zone, interplate stresses, and the ability of rupture zones to coalesce, all need to be evaluated carefully. Within the seismogenic zone, it is critical to understand the physical, chemical, and hydrogeological properties, as well as thickness and geometry of the slip zone. These goals are among the key objectives of the current IODP NanTroSEIZE drilling program (Kinoshita et al., 2008).

How are plate boundary motions partitioned among interplate thrust faults and splay faults, and how does this partitioning affect the tsunamigenic potential? Seismic reflection profiles reveal splay faults that diverge from the basal thrust, with considerable cumulative seafloor displacement (Fig. 6). Seismic imaging over the Nankai Margin in the NanTroSEIZE

drilling area shows evidence for recent slumping and active splay faulting across older more seaward faults (Moore et al., 2007), suggesting co-seismic slip may propagate from the décollement zone all the way to the seafloor. Similar geometries are observed along other subduction margins, and they may contribute to the generation of devastating tsunami during major earthquakes. Possible evidence for active slip on such a splay fault during the 26 December 2004 Sumatra earthquake comes from tsunami arrivals on the coastline earlier than expected for a fault source on the main interplate thrust (Plafker et al., 2006), one of several hypotheses currently being tested (Fig. 7) by new surveys over the Sumatra margin (Henstock et al., 2006; Mosher et al., 2008; Plafker et al., 2006).
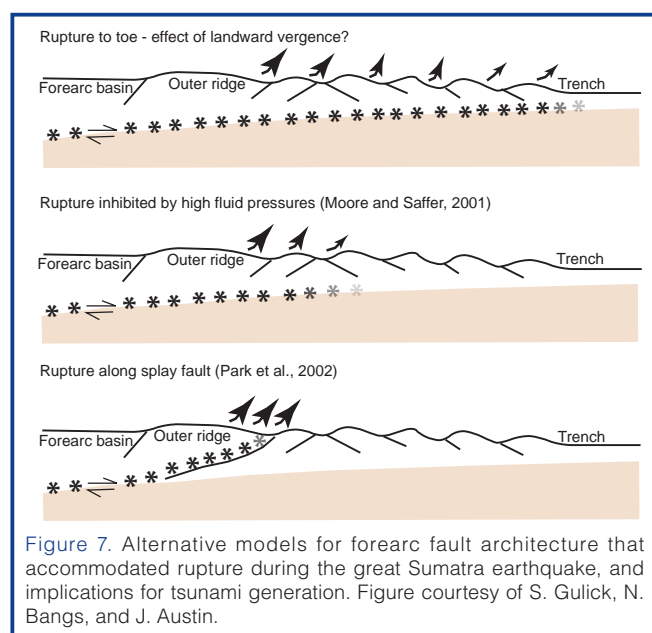
Figure 7. Alternative models for forearc fault architecture that accommodated rupture during the great Sumatra earthquake, and implications for tsunami generation. Figure courtesy of S. Gulick, N. Bangs, and J. Austin.

What physical processes control the onset of slow (tsunami) earthquakes? Some earthquakes launch destructive tsunami far in excess of their moment magnitudes. Such tsunami earthquakes (Kanamori, 1972) include the devastating 1896 Sanriku-oki earthquake in northeastern Japan, the M_w 8.5 earthquake of 1946 off Unimak Island in Alaska, and the northern rupture zone of the 2004 Sumatra earthquake (Stein and Okal, 2005). The sources for earthquake and tsunami may lie beneath the outer prism at very shallow depths. Further studies must also be carried out to test the hypothesis that sediments might play a role in slow earthquake ruptures (Kanamori, 1972), as some documented examples occur in sediment-starved settings such as Nicaragua (McIntosh et al., 2007). Drilling strategies will require exploring the structure and properties of the most frontal portions of the prisms, with comparisons to subduction systems that do not to produce slow earthquakes.

Volcanic Processes

Many oceanic and coastal volcanoes (e.g., in Hawaii, the Canary Islands, and Alaska) show evidence of large-scale flank collapse (Coombs et al., 2007; Masson et al., 2002;

Moore et al., 1989, 1994; Urgeles et al., 1999) and occasionally abortive slope failure (Day et al., 1997). Enormous debris fields composed of volcanic blocks and far-flung turbidite deposits occur most prominently around the Hawaiian oceanic island volcanoes (Fig. 8A). Modeled tsunami for such intraoceanic landslide sources produce enormous wave heights that can devastate coastlines around the entire ocean basin (Satake et al., 2002). They may also deposit marine coral deposits high on the nearby volcano flanks (McMurtry et al., 2004). Large-scale slope failure also may be accompanied by explosive volcanic eruptions that release large quantities of ash and vapor into the atmosphere, with short- and long-term detrimental effects on climate and society. Immediate hazards include airborne lateral blasts, column-collapse pyroclastic flows, ashfall, respiratory hazards, terrestrial dome-collapse pyroclastic flows, debris flows, and lahars (Herd et al., 2005; Saito et al., 2001). Explosive submarine eruptions pose unknown risks to nearby communities, as they can generate tsunami with shallow eruptions, but also release density currents and ash plumes (Belousev et al., 2000; Fiske et al., 1998; White et al., 2003). The far-flung materials generated by explosive eruptions are often the unique keys to recognizing and dating such events, providing important constraints on source, magnitude, and frequency (Fig. 8B).

Scars in the subaerial and submarine slopes of silicic volcanoes—such as Mt. Etna in Sicily, Kiska, Tanaga, and Augustine in Alaska, and Montserrat in the West Indies—and interpreted debris deposits attest to past slope failures (Coombs et al., 2007; Le Friant et al., 2004; Pareschi et al., 2006b). Although smaller in scale than Hawaiian landslides, such events can cause tsunami that will impact nearby shorelines with little warning. A tsunami from Mt. Etna would strike eastern Mediterranean coasts very quickly (Fig. 9; Pareschi et al., 2007). The explosive eruption of Krakatau volcano, Indonesia in 1883 produced a far-flung tsunami and caused untold damage. Smaller volcanic failures at island arc volcanoes, such as at Oshima-Oshima Island in the Japan Sea (1741) and Ritter Island in the Bismarck volcanic arc of New Guinea (1888), are more frequent and invariably produce regionally destructive tsunami (Day et al., 2005).

In some settings, the flanks of active volcanoes also exhibit slow outward flank displacements. This is best documented in Hawaii, where the south flank of Kilauea volcano is moving seaward at rates up to 10 cm y^{-1} (Denlinger and Okubo, 1995; Owen et al., 2000). Such volcanic spreading is primarily gravitationally driven but is also influenced by magmatic pressures and/or hot cumulates at depth that push the flank outward (Clague and Denlinger, 1994; Swanson et al., 1976). Slip is modeled to occur along a décollement that lies near the base of the volcanic edifice (Fig. 10), a geometry analogous to subduction, with a frontal accretionary prism of volcanic-lastic strata (Morgan and Clague, 2003; Morgan et al., 2000, 2003). Seaward slip is punctuated by large earthquakes (up to M 8) that may trigger coseismic slumping (Lipman et al., 1985; Ma et al., 1999). "Silent" slip events also have been recognized, with apparently periodic recurrence and offshore slip surfaces (Brooks et al., 2006; Cervelli et al., 2002). The first geodetic study over Kilauea's submarine south flank now confirms offshore fault slip, which produces vertical flank displacements up to 5 cm y^{-1} (Fig. 10; Phillips et al., 2008). However, the temporal and mechanical relationships among slow slip, seismic slip, and large scale flank failure in Hawaii are still very poorly known.

In general, the direct causes of volcano flank motions and failures are not well understood. Below are four key questions associated with volcanic geohazards that can be addressed by ocean drilling and relate to understanding the nature and controls on flank mobility and stability, and the triggering mechanisms.

What conditions and/or triggers lead to large-scale flank collapse in volcanic settings? Potential causes for volcano flank deformation and collapse include the presence of weak or

Figure 8. [A] Landslides and slumps around Hawaii (mapped by Moore et al., 1989 and more recent work from Tom Sisson). Red outlines debris avalanche fields; blue outlines slumps; islands are in gray. Location of seismic line and ODP Site 1223 indicated in white. Bathymetry from Eakins et al. (2004). [B] Portion of reflection profile across ODP drill site, showing multiple reflective turbidite horizons. [C] Representative drill core from ODP Site 1223, showing volcaniclastic sandstone/tuff unit overlying bioturbated claystone, with intervening erosional boundary. Figures B and C modified from Shipboard Scientific Party (2003).

overpressured lithologies, thermal pres-surization of groundwater or gas, and unique volcano-tectonic forcing (Elsworth and Day, 1999; Elsworth and Voight, 1995; Iverson, 1995; Reid, 2004; **Voight and Elsworth, 1997**). Accelerations induced by earthquakes or explosive eruptions may serve as triggers. The types and scales of slope failures and their tsunamigenic potential depend on these para-meters, the structure and stratigraphy of the edifice, and the rheology of the failed material. Thus, addressing this question requires direct sampling and measurement of the flanks to constrain subsurface stress, pore pressure, temperature, fluid chemistry, and composition, as well as their spatial and temporal variability. Additionally, core records may resolve linkages between eruptive and flank failures and provide information about emplacement mechanisms and rheology.

What are the frequencies, magnitudes, and distributions of large volcanic landslides? As the historic record of volcanic collapses is short, statistical data must be acquired through high resolution sampling of distal landslide deposits (e.g., turbidites, Fig. 8C) to constrain event frequency and size and to correlate these deposits regionally and globally (Shipboard Scientific Party, 2003). Ash stratigraphy offers great promise, especially where on-land ash units have been fingerprinted and dated and can be correlated with offshore deposits.

What causes/enables rapid volcano flank motion, and what are the hazard implications? The deep-seated causes for flank spreading, as observed in Hawaii, will be difficult to constrain through ocean drilling alone. However, drilling offers the only means to test interpretations for flank structure that controls deformation, and to constrain the properties of the materials involved. Additionally, offshore geodetic and seismic monitoring are crucial for understanding modes of flank deformation and identifying precursory phenomena in different settings. Such efforts are now in their nascent stages (Phillips et al., 2008).
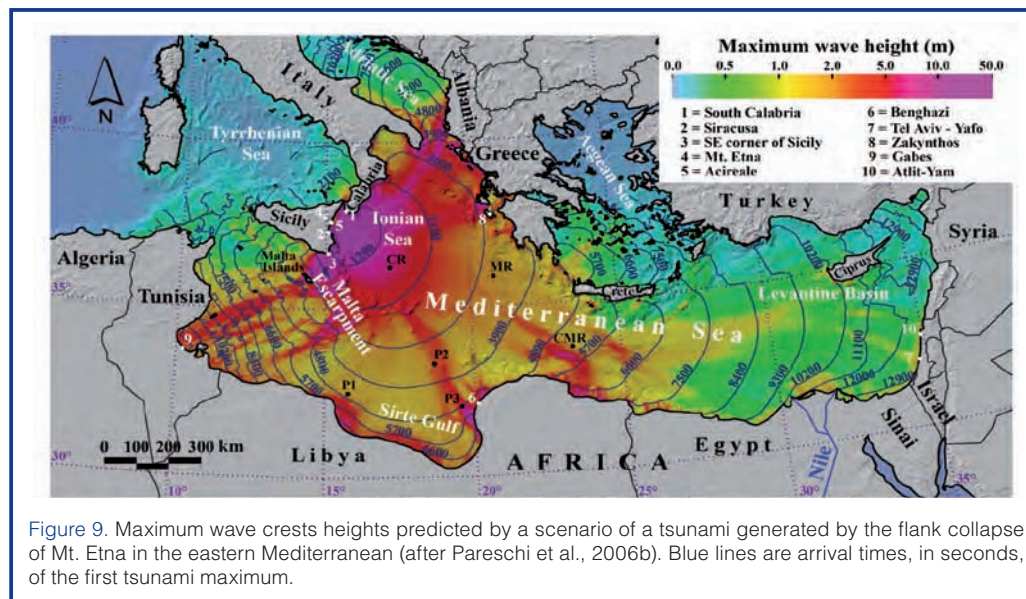

Figure 9. Maximum wave crests heights predicted by a scenario of a tsunami generated by the flank collapse of Mt. Etna in the eastern Mediterranean (after Pareschi et al., 2006b). Blue lines are arrival times, in seconds, of the first tsunami maximum.

What is the interplay between volcano growth and collapse? Landsliding and flank collapse occur throughout their evolution. Recent seismic and stratigraphic evidence suggest that flank failures are commonly buried by subsequent volcanic materials (Morgan et al., 2003). Thus, to better understand the growth and evolution of oceanic volcanoes, ocean drilling must be combined with geophysical surveys to constrain internal structure, composition and stratigraphy. In this way, we can begin to reconstruct volcanic history, estimate the volumes of past and incipient failures, and improve models of collapse effects (**e.g., tsunami,** landslide run-outs, etc.).

Other Active Tectonic Settings

Marine crustal earthquakes occur in a range of non-subduction and non-volcanic settings, including rifted margins, transform margins, and the occasional intra-plate or passive margin setting. These events tend to be relatively small, but can reach magnitudes of 6–8. Often, the sources and precise mechanisms of these earthquakes are unclear. Although earthquake damage may be local, the hazards can be great, as they are unexpected and commonly amplified by secondary events (e.g., tsunami, landslides, coastal collapse).
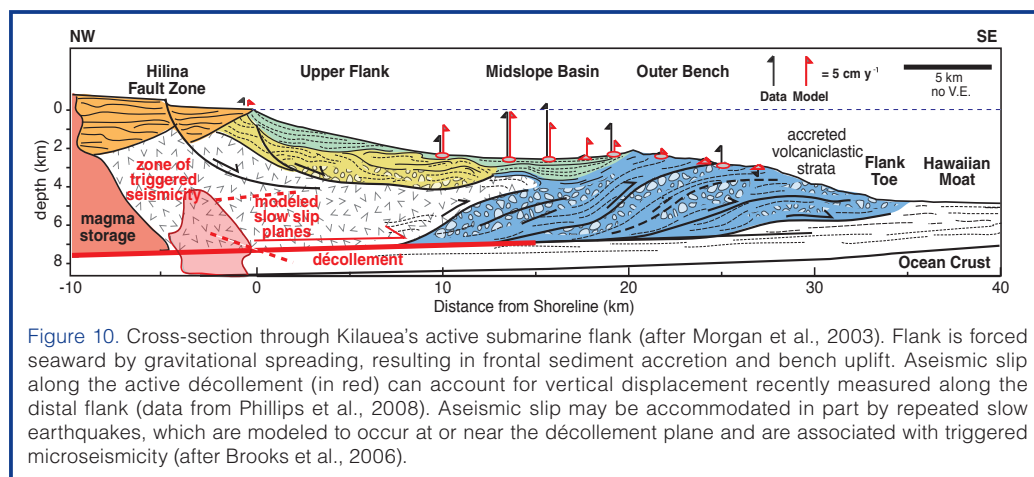
Figure 10. Cross-section through Kilauea's active submarine flank (after Morgan et al., 2003). Flank is forced seaward by gravitational spreading, resulting in frontal sediment accretion and bench uplift. Aseismic slip along the active décollement (in red) can account for vertical displacement recently measured along the distal flank (data from Phillips et al., 2008). Aseismic slip may be accommodated in part by repeated slow earthquakes, which are modeled to occur at or near the décollement plane and are associated with triggered microseismicity (after Brooks et al., 2006).
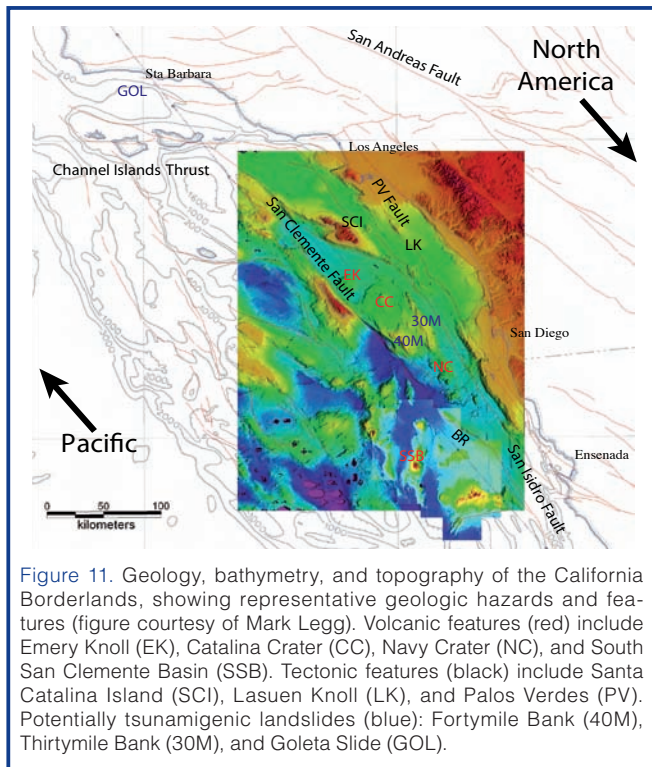
Figure 11. Geology, bathymetry, and topography of the California Borderlands, showing representative geologic hazards and features (figure courtesy of Mark Legg). Volcanic features (red) include Emery Knoll (EK), Catalina Crater (CC), Navy Crater (NC), and South San Clemente Basin (SSB). Tectonic features (black) include Santa Catalina Island (SCI), Lasuen Knoll (LK), and Palos Verdes (PV). Potentially tsunamigenic landslides (blue): Fortymile Bank (40M), Thirtymile Bank (30M), and Goleta Slide (GOL).

In addition, these sources have produced some of the most destructive historic geohazard events in terms of casualties and effects on populated coastal communities. Examples include the 1755 Lisbon earthquake (M >~8) and tsunami that resulted in 40,000–60,000 casualties (Gracia et al., 2003); the 1908 Messina Strait earthquake (M ~7–7.5) and tsunami causing 60,000 or more casualties (Amoruso et al., 2004; Billi et al., 2008); and the 373 BCE earthquake and tsunami, which completely destroyed the classical city of Helike on the southwestern shore of the Gulf of Corinth (Liritzis et al., 2001).

Young oceanic rift environments (e.g., the Gulf of Corinth) can produce up to M ~6–7 earthquakes that can trigger submarine landslides and tsunamis, as well as liquefaction and coastal failure. These processes are enabled by high sedimentation rates and steep fan delta slopes and faulted margins (Bell et al., 2008; McNeill et al., 2005). However, the high sedimentation rates provide a unique opportunity for drilling to unravel the tectonic and hazard history and to link it to the historic record. Oceanic transform margins, such as the California Borderlands (Fig. 11; Legg et al., 2007) and the North Anatolian Fault crossing the Sea of Marmara, are also subject to intermittent earthquakes, commonly with complex mechanisms. Irregular seafloor and oversteepened slopes can create additional risks, as earthquakes can trigger submarine landslides and tsunami that impact nearby populated regions (e.g., southern California or western Turkey; Borrero et al., 2004; McHugh et al., 2006).

The knowledge of geohazards in these settings is very incomplete. The following are two key questions that can be addressed by ocean drilling.

What are the potential earthquake and related hazards in active non-subduction settings? Ocean drilling offers the opportunity to constrain the types of hazards that exist in non-subduction settings, by testing structural and stratigraphic interpretations for the margins, including the frequency, timing, and rates of fault slip. For example, are there linkages between earthquakes and triggered mass flows or slope failures and tsunami? Additionally, drilling these settings will contribute to other fundamental issues about active rift and transform structure and processes, sedimentation, and linkages to climatic events and paleoceanography.

Can the history of past earthquakes be extracted from the sedimentary record? High sedimentation rates in some settings preserve high-resolution records of local earthquake-generated turbidite-homogenite units. These event deposits may have recognizable characteristics distinct from other sedimentary units. Careful dating of seismoturbidites can provide event ages and recurrence intervals. Such a record of seismoturbidites has been extracted from the Sea of Marmara for the last 16 ka, validating the approach and revealing unrecorded events that must be accounted for in probabilistic earthquake risk assessment (McHugh et al., 2006; Sari and Cagatay, 2006). Similar records may be reconstructed in other settings for which the historic record is limited, but earthquakes and associated hazard risks are high.

Bolide Impacts

Major bolide impacts, while infrequent, rank as potentially the most devastating of all geohazards, with the capability of wiping out civilization as we know it (Chapman, 2004; Chapman and Morrison, 1994; Collins et al., 2005). Representative examples include Meteor Crater in Arizona and Chicxulub Impact Crater in Mexico (Fig. 12), which approximately define the known size extremes on Earth (<100 m to >300 km in diameter). Currently about 175 impact craters are recognized on Earth, of which about one-third are no longer visible at the Earth's surface due to erosion or post-impact burial. Local effects of impact include ejecta deposition, airblasts, thermal radiation, seismic shaking, and tsunami. Global effects include thermal infra-red pulses, dust in the atmosphere, climatically active gases, acid trauma, and biological turn-over (Gulick et al., 2008; Ivanov et al., 1996; Koeberl and MacCleod, 2002; Pierazzo et al., 1998; Robertson et al., 2004; Toon et al., 1997). Tsunami are the most immediate hazard, with large regional effects. For example, a 400-m asteroid hitting the Atlantic could produce basin-wide run-ups of >60 m (Ward and Asphaug, 2000), although actual run-ups may be lessened by shallow continental shelves (Hofman et al., 2007; Korycansky and Lynett, 2005; Weiss and Wünneman, 2007).

The best-known impact crater is Chicxulub, which struck the Yucatan penisula ~65 Ma (Alvarez et al., 1980; Gulick et

al., 2008; Hildebrand et al., 1991; Morgan et al., 1997). Of an estimated impact energy of 2 x 10^{23} J (~100 million atomic bombs), only one percent was converted to tsunami and hurricane force winds (Pope et al., 1997). The remainder caused melting, vaporization, and ejecta. Deep-sea cores reveal evidence for large impacts in the form of tektites, ash, and dust (MacLeod et al., 2007; Norris et al., 1999), indicating the extraordinary reach of impact ejecta. Drilling through these well-preserved deposits in the ocean basins can yield valuable constraints on the energies and chemical signatures associated with such impacts and the associated hazards (Gohn et al., 2008; Morgan et al., 2005; Pope et al., 1997). One can also recognize sharp contrasts in biota before and after an event, indicating dramatic changes in environment induced by long-term climatic changes (Gulick et al., 2008; MacLeod et al., 2007; Pope et al., 1997).

What are the frequency, spatial distribution, and magnitude of impact events, and what effects did they have on global environment and biota? What are the impact process and resulting structure, and how can these be used to calibrate models? The Earth has a 40% chance per 100 years of getting hit by a Meteor Crater-sized bolide, and to our knowledge has been struck with at least three Chicxulub-sized bolides in the last two billion years, and with innumerable smaller ones, many of which are no longer recognizable (Grieve, 1998). Given the rarity of impacts, however, drilling offers the only direct means to investigate the internal structure and associated deposits generated by such an event. Drilling ejecta both nearby and far from known impact sites will help to understand the effects of impacts of varying size. Additionally, drilling is necessary to document changes in biological diversity, both locally and globally. Finally,

drilling-obtained constraints on impact structure and distribution of deposits can be used to calibrate models, which are used to understand the impact process and the associated hazards.

Overarching Scientific Questions That Can Be Addressed by Ocean Drilling

The topical review provided by the IODP Geohazards Workshop revealed a number of common themes and problems for which ocean drilling is ideally suited. Prominent among these are to construct detailed stratigraphic records that will help to establish links between event distribution and recurrence, source, and intensity of hazardous events and associated risks. Another theme is to characterize *in situ* properties and processes that govern unstable seafloor motions.

What are the frequencies, magnitudes, and distributions of geohazard events? The assessment of natural hazards and related risks requires information about event sizes, distributions, and recurrence intervals. These data can only be obtained through distributed drilling integrated with high-resolution stratigraphy and geochronology. The potential of this approach has been shown through stratigraphic studies of the Madeira Abyssal Plain (Fig. 13; Weaver, 2003). To date, only a few large-scale events (e.g., Storegga slide) have been dated with sufficient accuracy. Many medium- and small-sized submarine slides have been imaged in detail, but accurate dating is still lacking. Dating of turbidites offshore of the Cascadia margin has provided a compelling record of repeating earthquakes throughout the Holocene (Goldfinger et al., 2003, 2008), however similar data are lacking for the deeper record and for most other subduction zones. Turbidites of volcanic origin and ash deposits can also provide a record of recurring landslides and explosive eruptions, but these deposits are incompletely characterized. The study of known impact deposits is necessary to develop a clearer set of guidelines for distinguishing proximal and distal impact deposits in the stratigraphic record. A more complete inventory of impact events in the geologic record will ultimately allow an assessment of recurrence intervals.

Figure 12. Seismic profile across Chicxulub, Mexico impact crater showing proposed drilling transect combining ocean and continental drilling. Drilling objectives include 1) earliest Tertiary sediments to document the resurgence of life, 2) impact-induced megabreccia and potential exotic organisms, 3) impact morphometric features, such as a peak ring, to constrain their origins, and 4) lithology of the melt sheet to differentiate among impact models (modified after Morgan et al., 2007). Inset shows gravity data over Chicxulub, revealing distinct crater structure and proposed IODP/ICDP drill sites (gravity image courtesy of Pilkington and A.R. Hildebrand).

Can the tsunamigenic potential of past and future events be assessed? The tsunamigenic potential of seafloor deformation is a function of a number of
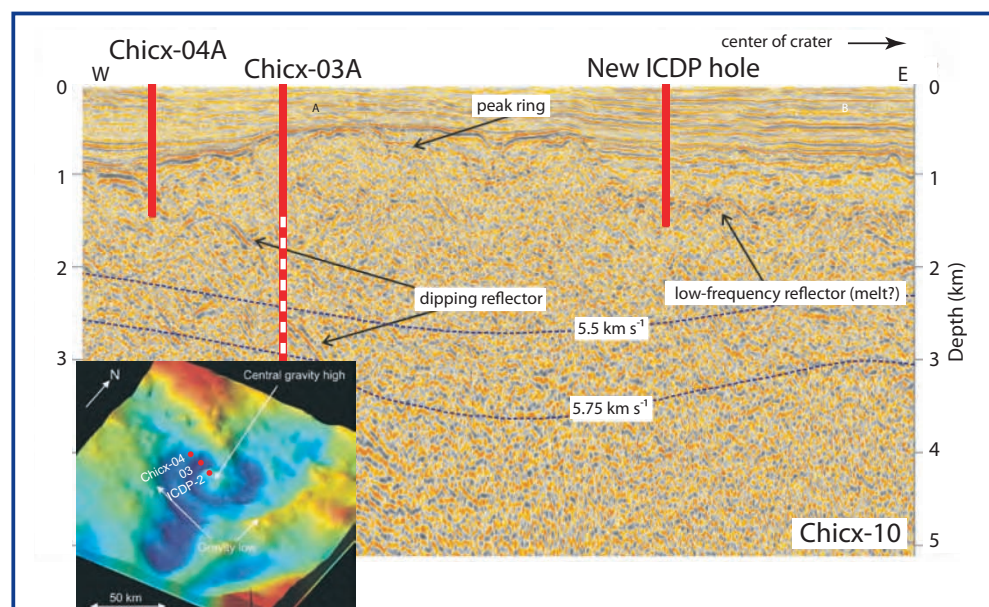
different parameters. The most critical ones relate to the pre-failure, failure, **and early post-failure behavior of the** deforming mass, as these influence the magnitudes, rates, and areas of seafloor displacement. Additionally, the geometry of subsurface structures and source mechanisms will control the deformation. Constraining the geomechanical properties and associated flow laws requires drilling and coring, *in situ* geotechnical measurements, and dedicated laboratory analyses. Extrapolating these results across broad regions requires 3D characterization of the deposits and underlying structure, as well as identification of past failure zones. Finally, the tsunamigenic potential will need to be evaluated through modeling, constrained by detailed observations.

Do precursory phenomena exist, and can they be recognized? In order to improve our predictive capability we need to determine which transient signals might indicate imminent seafloor deformation (Fig. 14). Transient physical parameters deemed to be important include pore pressure, pore fluid chemistry, temperature, **and seafloor deformation.** Microseismicity could indicate incipient failure or concurrent "silent" slip. *In situ* monitoring will be critical for recognizing and correlating precursory phenomena; it **should include seismometers, submarine geodetic obser-** vatories, pressure sensors, and flow meters installed at critical intervals. Increased strain rates, enhanced fluid flow, and geochemical transients may be inverted to resolve the deformation source and mechanism (Brown et al., 2005). And finally, *in situ* data can be integrated through predictive modeling to better understand their linkages to hazards.

What are the physical and mechanical properties of materials prone to failure? Subduction megathrusts, submarine landslides, and volcanic detachments are often localized at distinct stratigraphic levels, which must define "weak" horizons prone to failure. The physical and mechanical properties of these units strongly influence the mode of failure; their depths and distributions control the failure volume. Passive margins in glaciated settings tend to develop a compositional layering that may localize slip. In other settings, rapid sedimentation, differential burial and diagenesis, and overpressures can create weak layers. Recognition of critical horizons and conditions that may promote localized failure requires drilling and geotechnical characterization (Fig. 14), as well as laboratory studies of slip behavior and evolving rheology under specific loading conditions (e.g., **earthquake shaking, pore pressurization,** etc.).

What are the roles of preconditioning vs. triggering in rapid seafloor deformation? Preconditioning includes changes in physical properties and mechanical differences that occur between quasi-stable submarine slopes prior to failure. Examples include the development of weak materials, elevation of pore pressures, gas hydrate formation, structural geometry, fault development, and volcanism. Triggering mechanisms initiate the failure and may include seismic events, migration and pressurization of pore fluids, destabilization of gas hydrates, volcanic activity, and storms. Both sets of properties and processes must play a role in the onset of seafloor deformation, but their relative importance will vary from place to place. Knowledge of the range of material properties and potential triggering mechanisms in each geologic setting will be critical to assessing associated
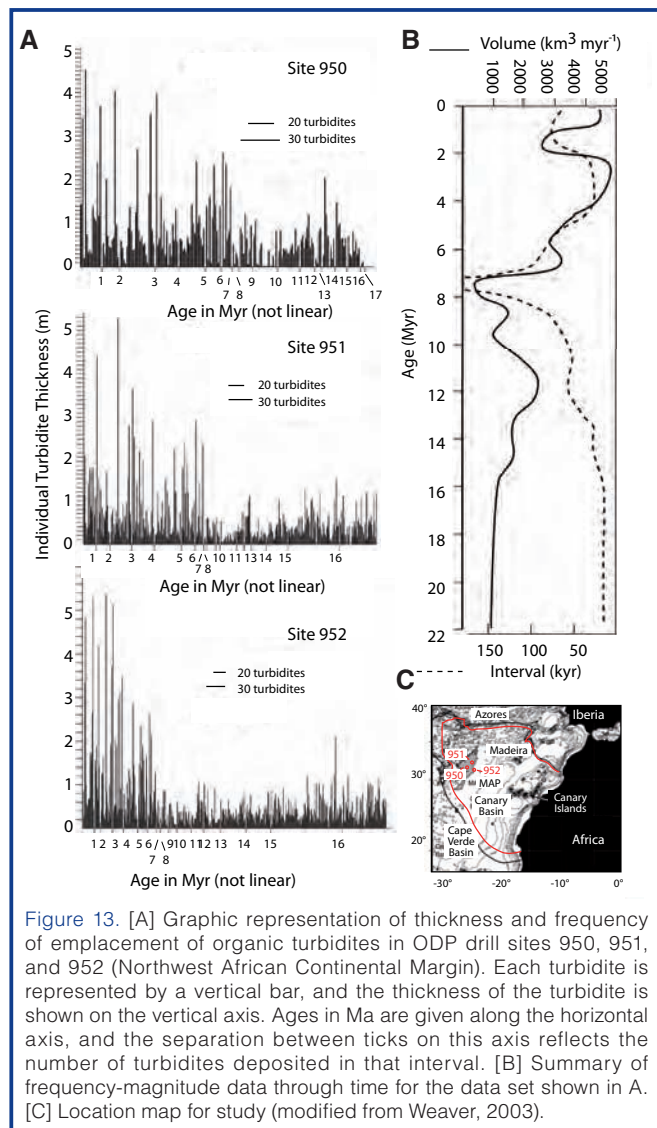

Figure 13. [A] Graphic representation of thickness and frequency of emplacement of organic turbidites in ODP drill sites 950, 951, and 952 (Northwest African Continental Margin). Each turbidite is represented by a vertical bar, and the thickness of the turbidite is shown on the vertical axis. Ages in Ma are given along the horizontal axis, and the separation between ticks on this axis reflects the number of turbidites deposited in that interval. [B] Summary of frequency-magnitude data through time for the data set shown in A. [C] Location map for study (modified from Weaver, 2003).
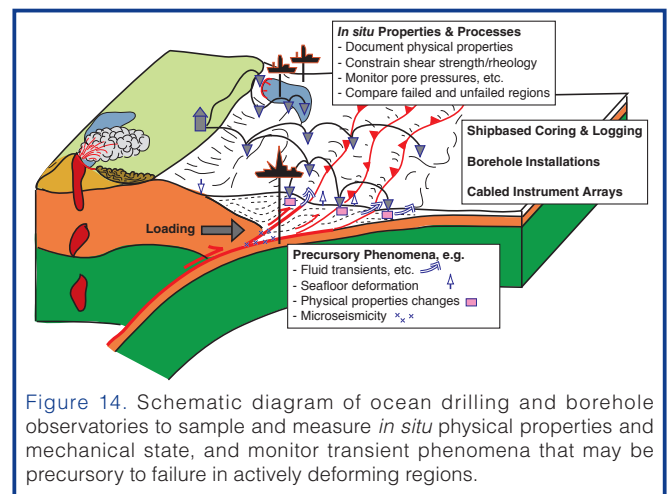

Figure 14. Schematic diagram of ocean drilling and borehole observatories to sample and measure *in situ* physical properties and mechanical state, and monitor transient phenomena that may be precursory to failure in actively deforming regions.

geohazards. Ocean drilling and observatory installations can measure critical physical properties and record transient phenomena that might distinguish between these two contributions in a range of settings.

Technological Opportunities and Requirements for Geohazards Studies

Site Surveys: Standard site surveys for geohazard objectives can provide two types of information:

(1) Definition of the geophysical, stratigraphic, and structural framework of the area capable of generating the geohazard. Swath bathymetry and acoustic backscatter imagery are necessary to identify morphological features, associated surficial deposits, or subsurface structure (i.e., for placement of boreholes or observatories). Seismic reflection profiling, particularly in 3D, serves to constrain the internal structural and stratigraphic architecture of the region with which to interpret past events and their temporal and spatial distribution.

(2) Pinpointing the exact locations for future drilling and assessing what knowledge would be gained at each site. Information can be gleaned from high-resolution seafloor acoustic images coupled with 3D seismic reflection images to identify reflections and impedance contrasts that might indicate target horizons, fault traces, or fluid pathways. Submersible dives can provide detailed information at the proposed point of entry, including local fluid or heat flow data.

Drilling and Coring: IODP operations provide some standard tools and capabilities, which can be utilized for geohazards studies. In some cases, integrated shoreline-crossing structures, such as Chicxulub crater, can also benefit from joint IODP–ICDP efforts.

Logging-while-drilling (LWD) tools are available for typical IODP drilling conditions. These routinely include gamma ray, resistivity, neutron density, porosity, and pressure-while-drilling. Although the costs and technologic requirements for LWD are high compared to wireline logging, this approach offers two key advantages in unstable materials consistent with geohazards. (1) Rapid sampling allows for evaluation of more pristine sedimentary intervals and assures data collection regardless of borehole stability. (2) The availability of real-time logs permits rapid assessment of lithologic environments and conditions.

In situ geotechnical tools are used routinely in the geotechnical community and should become an integral part of IODP geohazards investigations. These tools can make discrete measurements from the seafloor to tens of meters depth or deeper depending on the strength of the sediment. Penetration probes (e.g., Davis-Villinger Temperature Pressure Probe (DVTPP) and Temperature-Two-Pressure

(T2P)) can be used to evaluate *in situ* fluid pressure and sediment properties such as hydraulic conductivity and coefficient of consolidation. Moreover, implementation of existing tests, such as cone penetration tests (CPT), will greatly improve the quality of data near the seafloor, where wireline and LWD tools do not provide robust data. CPTs collect information on lithology, frictional and cohesive strength, and *in situ* pressure. Additional modules can be incorporated in CPTs to constrain formation resistivity, natural gamma radiation, and formation velocity. Incorporating these types of measurements into IODP operations would increase the quality of petrophysical data of near-surface sections prone to failure.

Development and application of certain *in situ* tools could greatly expand understanding of *in situ* pressures and stress. Pore pressure can be measured with downhole tools (DVTPP, T2P) or with instrumented boreholes such as Circulation Obviation Retrofit Kits (CORKs). Vertical stress can be evaluated from density data. Horizontal stress has not been measured within DSDP/ODP/IODP, but should be pursued to obtain more reliable estimates of failure potential. *In situ* strength should be measured and can be evaluated with fracture tests. Large-scale hydrologic tests can also help to up-scale the core measurements. These tests include injection tests, slug tests, and cross-borehole tracer studies.

Heterogeneous deposits may require new drilling technologies or the use of multiple coring devices, in particular to recover loose or chaotic materials. Recent advances in core catcher technology are compatible with the typical IODP drilling hardware and could be readily adapted. Overpressured settings common to unstable sediments have been successfully drilled by IODP (e.g., Expedition 308) and are routinely drilled by industry. In near-surface settings, overpressure can be monitored and evaluated through measurement-while-drilling (MWD) and/or LWD operations to assess risk prior to coring operations. When exploring deeper, overpressured targets, riser drilling with the *DV Chikyu* can provide the borehole control to prevent borehole collapse or blowout.

Complete characterization of the geotechnical properties (strength, permeability, compressibility, rheology) of slide-prone layers and bounding strata requires combined logging, coring, and shore-based studies. Reliable geotechnical data can be integrated with geophysical data to extrapolate the interpretations from the borehole to a local or regional scale. All coring activities will also require long-term onshore testing to define the requisite material properties. As the laboratory studies are integral to the overall scientific objectives, reliable means to support the shore-based laboratory component should be included in the planning.

Borehole Observatories and Cabled Arrays: Technological advances in borehole observatories and offshore cabled

arrays allow critical real-time data acquisition. Sub-seafloor failure may be preceded by precursory surface deformation or microseismicity, which must be monitored locally (Fig. 14). Cabled ocean bottom seismometer (OBS) arrays lasting from weeks to months can be coupled with long-term seafloor geodetic observatories or transponder-based acoustic GPS, seafloor pressure sensors, and flow meters to detect transient signals. Local physical property changes may also indicate internal deformation and can be monitored through changes in pressure or acoustic travel time (Fig. 14). Such real-time *in situ* data sets provide necessary constraints on the depths, rates, and modes of sub-seafloor deformation, for predictive purposes and for drilling future boreholes.

Real-time monitoring is particularly valuable during the late stages of the failure process, if that can be determined. During this period, properties are rapidly changing, offering the unique opportunity to capture the failure event including pre-, syn-, and post-event transients. The logic of this approach is quite obvious in subduction zones, which is understood in the context of the seismic cycle, but the same approach is transferable to other settings in which unstable failure processes are anticipated (for example, gravitationally driven landslides on continental margins or volcanic edifices). In each environment, a combination of surface and subsurface sensors and monitoring strategies are required to provide sufficient constraints on long-term build-up of strain (preconditioning) and transient events that might signal the onset of instability and hazardous conditions (triggers). In all cases, multiple co-located data sets must be collected to obtain necessary information about the underlying physics of the system, as well as to constrain complex numerical models to address the underlying driving processes. In fact, such modeling is ideally carried out prior to observatory emplacement to ensure that the observations are well located and of sufficient accuracy to address the critical scientific questions being posed.

Ocean drilling also offers the exciting potential to develop offshore tsunami warning facilities. Presently, warnings of earthquake-generated tsunami are issued by authorities based on seismic data monitored by regional or global seismic networks. The verification of tsunami warnings is made by monitoring tsunami heights along the coast with tide gauges. However, the lack of accurate knowledge of seafloor motions can lead to over- or under-estimations of wave height. Moreover, in many cases coastal detections of tsunami heights occur too late to issue warnings. If direct seafloor motions can be detected through monitoring of seafloor pressures, these data may be transmitted to shore more quickly than teleseismic data, which can be critical for local tsunami targets. Such data also offer the potential for predicting tsunami direction and magnitude well before coastal impact. Making information available in real time will require buoy telemetry or cabled networks, both expensive technologies. However, the costs of such installations must be balanced against the risks and consequences of not having on-site monitoring.

Concluding Remarks

The productive discussions during the IODP Geohazards Workshop led to several consensus points among the participants. One of the most important is a mandate to include geohazards in future science plans for IODP. Presently, geohazards are included only as peripheral objectives in the Initial Science Plan for IODP, although several IODP efforts already address critical geohazards concerns (e.g., NanTroSEIZE). A directed geohazards component of IODP would strongly complement those of other research entities, including various national hazards programs. Scientific drilling can provide critical ground truth to test models and hypotheses and to assess risks and associated geohazards.

Participants also noted the outstanding opportunities to mitigate and reduce the impacts of oceanic geohazards through improved warning systems, effective coastal evacuation plans, and infrastructural modifications, using actual data that allows rigorous risk assessment. For success, however, regional surveys and core analyses must be combined with *in situ* monitoring through cabled observatories or buoyed telemetry to obtain meaningful data in real time.

Finally, it was agreed that IODP now has the opportunity to define and engage in future research directions that will have clear relevance to all of society, because the impacts of oceanic geohazards are immediate and consequential and represent a clear danger to life on Earth.

References

Alvarez, L.W., Alvarez, W., Azaro, F., and Michel, H.V., 1980. Extraterrestrial cause for the Cretaceous–Tertiary extinction. *Science*, 208:1095–1108, doi:10.1126/science.208.4448.1095.

Amoruso, A., Crescentini, L., Neri, G., Orecchio, B., and Scarpa, R., 2004. Recent seismic activity of the Messina Straits area, Italy, and the magnitude 7, 1908 Messina earthquake. *EOS, Trans. Am. Geophys. Union*, 85(47), Fall Meet. Suppl., Abstract S52A-03.

Ando, M., 1975. Source mechanisms and tectonic significance of historical earthquakes along the Nankai Trough, Japan. *Tectonophysics*, 27:119–140, doi:10.1016/0040-1951(75)90102-X.

Atwater, B.F., 1987. Evidence for great Holocene earthquakes along the outer coast of Washington State. *Science*, 236:942–944, doi:10.1126/science.236.4804.942.

Atwater, B.F., Musumi-Rokkaku, S., Satake, K., Tsuji, Y., Ueda, K., and Yamaguchi, D.K., 2005. The orphan tsunami of 1700: Japanese clues to a parent earthquake in North America. *U. S. Geol. Surv. Prof. Pap., Report P 1707,* 133 pp.

Bell, R.E, McNeill, L.C., Bull, J.M., and Henstock, T.J., 2008. Active faulting within the offshore western Gulf of Corinth, Greece: Implications for models of continental rift deformation. *Geol. Soc. Am. Bull.*, 120:156–178, doi:10.1130/B26212.1.

Belousev, A., Voight, B., Belousova, M., and Muravyev, Y., 2000. Tsunamis generated by subaquatic volcanic explosions: unique data from 1996 eruption in Karymskoye Lake, Kamchatka, Russia. *Pure Appl. Geophys.*, 157:1135–1143, doi:10.1007/s000240050021.

Billi, A., Funiciello, R., Minelli, L., Faccenna, C., Neri, G., Orecchio, B., and Presti, D., 2008. On the cause of the 1908 Messina tsunami, southern Italy. *Geophys. Res. Lett.*, 35:L06301, doi:10.1029/2008GL033251.

Bondevik, S., Løvholt, F., Harbitz, C., Mangerud, J., Dawson, A., and Svendsen, J.-I., 2005. The Storegga Slide tsunami—comparing field observations with numerical simulations. *Mar. Petrol. Geol.*, 22:195–208, doi:10.1016/j.marpetgeo.2004.10.003.

Bondevik, S., Svendsen, J.I., Johnsen, G., Mangerud, J., and Kaland, P.E., 1997. The Storegga tsunami along the Norwegian coast, its age and run-up. *Boreas*, 26:29–53.

Borrero, J.C., Legg, M.R., and Synolakis, C.E., 2004. Tsunami sources in the Southern California Bight. *Geophys. Res. Lett.*, 31:L13211, doi:10.1029/2004GL020078.

Brooks, B.A., Foster, J.H., Bevis, M., Frazer, L.N., Wolfe, C.J., and Behn, M., 2006. Periodic slow earthquakes on the flank of Kilauea volcano, Hawaii. *Earth Planet. Sci. Lett.*, 246:207–216, doi:10.1016/j.epsl.2006.03.035.

Brown, K.M., Tryon, M.D., DeShon, H.R., Dorman, L.M., and Schwartz, S.Y., 2005. Correlated transient fluid pulsing and seismic tremor in the Costa Rica subduction zone. *Earth Planet. Sci. Lett.*, 238:189–203, doi:10.1016/j.epsl.2005.06.055.

Brudzinski, M.R., and Allen, R.M., 2007. Segmentation in episodic tremor and slip all along Cascadia. *Geology*, 35:907–910, doi:10.1130/G23740A.1.

Bünz, S., Mienert, J., Vanneste, M., and Andreassen, K., 2005. Gas hydrates at the Storegga Slide: Constraints from an analysis of multicomponent, wide-angle seismic data. *Geophysics*, 70:19–34, doi:10.1190/1.2073887.

Camerlenghi, A., Urgeles, R., Ercilla, G., and Bruckmann, W., 2007. Scientific ocean drilling behind the assessment of geo-hazards from submarine slides. *Sci. Drill.*, 4:45–47. doi:10.2204/iodp.sd.4.14.2007.

Cervelli, P., Segall, P., Johnson, K., Lisowski, M., and Miklius, A., 2002. Sudden aseismic fault slip on the south flank of Kilauea volcano. *Nature*, 415:1014–1018, doi:10.1038/4151014a.

Cita, M.B., and Aloisi, G., 2000. Deep-sea tsunami deposits triggered by the explosion of Santorini (3500 y BP), eastern Mediterranean. *Sed. Geol.*, 135:181–203, doi:10.1016/S0037-0738(00)00071-3.

Chapman, C.R., 2004. The hazard of near-Earth asteroid impacts on Earth. *Earth Planet. Sci. Lett.*, 222:1–15, doi:10.1016/j.epsl.2004.03.004.

Chapman, C.R., and Morrison, D., 1994. Impacts on the Earth by asteroids and comets: assessing the hazard. *Nature*, 367:33–40, doi:10.1038/367033a0.

Clague, D.A., and Denlinger, R.P., 1994. Role of olivine cumulates in destabilizing the flanks of Hawaiian volcanoes. *Bull. Volcanol.*, 56:425–434, doi:10.1007/BF00302824.

Collins, G.S., Melosh, H.J., and Marcus, R.A., 2005. Earth impact effects program: a web-based computer program for calculating the regional environmental consequences of a meteoroid impact on Earth. *Meteor. Planet. Sci.*, 40:817–840.

Coombs, M.L., White, S.M., and Scholl, D.W., 2007. Massive edifice failure at Aleutian arc volcanoes. *Earth Planet. Sci. Lett.*, 256:403–418, doi:10.1016/j.epsl.2007.01.030.

Day, S.J., Carrecedo, J.C., and Guillou, H., 1997. Age and geometry of an aborted rift flank collapse: the San Andres fault system, El Hierro, Canary Islands. *Geol. Mag.*, 134(4):523–537.

Day, S., Silver, E., Ward, S., Gary, H., Amelia, L., and Llanes-Estrada, P., 2005. Comparison of the submarine 1888 Ritter and the subaerial 1980 Mount St. Helens debris avalanche deposits. *EOS, Trans. Am. Geophys. Union*, Fall Meeting Suppl., Abstract V13F-01.

Denlinger, R., and Okubo, P., 1995. Structure of the mobile south flank of Kilauea volcano, Hawaii. *J. Geophys. Res.*, 100:24499–24507.

Dugan, B., and Flemings, P.B., 2000. Overpressure and fluid flow in the New Jersey continental slope: implications for slope failure and cold seeps. *Science*, 289:288–291, doi:10.1126/science.289.5477.288.

Eakins, B., Robinson, J.E., Kanamatsu, T., Naka, J., Smith, J.R., Takahashi, E., and Clague, D.A., 2004. Hawaii's Volcanoes Revealed. *U.S. Geol. Surv. Invest. Ser. I-2809*.

Elsworth, D., and Day, S.J., 1999. Flank collapse triggered by intrusion: the Canarian and Cape Verde archipelagoes. *J. Volc. Geotherm. Res.*, 94:323–340, doi:10.1016/S0377-0273(99)00110-9.

Elsworth, D., and Voight, B., 1995. Dike intrusions as a trigger for large earthquakes and the failure of volcano flanks. *J. Geophys. Res.*, 100:6005–6024, doi:10.1029/94JB02884.

Fiske, R.S., Cashman, K.V., Shibata, A., and Watanabe, K., 1998. Tephra dispersal from Myojinsho, Japan, during its shallow submarine eruption of 1952-1953. *Bull. Volcanol.*, 59:262–275, doi:10.1007/s004450050190.

Flemings, P.B., Behrmann, J.H., John, C.M., and the Expedition 308 Scientists, 2006. *Proc. IODP 308*: College Station, Texas (Integrated Ocean Drilling Program Management International, Inc.), doi:10.2204/iodp.proc.308.2006.

Gohn, G.S., Koeberl, C., Miller, K.G., Reimold, W.U., Browning, J.V., Cockell, C.S., Horton, J.W., Jr., Kenkmann, T., Kulpecz, A. A., Powars, D.S., Sanford, W.E., and Voytek, M.A., 2008. Deep drilling into the Chesapeake Bay impact structure. *Science*, 320:1740–1745, doi:10.1126/science.1158708.

Goldfinger, C., Hans-Nelson, C., Johnson, J.E., and Shipboard

Scientific Party, 2003. Holocene earthquake records from the Cascadia subduction zone and northern San Andreas Fault based on precise dating of offshore turbidites. *Ann. Rev. Earth Planet. Sci.*, 31:555–577, doi:10.1146/annurev. earth.31.100901.141246.

Goldfinger, C., Nelson, C.H., Morey, A., Johnson, J.E., Gutierrez-Pastor, J., Eriksson, A.T., Karabanov, E., Patton, J., Gracia, E., Enkin, R., Dallimore, A., and Dunhill, G., 2008. Turbidite event history: methods and implications for Holocene paleoseismicity of the Cascadia subduction zone. *USGS Professional Paper 1661-F,* 178 p., in preparation.

Gracia, E., Danobeitia, J., Verges, J., and PARSIFAL Team, 2003. Mapping active faults offshore Portugal (36 degrees N-38 degrees N): implications for seismic hazard assessment along the southwest Iberian margin. *Geology*, 31:83–86, doi:10.1130/0091-7613(2003)031<0083:MAFOPN>2.0.CO;2.

Grieve, R.A.F., 1998. Extraterrestrial impacts on earth: the evidence and the consequences. *Geol. Soc., London Spec. Publ.*, 140:105–131.

Gulick, S., Barton, P.J., Christeson, G.L., Morgan, J.V., McDonald, M., Mendoza-Cervantes, K., Pearson, Z.F., Anush, S., Urrutia, J., Vermeesch, P.M., and Warner, M.R., 2008. Importance of pre-impact crustal structure for the asymmetry of the Chicxulub impact crater. *Nat. Geosci.*, 1:131–135, doi:10.1038/ngeo103.

Henstock, T.J., McNeill, L.C., and Tappin, D.R., 2006. Seafloor morphology of the Sumatran subduction zone: surface rupture during megathrust earthquakes? *Geology*, 34:485–488, doi:10.1130/22426.1.

Herd, R.A., Edmonds, M., and Bass, V.A., 2005. Catastrophic lava dome failure at Soufriere Hills Volcano, Montserrat. *J. Volc. Geotherm. Res.*, 148:234–252, doi:10.1016/j. jvolgeores.2005.05.003.

Hieke, W., 2000. Transparent layers in seismic reflection records from the central Ionian Sea (Mediterranean): evidence for repeated catastrophic turbidite sedimentation during the Quaternary. *Sed. Geol.*, 135:89–98, doi:10.1016/ S0037-0738(00)00065-8.

Hildebrand, A.R., Penfield, G.T., Kring, D.A., Pilkington, M., Zanoguera, A.C., Jacobsen, S.B., and Boynton, W.V., 1991. A possible Cretaceous–Tertiary boundary impact crater on the Yucatan peninsula, Mexico. *Geology*, 19:867–871, doi:10.1130/0091-7613(1991)019<0867:CCAPCT>2.3.CO;2.

Hofmann, K., Wünnemann, K., and Weiss, R., 2007. Oceanic impacts —types and characteristics of induced water waves. *38th Lun. Planet. Sci. Conf.*, League City, Texas, 12–16 March 2007, abstract #1586.

Ivanov, B.A., Badukov, D.D., Yakovlev, O.I., Gerasimov, M.V., Dikov, Y.P., Pope, K.O., and Ocampo, A.C., 1996. Degassing of sedimentary rocks due to Chicxulub impact: hydrocode and physical simulations. *Geol. Soc. Am. Spec. Pap.*, 307:125–140.

Iverson, R.M., 1995. Can magma-injection and groundwater forces cause massive landslides on Hawaiian volcanoes? *J. Volc. Geotherm. Res.*, 66:295–308, doi:10.1016/0377-0273 (94)00064-N.

Kanamori, H., 1972. Mechanism of tsunami earthquakes. *Phys. Earth Planet. Int.*, 6:346–359, doi:10.1016/0031-9201(72)90058-1.

Kennett, J.P., Cannariato, K.G., Hendy, I.L., and Behl, R.J., 2000.

Carbon isotopic evidence for methane hydrate instability during Quaternary interstadials. *Science*, 288:128–133, doi:10.1126/science.288.5463.128.

Kinoshita, M., Tobin, H., Moe, K.T., and the Expedition 314 Scientists, 2008. NanTroSEIZE Stage 1A: NanTroSEIZE LWD transect. *IODP Prel. Rept., 314*. doi: 10.2204/iodp.pr.314.2008.

Koeberl, C., and MacLeod, K., 2002. Catastrophic events and mass extinctions: impacts and beyond. *Geol. Soc. Am., Spec. Pap., 356*, 746 pp.

Korycansky, D.G., and Lynett, P.J., 2005. Offshore breaking of impact tsunami: the Van Dorn effect revisited. *Geophys. Res. Lett.*, 32:L10608, doi:10.1029/2004GL021918.

Lander, J.F., and Lockridge, P.A., 1989. *United States Tsunamis*. Publication 41-2. U.S. Department of Commerce.

Lee, H.J., Kayen, R.E., Gardner, J.V., and Locat, J., 2003. Characteristics of several tsunamigenic submarine landslides. *In* Locat, J., and Mienert, J. (Eds.), *Submarine Mass Movements and Their Consequences*, Dordrecht (Kluwer Academic Publishers), 357–366.

Le Friant, A., Harford, C.L., Deplus, C., Boudon, G., Sparks, R.S.J., Herd, R.A., and Komorowski, J.C., 2004. Geomorphological evolution of Montserrat (West Indies): importance of flank collapse and erosional processes. *J. Geol. Soc. London*, 161:147–160, doi:10.1144/0016-764903-017.

Legg, M.R., Goldfinger, C., Kamerling, M.J., Chaytor, J.D., and Einstein, D.E., 2007. Morphology, structure and evolution of California continental borderland restraining bends. *Geol. Soc. Spec. Publ.*, 290:143–168, doi:10.1144/SP290.3.

Lipman, P.W., Lockwood, J.P., Okamura, R.T., Swanson, D.A., and Yamashita, K.M., 1985. Ground deformation associated with the 1975 magnitude-7.2 earthquake and resulting changes in activity of Kilauea Volcano, Hawaii. *U.S. Geol. Surv. Prof. Pap. Rep. P 1276,* 45 pp.

Liritzis, I., Katsanopoulou, D., Soter, S., and Galloway, R.B., 2001. In search of ancient Helike, Gulf of Corinth, Greece. *J. Coast. Res.*, 17:118–123.

Longva, O., Janbu, N., Blikra, L.H., and Bøe R., 2003. The 1996 Finneidfjord slide: seafloor failure and slide dynamics. *In* Locat, J., and Mienert, J. (Eds.), *Submarine Mass Movements and Their Consequences*, Dordrecht (Kluwer Academic Publishers), 531–538.

Ma, K.-F., Kanamori, H., and Satake, K., 1999. Mechanism of the 1975 Kalapana Hawaii earthquake, inferred from tsunami data. *J. Geophys. Res.*, 104:13153–13167, doi:10.1029/1999JB 900073.

MacLeod, K.G., Whitney, D.L., Huber, B.T,. and Koeberl, C., 2007. Impact and extinction in remarkably complete Cretaceous-Tertiary boundary sections from Demerara Rise, tropical western North Atlantic. *GSA Bull.*, 119:101–115.

Masson, D.G., Watts, A.B., Gee, M.J.R., Urgeles, R., Mitchell, N.C., Le Bas, T.P., and Canals, M., 2002. Slope failures on the flanks of the western Canary Islands. *Earth-Sci. Rev.*, 57:1–35, doi:10.1016/S0012-8252(01)00069-1.

McHugh, C.M.G., Seeber, L., Cormier, M.-H., Dutton, J., Cagatay, N., Polonia, A., Ryan, W.B.F., and Gorur, N., 2006. Submarine earthquake geology along the North Anatolia Fault in the Marmara Sea, Turkey: a model for transform basin sedimentation. *Earth Planet. Sci. Lett.*, 248:661–684, doi:10.1016/j. epsl.2006.05.038.

McIntosh, K.D., Silver, E.A., Ahmed, I., Berhorst, A., Ranero, C.R., Kelly, R.K., and Flueh, E.R., 2007. The Nicaragua Convergent Margin: seismic reflection imaging of the source of a tsunami earthquake. *In* Dixon, T., and Moore, J.C. (Eds.), *The Seismogenic Zone of Subduction Thrust Faults*, New York (Columbia University Press), 257–287.

McMurtry, G.M., Fryer, G.J., Tappin, D.R., Wilkinson, I.P., Williams, M., Fietzke, J., Garbe-Schoenberg, D., and Watts, P., 2004. Megatsunami deposits on Kohala volcano, Hawaii, from flank collapse of Mauna Loa. *Geology*, 32:741–744, doi: 10.1130/G20642.1.

McNeill, L.C., Cotterill, C.J., Henstock, T.J., Bull, J.M., Stefator, A., Collier, R.E.L., Paptheodorou, G., Ferentinos, G., and Hicks, S.E., 2005. Active faulting within the offshore western Gulf of Corinth, Greece: Implications for models of continental rift deformation. *Geology*, 33:241–244, doi:10.1130/G21127.1.

Mienert, J., Vanneste, M., Bunz, S., Andreassen, K., Haflidason, H., and Sejrup, H.P., 2005. Ocean warming and gas hydrate stability on the mid-Norwegian margin at the Storegga Slide. *Mar. Petrol. Geol.*, 22:233–244, doi:10.1016/j.marpetgeo.2004.10.018.

Moore, G.F., Bangs, N.L., Taira, A., Kuramoto, S., Pangborn, E., and Tobin, H.J., 2007. Three-dimensional splay fault geometry and implications for tsunami generation. Science, 318:1128, doi: 10.1126/science.1147195.

Moore, J.G., Clague, D.A., Holcomb, R.T., Lipman, P.W., Normark, W.R., and Torresan, M.E., 1989. Prodigious submarine landslides on the Hawaiian Ridge. *J. Geophys. Res.*, 94:17465–17484, doi:10.1029/JB094iB12p17465.

Moore, J.G., Normark, W.R., and Holcomb, R.T., 1994. Giant Hawaiian landslides. *Ann. Rev. Earth Planet. Sci.*, 22:119–144, doi:10.1146/annurev.ea.22.050194.001003. [First sentence of volcanic processes]

Morgan, J., Christeson, G., Gulick, S., Grieve, R., Urrutia, J., Barton, P., Rebolledo, M., and Melosh, J., 2007. Joint IODP/ICDP scientific drilling of the Chicxulub impact crater. *Sci. Drill.*, 4:42–44.

Morgan, J., Warner, M., and the Chicxulub Working Group, 1997. Size and morphology of the Chicxulub impact crater. *Nature*, 390:472–476, doi:10.1038/37291.

Morgan, J., Warner, M., Urrutia-Fucugauchi, J., Gulick, S., Christeson, G., Barton, P., Rebolledo-Vieyra, M., and Melosh, J., 2005. Chicxulub crater seismic survey prepares way for future drilling. *EOS, Trans. Am. Geophys. Union*, 86:325–328, ISSN: 0096-3941.

Morgan, J.K., and Clague, D.A., 2003. Volcanic spreading on Mauna Loa volcano, HI: evidence from accretion, alteration, and exhumation of volcaniclastic sediments. *Geology*, 30:411–414, doi:10.1130/0091-7613(2003)031<0411:VSOMLV>2.0.CO;2.

Morgan, J.K., Moore, G.F., and Clague, D.A., 2003. Slope failure and volcanic spreading along the submarine south flank of Kilauea volcano, HI. *J. Geophys. Res.*, 108(B9):2415, doi:10.1029/2003JB002411.

Morgan, J.K., Moore, G.F., Hills, D.J., and Leslie, S.C., 2000. Overthrusting and sediment accretion along Kilauea's mobile south flank, Hawaii: evidence for volcanic spreading from marine seismic reflection data. *Geology*, 28:667–670, doi:10.1130/0091-7613(2000)28<667:OASAAK>2.0.CO;2.

Mosher, D.C., Austin, J.A., Jr., Fisher, D., and Gulick, S.P., 2008. Deformation of the northern Sumatra accretionary prism: evidence for strain partitioning from high-resolution seismic reflection profiles and ROV observations. *Mar. Geol.*, 252(3-4):89–99, doi:10.1016/j.margeo.2008.03.014.

Norris, R.D., Huber, B.T., and Self-Trail, J.M., 1999. Synchroneity of the K-T oceanic mass extinction and meteorite impact: Blake Nose, western North Atlantic. *Geology*, 27:419–422.

Owen, S., Segall, P., Lisowski, M., Miklius, A., Denlinger, R., and Sako, M., 2000. Rapid deformation of Kilauea volcano: global positioning system measurements between 1990 and 1996. *J. Geophys. Res.*, 105:18983–18998, doi:10.1029/2000JB900109.

Panieri, G., 2003. Benthic foraminifera response to methane release in an Adriatic Sea pockmark. *Riv. Ital. Paleontol. Strat.*, 109:549–562.

Pareschi, M.T., Boschi, E., and Favalli, M., 2006a. The lost Tsunami. *Geophys. Res. Lett.*, 33:L22608, doi:10.1029/2006GL027790.

Pareschi, M.T., Boschi, E., and Favalli, M., 2007. Holocene tsunamis from Mount Etna and the fate of Israeli Neolithic communities. *Geophys. Res. Lett.*, 34:L16317, doi:10.1029/2007GL030717.

Pareschi, M.T., Boschi, E., Mazzarini, F., and Favalli, M., 2006b. Large submarine landslides offshore Mt. Etna. *Geophys. Res. Lett.*, 33:L13302, doi:10.1029/2006GL026064.

Park, J.-O., Tsuru, T., Kodaira, S., Cummins, P.R., and Kaneda, Y., 2002. Splay fault branching along the Nankai subduction zone. *Science*, 297(5584):1157–1160. doi:10.1126/science.1074111.

Phillips, K.A., Chadwell, C.D., and Hildebrand, J.A., 2008. Vertical deformation measurements on the submerged south flank of Kilauea volcano, Hawai'i reveal seafloor motion associated with volcanic collapse. *J. Geophys. Res.*, 113:B05106, doi.10.1029/2007JB005124

Pierazzo, E., Kring, D.A., and Melosh, H.J., 1998. Hydrocode simulation of the Chicxulub impact event and the production of climatically active gases. *J. Geophys. Res.*, 103:28607–28625, doi:10.1029/98JE02496.

Piper, D.J.W., Cochonat, P., and Morrison, M.L., 1999. The sequence of events around the epicentre of the 1929 Grand Banks earthquake: initiation of debris flows and turbidity current inferred from sidescan sonar. *Sedimentology*, 46:79–97, doi:10.1046/j.1365-3091.1999.00204.x.

Plafker, G., Nishenko, S., Cluff, L., and Syahrian, M., 2006. The cataclysmic 2004 tsunami on NW Sumatra; preliminary evidence for a near-field secondary source along the western Aceh Basin. *Seism. Res. Lett.*, 77:231.

Pope, K.O., Baines, K.H., Ocampo, A., and Ivanov, B.A., 1997. Energy, volatile production, and climatic effects of the Chicxulub Cretaceous/Tertiary impact. *J. Geophys. Res.*, 102:21645–21664, doi:10.1029/97JE017434.

Reid, M.E., 2004. Massive collapse of volcano edifices triggered by hydrothermal pressurization. *Geology*, 32:373–376, doi:10.1130/G20300.1.

Robertson, D.S., McKenna, M.C., Toon, O.B., Hope, S., and Lillegraven, J.A., 2004. Survival in the first hours of the Cenozoic. *GSA Bull.*, 116(5):760–768, doi:10.1130/B25402.1.

Saito, T., Eguchi, T., Takayama, K., and Taniguchi, H., 2001. Hazard predictions for volcanic explosions. *J. Volc. Geotherm. Res.*, 106:39–51, doi:10.1016/S0377-0273(00)00265-1.

Sari, E., and Cagatay, M.N., 2006. Turbidites and their association with past earthquakes in the deep Cinarcik Basin of the Marmara Sea. *Geo-Mar. Lett.*, 26:69–76, doi:10.1007/s00367-006-0017-3.

Satake, K., Shimazaki, K., Tsuji, Y., and Ueda, K., 1996. Time and size of a giant earthquake in Cascadia inferred from Japanese tsunami records of January 1700. *Nature*, 379:246–249, 1996, doi:10.1038/379246a0.

Satake, K., Smith, J.R., and Shinozaki, K., 2002. Three-dimensional reconstruction and tsunami model of the Nuuanu and Wailau giant landslides, Hawaii. *In* Takahashi, E., Lipman, P.W., Garcia, M.O., Naka, J., and Aramaki, S. (Eds.), *Hawaiian Volcanoes – Deep Underwater Perspective. Am. Geophys. Un. Geophys. Monogr. 128*, 333–346.

Sen Gupta, B.K., Platon, E., Bernhard, J.M., and Aharon, P., 1997. Foraminiferal colonization of hydrocarbon-seep bacterial mats and underlying sediment, Gulf of Mexico slope. *J. Foramin. Res.*, 27:292–300.

Shipboard Scientific Party, 2003. Site 1223. *In* Stephen, R.A., Kasahara, J., and Acton, G.D. (Eds.), *Proc. ODP, Init. Repts., 200.* College Station, Texas (Ocean Drilling Program), 1–159, doi:10.2973/odp.proc.ir.200.103.2003.

Solheim, A., Bryn, P., Sejrup, H.P., Mienert, J., and Berg, K., 2005. Ormen Lange—an integrated study for the safe development of a deep-water gas field within the Storegga Slide Complex, NE Atlantic continental margin; executive summary. *Mar. Petrol. Geol.*, 22:1–9, doi:10.1016/j.marpetgeo.2004.10.001.

Stein, S., and Okal, E.A., 2005. Speed and size of the Sumatra earthquake. *Nature*, 434:581–582, doi:10.1038/434581a.

Sultan, N., Cochonat, P., Canals, M., Cattaneo, A., Dennielou, B., Haflidason, H., Laberg, J.S., Long, D., Mienert, J., Trincardi, F., Urgeles, R., Vorren, T.O., and Wilson, C., 2004. Triggering mechanisms of slope instability processes and sediment failures on continental margins: a geotechnical approach. *Mar. Geol.*, 213:291–321, doi:10.1016/j.margeo.2004.10.011.

Swanson, D.A., Duffield, W.A., and Fiske, R.S., 1976. Displacement of the south flank of Kilauea volcano: The result of forceful intrusion of magma into the rift zones. *U.S. Geol. Surv. Prof. Paper 963*, 1–30.

Synolakis, C.E., Bardet, J.-P., Borrero, J.C., Davies, H.L., Okal, E.A., Silver, E.A., Sweet, S., and Tappin, D.R., 2002. The slump origin of the 1998 Papua New Guinea tsunami. *Proc. Roy. Soc. London A*, 458:763–789, doi:10.1098/rspa.2001.0915.

Tappin, D.R., Watts, P., McMurty, G.M., Lafoy, Y., and Matsumoto, T., 2001. The Sissano, Papua New Guinea tsunami of July 1998 – offshore evidence of the source mechanism. *Mar. Geol.*, 175:1–23, doi:10.1016/S0025-3227(01)00131-1.

Tobin, H., and Kinoshita, M., 2007. The IODP Nankai Trough Seismogenic Zone Experiment. *Sci. Drill., Spec. Ed.* 1:39–41.

Toon, O.B., Zahnle, K., Morrison, D., Turco, R.P., and Covey, C., 1997. Environmental perturbations caused by the impacts of asteroids and comets. *Rev. Geophys.*, 35:41–78, doi:10.1029/96RG03038.

Urgeles, R., Masson, D.G., Canals, M., Watts, A.B., and Le Bas, T., 1999. Recurrent large-scale landsliding on the west flank of La Palma, Canary Islands. *J. Geophys. Res.*, 104:25331–25348, doi:10.1029/1999JB900243.

Voight, B., and Elsworth, D., 1997. Failure of volcano slopes. *Geotechnique*, 47:1–31.

Ward, S.N., and Asphaug, E., 2000. Asteroid impact tsunami: A probabilistic hazard assessment. *Icarus*, 145:64–78.

Weaver, P.P.E., 2003 Northwest African continental margin: history of sediment accumulation, landslide deposits, and hiatuses as revealed by drilling the Madeira abyssal plain. *Paleoceanography*, 18(1):1009, doi:10.1029/2002PA000758.

Weiss, R., and Wünnemann, K., 2007. Large waves caused by oceanic impacts of meteorites. *In* Kunda, A. (Ed.), *Tsunami and Nonlinear Waves*. Berlin-Heidelberg (Springer), 235–260.

Whelan, M., 1994. The night the sea smashed Lord's Cove. *Canad. Geograph.*, 114(6):70–73.

White, J.D.L., Smellie, J.L., and Clague, D.A., 2003. A deductive outline and topical overview of subaqueous explosive volcanism. *In* White, J.D.L., Smellie, J.L., and Clague, D.A. (Eds.), *Explosive Subaqueous Volcanism, Am. Geophys. Un. Monogr. 140*, Washington, DC (American Geophysical Union), 1–20.

Authors

Julia K. Morgan, Department of Earth Science, Rice University, 6100 Main Street, Houston, Texas, 77005, U.S.A., e-mail: morganj@rice.edu.

Eli Silver, Earth and Planetary Sciences Department, University of California at Santa Cruz, Santa Cruz, Calif., 95064, U.S.A., e-mail: esilver@pmc.ucsc.edu.

Angelo Camerlenghi, ICREA, c/o GRC Geociences Marines, Facultat de Geologia, Universitat de Barcelona, Spain, e-mail: acamerlenghi@ub.edu.

Brandon Dugan, Department of Earth Science, Rice University, 6100 Main Street, Houston, Texas, 77005, U.S.A., e-mail: dugan@rice.edu.

Stephen Kirby, Western Earthquake Hazard Team, United States Geological Survey, 345 Middlefield Road, MS 977, Menlo Park, Calif., 94025, U.S.A., e-mail: skirby@usgs.gov.

Craig Shipp, Geohazards Assessment and Pore Pressure Prediction Team, Shell International Exploration and Production, Inc., 200 North Dairy Ashford, Houston, Texas, 77079, U.S.A., e-mail: Craig.Shipp@shell.com.

Kiyoshi Suyehiro, Japan Agency for Marine-Earth Science and Technology, Japan, e-mail: suyehiro@jamstec.go.jp.

New Focus on the Tales of the Earth—Legacy Cores Redistribution Project Completed

by John Firth, Lallan Gupta, and Ursula Röhl

Scientific drilling for marine cores began in 1968 under the auspices of the Deep Sea Drilling Project (DSDP), whose initial discoveries included salt domes on the sea floor and formation of oceanic crust by sea-floor spreading along the mid-ocean ridges rift zone. Analyses of cores in various laboratories all over the world provided key information toward a better understanding of Earth's past, present, and future including the geology of the sea floor, evolution of the Earth, and past climatic changes. With an eye towards future development of analytical tools for core-based research, it was important to maintain cores in as close to their original condition as possible for the years to come. This led to the establishment of large repositories curating cores at 4ºC, conducting sub-sampling, and facilitating non-destructive observation of cores while following well-defined curation policies.

Collection management of scientific ocean drilling cores has always been a shared responsibility. Beginning with DSDP, drill cores from the world's oceans were all stored in the United States and separated geographically into two regions. The East Coast Repository (ECR) at Lamont-Doherty Geological Observatory in Palisades, New York was responsible for taking care of cores from the Gulf of Mexico, Atlantic Ocean, Southern Ocean (loosely defined as south of 60°S latitude) and their peripheral seas, whereas the West Coast Repository (WCR) at Scripps Institution of Oceanography in San Diego, California was responsible for cores from the Pacific and Indian Oceans and their peripheral seas. At the end of fifteen years of DSDP operations in 1983, the 96 km of recovered core were almost evenly split between the two DSDP repositories.

With the advent of the Ocean Drilling Program (ODP), the WCR was completely filled. The Gulf Coast Repository (GCR) was built at Texas A&M University in College Station to store new cores from the Pacific and Indian Oceans, and ECR continued to set up new core storage available for its portion of the globe. A satellite repository of the GCR at the New Jersey Geological Survey/Rutgers University stores land-based cores from ODP Legs 150X and 174AX drilled from 1993 through 1997; these are scientifically related to the ODP Leg 150 and 174A marine cores taken off the New Jersey margin. In 1994, space at the ECR was becoming limited, and the international partners of ODP requested a new repository in Europe, closer to many of the scientists
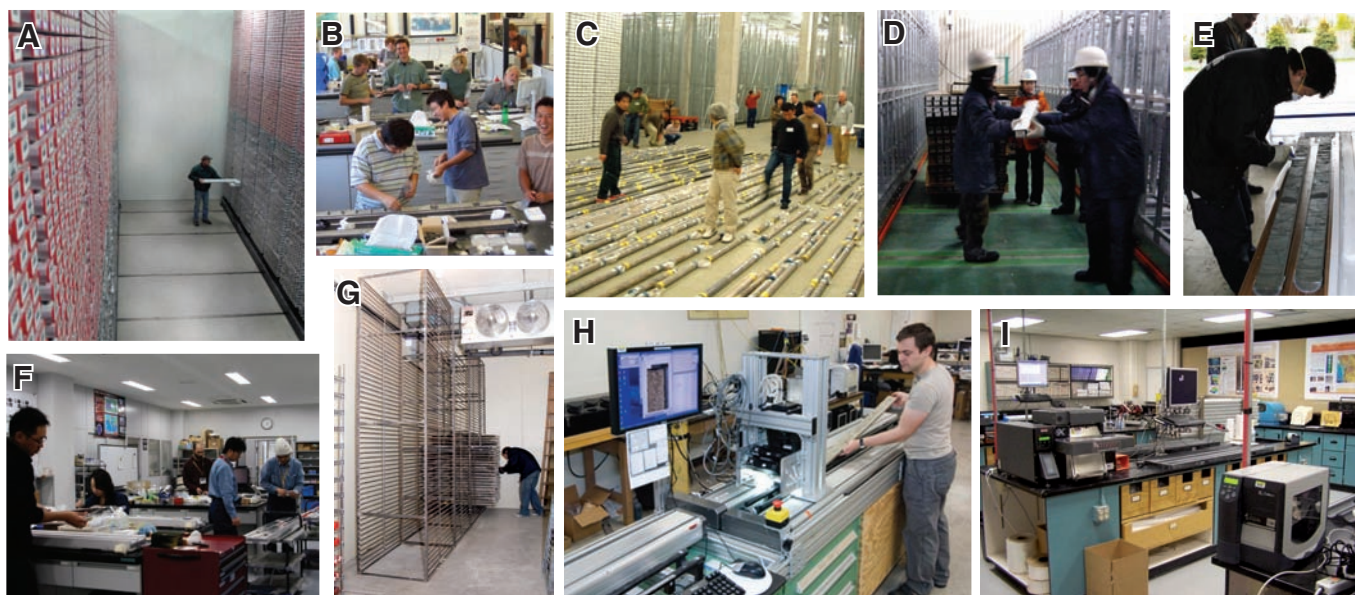
The New Repositories in Action: [A] The 5.5-m-high movable core racks in the BCR (© MARUM). [B] On-shore core description and sampling party for IODP Expedition 307 at the BCR (© IODP-BCR). [C] IODP Expedition 310 ("Tahiti Sea Level") Onshore Science Party at BCR: cores laid out in the reefer before the splitting, analyses, and sampling started. (© IODP-ESO). [D] First legacy cores arrive at the KCC (© IODP-JPIO). [E] IODP NanTroSEIZE Stage 1A core sections (© IODP-JPIO). [F] Sampling of the NanTroSEIZE Stage 1A cores at the KCC (© IODP-JPIO). [G] New high density core racks in the GCR for storage of the oldest DSDP cores beginning with Leg 1 (© IODP-USIO).[H] Legacy core being re-analyzed with newly developed digital imaging system for the *JOIDES Resolution*, in the new GCR lab facility (© IODP-USIO). [I] New GCR sampling station with automated sample bagging machine (© IODP-USIO).

outside of North America. The Bremen Core Repository (BCR) in Bremen, Germany thus began operations by taking over the ECR's Atlantic/Southern Ocean responsibilities starting with ODP Leg 151.

After twenty years of ODP operations, another 222 km of core had been collected, with the ECR containing roughly 75 km, the WCR still at roughly 50 km, the GCR at 120 km, and the BCR at 75 km. These DSDP and ODP cores are now referred to as 'legacy' cores.

In the early phase of the Integrated Ocean Drilling Program (IODP) in 2004, several new developments along with concerns of the scientific community provided an impetus to re-evaluate the core storage strategy for both legacy and new cores.

The oldest cores stored at the WCR and ECR were in relatively less demand by the international scientific community than the more recent cores at the GCR and BCR. This reflects a normal trend for all cores, where the greatest usage in terms of sampling usually occurs within the first five years, after which usage steadily declines. The cost of maintaining these low-usage core collections at their original locations was quite high compared to the cost of the more recent collections, simply because of the need to pay for rental space, utilities for cold storage, and complete core sampling labs and staff at these facilities. It was apparent that combining these old collections with the newer ones would reduce costs.

In early 2005 the BCR collection was moved from the former harbor area of Bremen to the MARUM–Center for Marine Environmental Sciences building on the campus of Bremen University. The new core reefer in the MARUM building and additional laboratory and office space greatly facilitate core sampling and analysis. The infrastructure of the MARUM and of the Faculty of Geosciences, University of Bremen, features a unique set of high capacity facilities, for both the initial handling and for highly sophisticated analyses of marine sediments, including three XRF core scanners and an X-ray CT scanner. The new BCR has approximately tripled the capacity of the old facility.

In April 2004, JAMSTEC (Japan Agency for Marine-Earth Science and Technology) and Kochi University established a new marine core research center (nicknamed Kochi

Core Center, or KCC, in June 2006) on the Monobe campus of the university in Nankoku City, Japan. The center has a movable rack system for core storage, a number of large liquid N_2 freezers for the storage of microbiological and hydrate samples, and a large set of state-of-the-art analytical equipment including X-ray CT and XRF core scanners. Curation of the IODP and legacy cores at KCC is managed by JAMSTEC, while the analytical facility is maintained through collaboration of the university and JAMSTEC.

Texas A&M University committed to ensuring greater core storage capacity and to creating a shore-based analytical laboratory facility adjacent to the GCR as part of its contribution to the IODP. The laboratory space was used in 2007 and 2008 for development of new shipboard analytical tools for the newly refurbished *DV JOIDES Resolution*, and it is ready for installation of its first instrument, an XRF core scanner, in the spring of 2009. The GCR has nearly 100 km of additional core storage capacity, contains some additional oceanographic cores, and serves also as the core storage site for the San Andreas Fault Observatory at Depth project of the International Continental Scientific Drilling Program (ICDP).

IODP became a multi-platform operation with the construction of the *DV Chikyu* and with the conception of ECORD′s Mission Specific Platforms (MSP) for drilling projects not achievable using either the U.S. non-riser *DV JOIDES Resolution* or Japan's riser *DV Chikyu*.

The addition of analytical facilities complementing the core repositories was an important advancement for improving service to the community. For example, the facilities can be utilized to complete analytical work not carried out on board. MSPs are normally not equipped with the laboratory facilities that scientists are accustomed to on other IODP drilling vessels. The Onshore Science Party (OSP) at BCR takes place after MSP offshore operations (which capture, at
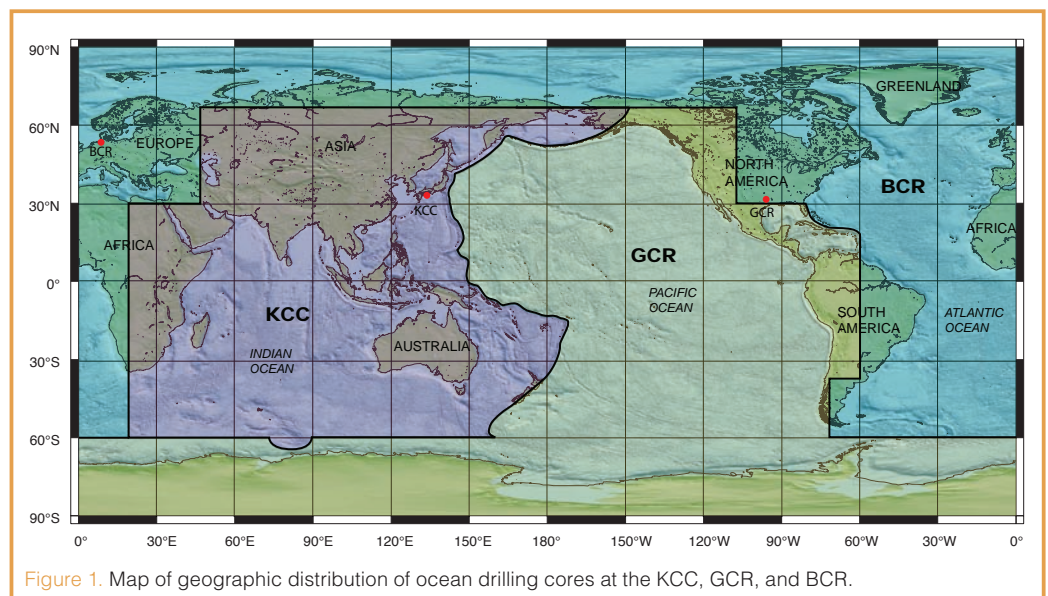

Figure 1. Map of geographic distribution of ocean drilling cores at the KCC, GCR, and BCR.

a minimum, mostly ephemeral properties) are completed. At the OSP in Bremen, cores are split and scientists have their first opportunity to study, analyze, and sample the cores in detail. The utilization of the facility for personal research also provides the advantage of minimal deterioration in the core sample quality, which would otherwise be a concern (e.g., contamination and rise in temperature during shipment of samples from a repository to a researcher's laboratory) especially for microbiological research.

All of these new developments were discussed among the Implementing Organizations (IOs), their funding agencies, and Integrated Ocean Drilling Program–Management International (IODP-MI). Consequently a decision was made that the storage of cores from the world's oceans should now reflect the three-way partitioning of drilling responsibilities in the new program. A project was approved and funded to close the ECR and WCR, consolidate their cores with those of the BCR and GCR, and re-distribute the collections among the three primary repositories to a new geographic system that is fairly balanced in terms of volume of core material, and which would include future IODP cores. After two years of work, about two-thirds of the DSDP/ODP core collection (>200 km) were moved, and the ECR and WCR were both officially closed on 30 September 2008. In addition, the first phase of IODP drilling recovered more than 15 km of new cores between 2004 and 2008. The current status of all scientific ocean drilling cores at the three IODP repositories (Fig. 1) is as follows:

> - The GCR stores cores from the Pacific Ocean plate, the Southern Ocean south of 60°S latitude (except Kerguelan Plateau), the Gulf of Mexico, and the Caribbean Sea. It presently houses over 109 km of core.
> - The BCR stores cores from the North and South Atlantic, the Mediterranean and Black Seas, and the Arctic Ocean. It now houses over 140 km of core.
> - The KCC stores cores from the Indian Ocean and marginal seas, as well as from the western and northern marginal seas of the Pacific region, defined by the plate boundaries that extend from the Aleutian Trench to the Macquarie Ridge. It now houses over 85 km of core.

This new disposition of cores not only renders a change of locations, but also provides an opportunity to extend the usefulness of even the oldest drill cores by making them easily available to new non-destructive analytical systems that did not exist when many of these cores were first obtained. Therefore, the consolidation of old and new cores from similar regions within three well-balanced core storage and analytical facilities around the world is intended to enhance the use of this vast and still growing collection. After completion of this gigantic moving project, the curatorial staff at all three repositories are now ready to provide improved service to the international scientific community, including that in the Asia-Pacific region.

Authors

John Firth, IODP-USIO, 1000 Discovery Drive, College Station, Texas 77845, U.S.A., e-mail: firth@iodp.tamu.edu.
Lallan Gupta, IODP-JPIO, Kochi Institute for Core Sample Research, Japan Agency for Marine-Earth Science and Technology (JAMSTEC), B200 Monobe, Nankoku, Kochi 783-8502, Japan, e-mail: gupta@jamstec.go.jp.
Ursula Röhl, Bremen Core Repository (BCR), MARUM— Center for Marine Environmental Sciences at Bremen University, Leobener Strasse, 28359 Bremen, Germany, e-mail: uroehl@marum.de.

Related Web Links

DSDP: http://www.deepseadrilling.org
ODP: http://www-odp.tamu.edu
IODP: http://www.iodp.org
SEDIS: http://sedis.iodp.org/front_content.php
BCR: http://marum.de/en/IODP_Core_Repository.html
ECORD: http://www.ecord.org
GCR: http://iodp.tamu.edu/curation/gcr/index.html
KCC: http://www.kochi-core.jp/en/index.html
Rutgers Satellite Repository: http://geology.rutgers.edu/corerepository.shtml
ICDP-SAFOD: http://safod.icdp-online.org
Access data and samples: http://www.iodp.org/weblinks/Tasks-Scientists/Request-Access-to-Samples/

Clues of Early Life: Dixon Island–Cleaverville Drilling Project (DXCL-DP) in the Pilbara Craton of Western Australia

by Kosei E. Yamaguchi, Shoichi Kiyokawa, Takashi Ito, Minoru Ikehara, Fumio Kitajima, and Yusuke Suganuma

Introduction

The Pilbara Craton in NW Australia (Fig. 1) exposes one of the well-preserved and least metamorphosed greenstone belts in the Archean. Greenstone belts are normally composed of a complex amalgam of meta-basaltic and meta-sedimentary rocks. Sedimentary rocks of the greenstone belts are good targets to search for clues of early Earth's environment and life.

In recent years, several scientific drilling programs (e.g.: Archean Biosphere Drilling Project (ABDP), Ohmoto et al., 2006; Deep Time Drilling Project (DTDP), Anbar et al., 2007, Kaufman et al., 2007; PDP: Pilbara Drilling Project, Philippot et al., 2007) were successfully completed in the western Pilbara area, where 3.5, 2.9, 2.7, and 2.5 Ga sedimentary units were drilled. However, there is a huge time gap in the samples drilled by ABDP and DTDP that represents middle Archean time , between 3.5 Ga and 2.9 Ga (i.e., ~600 Ma, equivalent to the duration of the entire Phanerozoic). The Cleaverville-Dixon Island area of the coastal Pilbara terrain (Fig. 1) is suited to filling in the missing record. It contains well-preserved volcano-sedimentary sequences (Cleaverville Group dated at 3.2 Ga) where hydrothermal vein systems, organic-rich siliceous sedimentary rocks, and iron-rich sedimentary rocks are developed (Kiyokawa et al., 2006). Such geological materials may be used to reconstruct past submarine hydrothermal

Figure 1. Aerial photo showing locations of drilling sites CL1, CL2, and DX for DXCL-DP in Cleaverville, northwestern coast of Pilbara district, Western Australia. Coordinates of the DX site are 20°39'21"S and 117°00'04"E. Aerial photo is taken from "Google Earth" (http://earth.google.com/).

activity and its influence on biological activity. Indeed, some attempts have been made to answer the key questions. However, the surface outcrops in this area are generally weathered to variable degrees; thus they are apparently not suitable for geo-biological and geochemical studies which require unaltered original chemical/isotopic compositions from the time of their formation in the middle Archean. Consequently, we carried out the "Dixon Island - Cleaverville Drilling Project (DXCL-DP)", to obtain "fresh" samples from the sedimentary sequences in the Cleaverville—Dixon Island area.

Scientific Objectives and Methods

The most important objective of the DXCL-DP is to understand the nature of the middle Archean (3.2 Ga) marine environment influenced by hydrothermal activity, through detailed and systematic study of fresh drill core samples. This objective has been pursued through (a) detailed stratigraphy of the whole section, (b) inorganic geochemistry of sedimentary rocks, (c) organic geochemistry of carbonaceous sedimentary rocks (i.e., characterization of the carbonaceous materials including insoluble macromolecular matter), (d) study of "microfossils", (e) geochemistry (including stable isotopes) of sulfide in sedimentary rocks, and (f) paleomagnetic study on oriented core samples in order to explore the presence and direction of the geomagnetic field in the early Earth. Various geochemical investigations of shales and cherts are used (e.g., major, minor, trace, and rare earth element geochemistry; C_{org}, N, S, and Fe isotope geochemistry, etc.) to fully extract the information from samples and to understand the influence of submarine hydrothermal activity on the biological and chemical fingerprints. From these data we intend to determine the original environmental information at the time of deposition.

Drilling Targets and Geological Background

Our drilling targets were deeply buried organic-rich black cherts and black shales of the Dixon Island Formation (DIF) and Snapper Beach Formation (SBF) (Fig. 2). Both formations belong to the 3.2 Ga Cleaverville Group and are exposed along the coasts of the Cleaverville area and Dixon Island. The Cleaverville Group is a well-preserved submarine sequence affected only by low-grade metamorphism (prehnite-pumpellyite facies) without intensive deformation
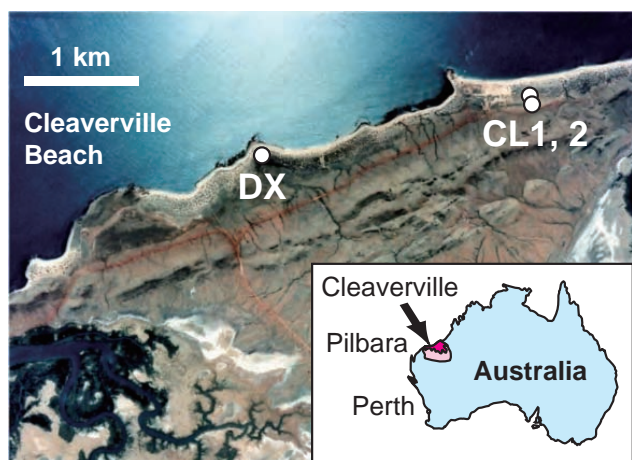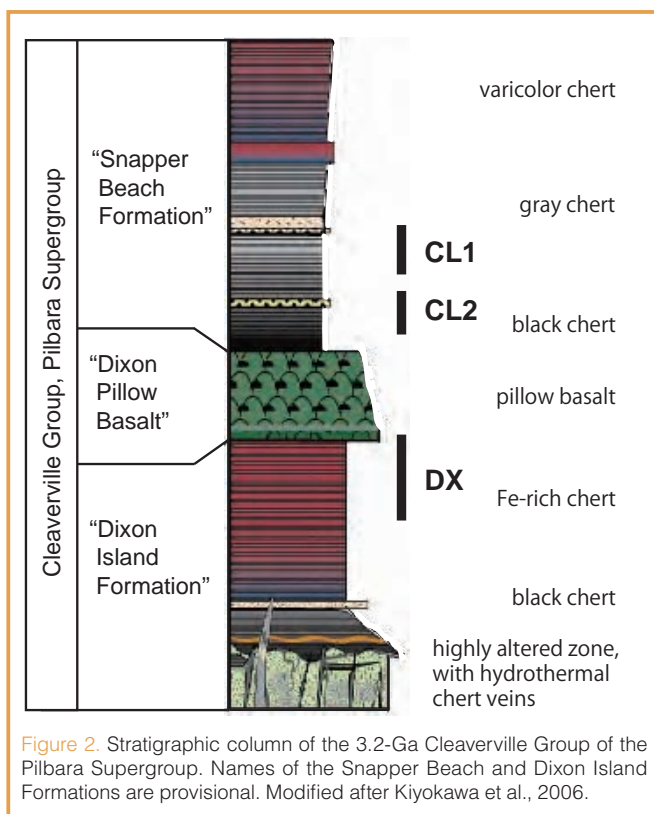
Figure 2. Stratigraphic column of the 3.2-Ga Cleaverville Group of the Pilbara Supergroup. Names of the Snapper Beach and Dixon Island Formations are provisional. Modified after Kiyokawa et al., 2006.

Figure 3. Photographs of drilling sites for DXCL-DP. [A] CL1 and CL2, and [B] DX.

(Kiyokawa et al., 2002). It is composed of volcanic rock units and chemical-volcano-sedimentary sequences. Interpretation of its depositional settings diverges among rift, horizontal tectonics, accreted oceanic crust, or accreted immature island arc (Hickman, 1983; Van Kranendonk et al., 2006).

The ~350-m-thick DIF in the lower part of the Cleaverville Group consists mainly of highly silicified volcanic-siliceous sequences that contain apparent microbial mats and fossilized bacteria-like structures within black chert and also includes a komatiite-rhyolite sequence bearing hydrothermal veins. The >300-m-thick SBF in the upper part of the Cleaverville Group contains a thick unit of reddish shale, bedded red-white cherts, and a banded iron formation. It also contains chert fragments bearing pyroclastic beds bearing chert fragments (Kiyokawa et al., 2006). We selected two coastal sites at the eastern part of the Cleaverville Beach for drilling (Fig. 3). The first site (CL1 and CL2) was intended to drill through the lower part of the SBF (distance between holes is 60 m along the core dip direction), and the other is the DX site which was targeted to drill the upper DIF.

Drilling Results

DXCL-DP was successfully completed in summer 2007 after continuous drilling from 31 July to 10 August. The orientation of the core, being perpendicular to the bedding plane, is 52° dip to the southwest for the CL1 and CL2 site

and 52° dip to the northwest for the DX site. Orientations of the core samples were taken using "Ezy-Mark" oriented system (2iC Australia Pty Ltd). As a cooling media during drilling, freshwater was used at CL1 and CL2 sites, and seawater at DX site; for both, partially hydrolyzed polyacrylamide lubricant was added. A summary of information on drilling sites (core length, direction, bedding, etc.) is presented in Table 1. Stratigraphic columns of CL1, CL2, and DX are shown in Fig. 4, and an example of drillcore (DX) in a core tray is shown in Fig. 5.

CL1. The CL1 drill core (66.1 m long; Fig. 4), covering the lower part of the SBF, consists of two units: black shale and reddish shale. The black shale unit was subdivided into five subunits (BS1 to BS5). BS1 (39.4–45 m) consists of highly fragmented but organic-rich massive and laminated black shales. BS2 (49–62 m) and BS3 (71–88 m) subunits consist of massive and partly laminated black shales. BS4 (92–94 m) and BS5 (99–105 m) subunits consist of organic-rich massive

Table 1. Summary of logistical information on DXCL-DP drill cores.

	DXCL-DP Drill Core		
Drilling Site	CL1	CL2	DX
Latitude	117°01'28.8"	117°01'20.1"	117°00'05.9"
Longitude	20°39'06.7"	20°39'35.0"	20°39'43.6"
Depth to Start Drilling	39.4 m	47.6 m	47.7 m
Depth to Finish Drilling	105.3 m	92.0 m	148.3 m
Total Drill Core Length	66.1 m	44.4 m	100.15 m
Stratigraphic Thickness	40.7 m	27.3 m	61.5 m
Core Directon	160°	159°	315°
Dip	52°	50°	52°

black shale with some fine sandstone layers. The laminated black shales with pyrite nodules occur at the deepest (but stratigraphically the uppermost) part. This unit partly contains graded thin sandstone beds with cross lamination. The reddish shale unit is either mostly fragmented laminated red-brown-black shale (44–49 m and 62–71 m) or well-laminated reddish to black shale (86–88 m and 95–99 m). The uppermost section down to 53 m depth is strongly fragmented. Changes of the bedding orientation occurred at 54–57 m, 60–62 m, 72–75 m, 80–84 m, and 89–92 m depth ranges that are accompanied by fragmentation of the rocks.

CL2. The CL2 drill core (44.4 m long; Fig. 4), covering the lowest part of the SBF, consists of three units: weathered yellowish-brown rock (WY), black shale (BS), and reddish shale (R) units. Boundaries between each units are highly fragmented. The WY unit, containing laminated white chert, is highly weathered. The BS unit was subdivided into five subunits, BS1 to BS5. Each unit mainly consists of massive black shale with well-laminated black shale and silt bed, and contains some fine sandstone with cross lamination. The R unit was also subdivided into five subunits (R1 to R5), which consist of reddish massive shale, white chert, and massive and well-laminated black-gray-red shale. The color changes between red and brown are gradual. The CL2 drillcore is generally more fragmented than CL1 and DX drillcores. Bedding orientation slightly changes at 75–76 m depth and 81–82 m depth.

DX. The DX drill core (100.2 m long; Fig. 4), covering the upper part of DIF, consists of four units: highly fragmented/deformed and well-laminated black shale (69–88 m, with disturbance at 85–88 m); well-laminated black shale with pyrite lamina (88–149 m; a partly yet highly deformed section at 101–110 m; see Fig. 5) with several cm-thick pyrite veins and 10–50-cm-thick massive sulfides at 138–139 m and 144–149 m depth ranges; massive and finely-laminated black shale; and reddish shale (110–118 m) units associated with

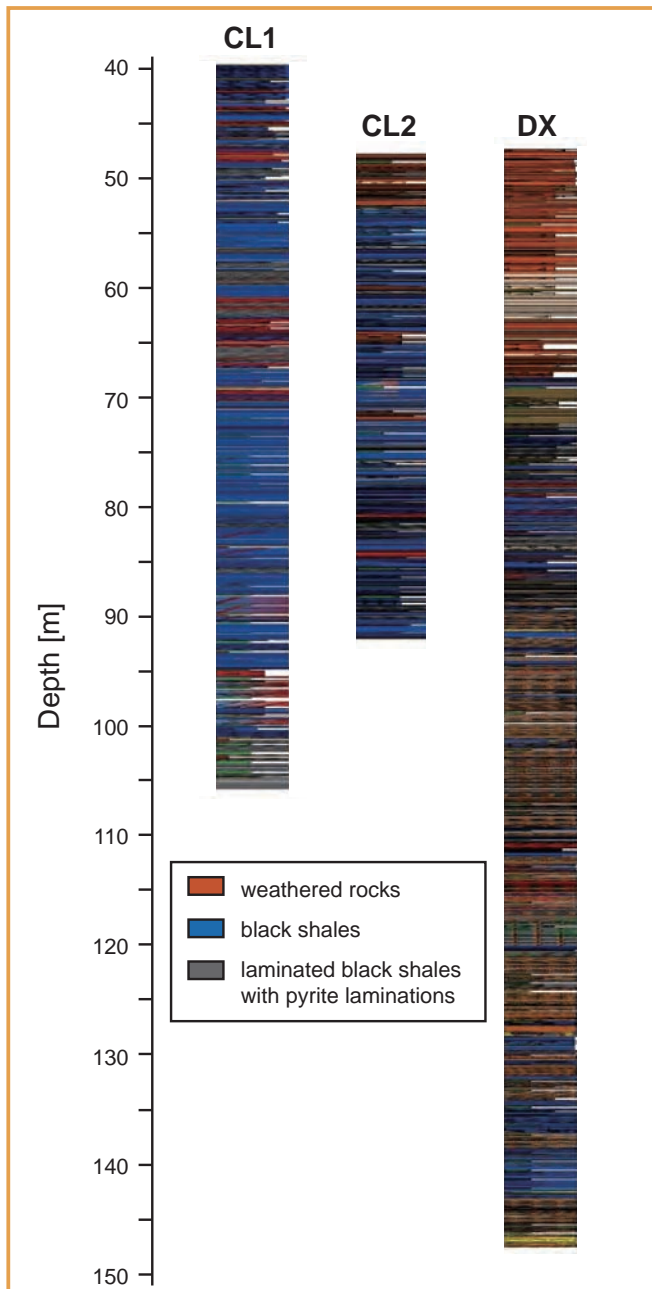Figure 4. Integrated stratigraphic columns for CL1, CL2, and DX in DXCL-DP based on fine-scale visual inspection of the drillcores. Note that the upper ~40-m sections of cores (highly-weathered by recent oxidation) were not sampled.
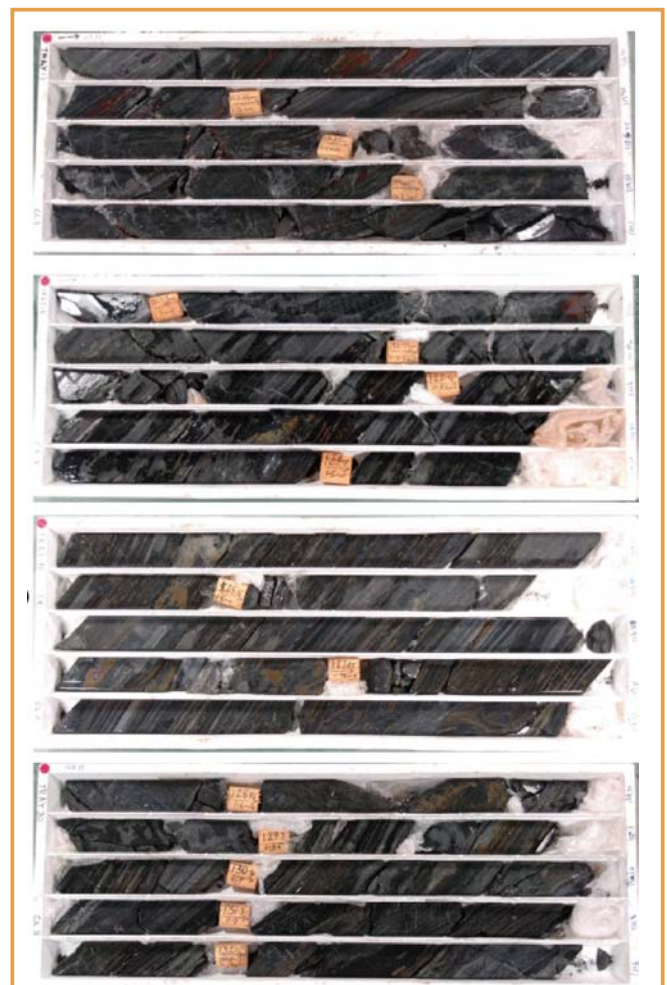

Figure 5. Representative drillcores (DX) in a core tray. Tray length is approximately 1 m. Modern-weathering-free black shales preserve pyrite laminations and pyrite nodules.

deformed/fragmented zones. The normal dip of the DX drillcore is approximately 50°. Gradual changes in the dip orientation are observed at the 110–123 m depth range that exhibit a few meter-scale open folds. The uppermost ~70 m of the drillcore DX is generally highly weathered. Its upper part (47.9–59 m) is massive and reddish, the middle part (59–63 m) contains bleached materials, and the lower part (63–69 m) is red but preserves the chilled margin structure of pillow basalts.

Summary

"Dixon Island–Cleaverville Drilling Project (DXCL-DP)" was successfully completed in summer 2007. Three holes were cored, the CL1 and CL2 cover the Snapper Beach Formation, while the DX drillcore covers the Dixon Island Formation, both of which belong to the Cleaverville Group. The CL1 and CL2 drillcores consist mainly of organic-rich massive black shales with little cross-laminated fine sandstone, and the DX drillcore contains very finely laminated black shales with lamination and veins of pyrite and weathered pillow basalt. These sulfide-containing black shales are not found anywhere in surface outcrops. It is the first discovery of these geological units.

A systematic combination of geological, sedimentological, geochemical, and geobiological approaches to the drillcore samples will be applied to obtain critical information on the characteristics of the samples and to understand the influence of submarine hydrothermal activity on the biological and chemical fingerprints. From these we intend to reconstruct the environmental conditions at the time of deposition.

Acknowledgements

References

Anbar, A.D., Duan, Y., Lyons, T.W., Arnold, G.L., Kendall, B., Creaser, R.A., Kaufman, A.J., Gordon, G.W., Scott, C., Garvin, J., and Buick, R., 2007. A whiff of oxygen before the Great Oxidation Event? *Science*, 317:1903–1906, doi:10.1126/science.1140325.

Hickman, A.H., 1983. Geology of the Pilbara Block and Its Environs. *Geological Survey of Western Australia*, *Bulletin* 127, 268 p.

Kaufman, A.J., Johnston, D.T., Farquhar, J., Masterson, A.L., Lyons, T.W., Bates, S., Anbar, A.D., Arnold, G.L., Garvin, J., and Buick, R., 2007. Late Archean biospheric oxygenation and atmospheric evolution. Science, 317:1900–1903.

Kiyokawa, S., Ito., T., Ikehara, M., and Kitajima, F., 2006. Middle Archean volcano-hydrothermal sequence: Bacterial microfossil-bearing 3.2 Ga Dixon Island Formation, coastal Pilbara terrane, Australia. Geological Society of America Bulletin, 118:3–22, doi:10.1130/B25748.1.

Kiyokawa, S., Taira, A., Byrne, T., Bowring, S., and Sano, Y., 2002. Structural evolution of the middle Archean coastal Pilbara terrain, Western Australia. Tectonics, 21:1–24, doi:10.1029/2001TC001296.

Ohmoto, H., Watanabe, Y., Ikemi, H., Poulson, S.R., and Taylor, B.E., 2006. Sulphur isotope evidence for an oxic Archaean atmosphere. Nature, 442:873–876, doi:10.1038/nature05044.

Philippot, P., Van Zuilen, M., Lepot, K., Thomazo, C., Farquhar, J., and Van Kranendonk, M.J., 2007. Early Archaean microorganisms preferred elemental sulfur, not sulfate. Science, 317:1534–1537, doi:10.1126/science.1145861.

Van Kranendonk, M.J., Hickman, A.H., Smithies, R.H., Williams, I.R., Bagas, L., and Farrell, T.R., 2006. Revised lithostratigraphy of Archean supracrustal and intrusive rocks in the northern Pilbara Craton, Western Australia. *Geological Survey of Western Australia*. Record 2006/15, p. 63.

Authors

Kosei E. Yamaguchi, Precambrian Ecosystem Laboratory, Japan Agency for Marine-Earth Science and Technology (JAMSTEC), 2-15 Natsushima, Yokosuka, Kanagawa, 237-0061, Japan, and NASA Astrobiology Institute (NAI), Present address: Department of Chemistry, Toho University, 2-2-1 Miyama, Funabashi, Chiba 274-8510, Japan, e-mail: kosei@chem.sci.toho-u.ac.jp.

Shoichi Kiyokawa, Department of Earth and Planetary Sciences, Kyushu University, 6-10-1 Hakozaki, Fukuoka 812-8581, Japan.

Takashi Ito, Faculty of Education, Ibaraki University, 2-1-1 Bunkyo, Mito, Ibaraki 310-8512, Japan.

Minoru Ikehara, Center for Advanced Marine Core Research, Kochi University, 200 Monobe, Nankoku, Kochi 783-8502, Japan.

Fumio Kitajima, Department of Earth and Planetary Sciences, Kyushu University, 6-10-1 Hakozaki, Fukuoka 812-8581, Japan.

Yusuke Suganuma, Ocean Research Institute, University of Tokyo, 1-15-1 Minamidai, Nakano, Tokyo 164-8639, Japan.

Complex Drilling Logistics for Lake El'gygytgyn, NE Russia

by Julie Brigham-Grette and Martin Melles

Introduction

Lake El'gygytgyn was formed by astrophysical chance when a meteorite struck the Earth 100 km north of the Arctic Circle in Chukotka 3.6 Myrs ago (Layer, 2000) on the drainage divide between the Arctic Ocean and the Bering Sea. The crater measures ~18 km in diameter and lies nearly in the center of what was to become Beringia, the largest contiguous landscape in the Arctic to have escaped continental scale glaciation. Within the crater rim today, Lake El'gygytgyn is 12 km in diameter and 170 m deep, enclosing 350–400 m of sediment deposited since the time of impact (Gebhardt et al., 2006). This setting makes the lake ideal for paleoclimate and impact research.

Deep Drilling Initiation

After several years of preparation, pre-site survey work, and arduous logistical planning, Lake El'gygytgyn is now the focus of a challenging interdisciplinary multi-national drilling campaign as part of the International Continental Scientific Drilling Program (ICDP). With drilling initiated in late fall 2008, the goal is to collect the longest time-continuous record of climate change in the terrestrial Arctic and to compare this record with those from lower latitude marine and terrestrial sites to better understand hemispheric and global climate change. Coring objectives include replicate overlapping lake sediment cores of 330 m and 420 m length at two sites (D1 and D2, Fig. 1) near the deepest part of the

Figure 1. [A] Digital elevation model, [B] drill site locations, projected onto a panoramic view of Lake El'gygytgyn in May facing north, [C] location of Lake El'gygytgyn at 67.5°N and 172°E, ~100 km north of the Arctic Circle in Chukotka, northeastern Russia (base map courtesy of Arctic Climate Impact Assessment).

lake. Coring will be continued 300 m (D1) and 100 m (D2) into the underlying impact breccia and brecciated bedrock in order to investigate the impact process and the response of the volcanic bedrock to the impact event. One additional land-based core (site D3, Fig. 1) measures ~200 m in lake sediments now overlain by frozen alluvial sediments on the lakeshore; D3 will allow a better understanding of sediment supply to the lake and spatial depositional heterogeneity since the time of impact. Drilling of the primary D1 and D2 sites will take place from February to the middle of May 2009 using the lake ice as a drilling platform. The project uses a new Global Lake Drilling 800m (GLAD800) system modified for extreme weather conditions by Drilling, Observation and Sampling of the Earths Continental Crust (DOSECC). Moreover, the science and logistics involves close cooperation with the Russian Academy of Sciences (Far East Geological Institute-Vladivostok; and Northeastern Interdisciplinary Scientific Research Institute-Magadan) and Roshydromet's Arctic and Antarctic Research Institute (AARI), St. Petersburg.

Pilot Cores and Initial Results

The impetus for deep drilling at Lake El'gygytgyn is largely based on field and laboratory studies carried out over the past decade. Seismic work in the lake and morphostratigraphic work in the catchment and surrounding region confirmed that the lake record is undisturbed, without evidence of glaciation or desiccation (Niessen et al., 2007; Glushkova and Smirnov, 2007). Short sediment cores demonstrated the sensitivity of this lacustrine environment to record high-resolution climatic change across NE Asia at millennial timescales (Brigham-Grette et al., 2007; Melles et al., 2007; Nowaczyk et al., 2007; Fig. 2). Documenting the dynamics and controls on the lake's seasonal ice cover (Nolan and Brigham-Grette, 2007) has been key to understanding lake circulation and has been critical to developing safety plans for ice thickening and engineering prior to drilling from the lake's frozen surface.

Logistical Challenges

Lake El'gygytgyn is located 255 km inland from the village of Pevek on the coast of the East Siberian Sea. Because there are no roads to the lake, maritime shipments with the drilling system, fuel, mud, drill pipe, etc. need to be delivered in the open water season by barge through the Bering Strait
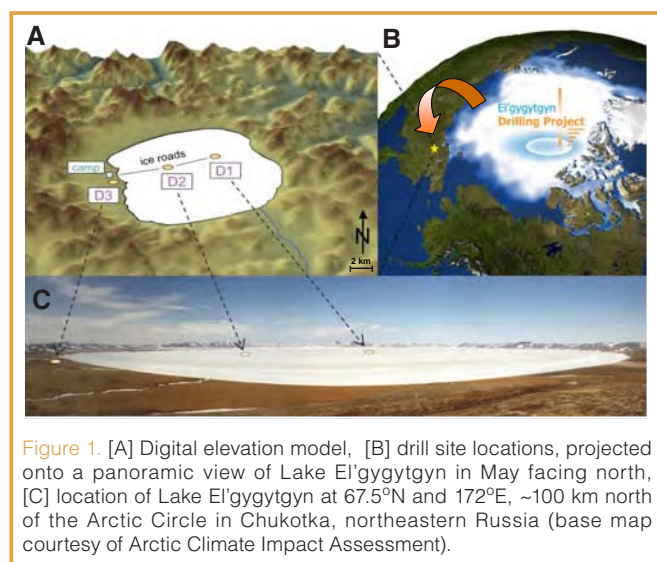
Figure 2. The new "Russian"GLAD assembled and modified by DOSECC in Salt Lake City in consultation with Alex Pyne (Antarctica Research Center, New Zeland).

by way of Vladivostok. Traversing the DOSECC drill rig and all supplies, pipe, and equipment from Pevek to Lake El'gygytgyn requires a 360-km overland bulldozer-supported trek after the rivers and tundra are well frozen and can sustain heavy loads. Most of the field party will reach the lake by helicopter out of Pevek.

Winter Drilling

Drilling in the extreme cold, darkness, and isolation of the Arctic required that the drilling system be completely enclosed and outfitted with a reliable heating system and adequate power and backup systems. Moreover, the drill system was designed to rest on a steel sledge for relocation and for cold air to circulate underneath the rig (to prevent melting). Crew changes and the transportation of cores from the rig on the lake ice to the science camp on the shore will be done in an enclosed personnel carrier. The drill sites on the lake ice are being carefully engineered for load require-ments of 1.5 m of ice achieved by clearing snow and flooding the ice over an area of about 100 m in diameter. These drill pads and the road back to camp will be monitored conti-nuously for cracks and wear. The sediment cores will be processed for whole-core physical properties and will be stored at the lake in a temperature-controlled container until they are flown to Pevek and staged for airfreight to St. Petersburg and later trucked to the University of Cologne for core opening and study by the international team. The archive halves of the core will go to LacCore, University of Minnesota.

Acknowledgements

References

Brigham-Grette, J., Melles, M., Minyuk, P., and Scientific Party, 2007. Overview and significance of a 250 ka paleoclimate record from El'gygytgyn Crater Lake, NE Russia. *J. Paleolimnol.*, 37:1–16, doi: 10.1007/s10933-006-9017-6.

Gebhardt, A.C., Niessen, F., and Kopsch, C., 2006. Central ring structure identified in one of the world's best-preserved impact craters, *Geology*, 34:145–148, doi:10.1130/G22278.1.

Glushkova, O.Y., and Smirnov, V.N., 2007. Pliocene to Holocene geomorphic evolution and paleogeography of the El'gygytgyn Lake region, NE Russia, *J. Paleolimnol.*, 37:37–47, doi:10.1007/s10933-006-9021-x.

Layer, P.W., 2000. Argon-40/argon-39 age of the El'gygytgyn impact event, Chukotka, Russia. *Meter. Planet. Sci.*, 35:591–599.

Melles, M., Brigham-Grette, J., Glushkova, O.Y., Minyuk, P.S., Nowaczyk, N.R., and Hubberten, H.W., 2007. Sedimentary geochemistry of a pilot core from Lake El'gygytgyn—a sensitive record of climate variability in the East Siberian Arctic during the past three climate cycles. *J. Paleolimnol.*, 37:89–104, doi:10.1007/s10933-006-9025-6.

Niessen, F., Gebhardt, A.C., and Kopsch, C., 2007. Seismic investiga-tion of the El'gygytgyn impact crater lake (Central Chukotka, NE Siberia): preliminary results. *J Paleolimnol.*, 37:49–63, doi:10.1007/s10933-006-9022-9.

Nolan, M., and Brigham-Grette, J., 2007. Basic hydrology, limnology, and meteorology of modern Lake El'gygytgyn, Siberia. *J. Paleolimnol.*, 37:17–35, doi:10.1007/s10933-006-9020-y.

Nowaczyk, N.R., Melles, M., and Minyuk, P., 2007. A revised age model for core PG1351 from Lake El'gygytgyn, Chukotka, based on magnetic susceptibility variations correlated to northern hemisphere insolation variations. *J Paleolimnol.*, 37:65–76, doi:10.1007/s10933-006-9023-8.

Authors

Julie Brigham-Grette, Department of Geosciences, University of Massachusetts, Amherst, Mass. 01003, U.S.A., e-mail: juliebg@geo.umass.edu.

Martin Melles, Institute of Geology and Mineralogy, University of Cologne, Zuelpicher Str. 49a D-50674 Cologne, Germany, e-mail: mmelles@uni-koeln.de.

Related Web Links

DOSECC: http://www.dosecc.org/html/glad800.html
El'gygytgyn Drilling Project: http://elgygytgyn.icdp-online.org

Photo Credits

Fig. 1: [A] photo by Conrad Kopsch, AWI; [B] photo by Volker Wennrich, University of Cologne; [C] base map courtesy of Arctic Climate Impact Assessment
Fig. 2: photo by David Zur, DOSECC

New Seismic Methods to Support Sea-Ice Platform Drilling

by Marvin A. Speece, Richard H. Levy, David M. Harwood,
Stephen F. Pekar, and Ross D. Powell

Introduction

The ANtarctic geological DRILLing Program (ANDRILL) is currently a consortium of five nations (Germany, Italy, New Zealand, the United Kingdom, and the United States of America). By drilling, coring and analyzing stratigraphic archives along the Antarctic continental margin, ANDRILL pursues its primary goal of better understanding the role the Antarctic cryosphere plays in the global climate system (Harwood et al., 2006). The ANDRILL drilling system was developed to operate on both ice shelf and sea-ice platforms (Harwood et al., 2006; Falconer et al., 2007; Naish et al., 2007; Florindo et al., 2008). While thick multiyear sea ice provides stable and safe drilling platforms, identifying drilling targets in regions where these sea-ice conditions occur can be problematic due to a paucity of marine seismic reflection data because near-constant sea ice limits ship access (Fig. 1). In response to this problem ANDRILL developed new over-sea-ice seismic methods to extend seismic reflection data coverage to regions of multiyear sea ice.
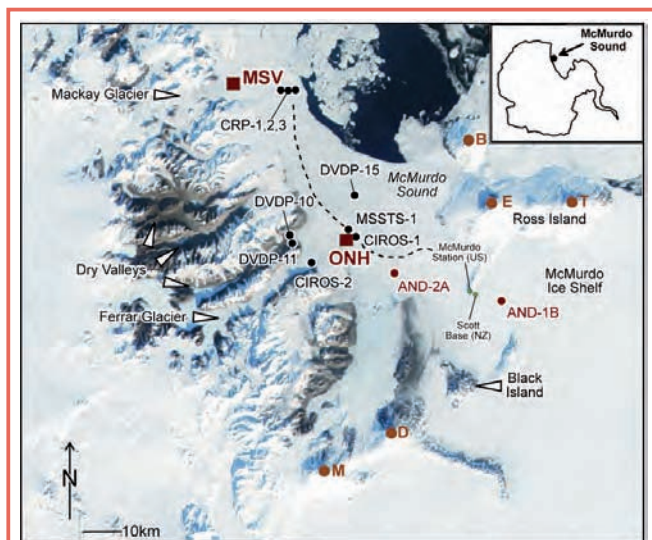

Figure 1. Location of key geographical features in southern McMurdo Sound, plus inset of Antarctica. The volcanic centers of Erebus (E), Terror (T), Bird (B), Discovery (D), and Morning (M) are annotated. The location of the two completed ANDRILL drill holes, AND-1B (McMurdo Ice Shelf), and AND-2A (Southern McMurdo Sound Project) are shown. The dashed line indicates the approximate margin of multiyear sea ice. Regions targeted for possible future drilling from sea-ice platforms include Offshore New Harbor (ONH) and Mackay Sea Valley (MSV). Also shown are the locations of previous stratigraphic drill holes (DVDP, CIROS, MSSTS, and CRP). (Modified after ANDRILL International Science Proposal, 2003; NASA MODIS image I.D.: Antarctica.A2001353.1445.250m).

Over-Sea-Ice Seismic Surveys

Previous over-sea-ice seismic experiments had limited success due to (1) poor source coupling caused by thin sea ice, (2) source-induced ice flexural modes that cause coherent noise, which is difficult to remove from data, and (3) source bubble-pulse effects caused by explosive seismic sources placed in the water column (Cobb, 1973; Cook, 1973; Mertz, 1981; McGinnis et al., 1985; Davy and Alder, 1989; Rendleman and Levin, 1990; Barrett et al., 2000; Bannister and Naish, 2002; Horgan and Bannister, 2004). During the austral spring-summer of 2005, approximately 28 km of over-sea-ice seismic reflection data were recorded in McMurdo Sound, Antarctica (Fig. 2) for ANDRILL's Southern McMurdo Sound (SMS) Project (Harwood et al., 2004). ANDRILL developed seismic survey techniques for the SMS Project that improved the quality of over-sea-ice seismic data (Betterly et al., 2007). A Generator-Injector (GI) air gun was used as the seismic source (Fig. 3A). Single air-gun-source marine seismic surveys typically use a GI technique, in which a secondary air pulse is injected into the primary air pulse on a short time delay. The injection of the secondary air pulse dampens the generation of the bubble pulse. The GI air gun was lowered into the water column via holes drilled through the sea ice. The GI air gun minimized the source bubble effects that plagued previous over-sea-ice experiments in the Antarctic. Moreover, a 60-channel seismic snow streamer consisting of vertically oriented gimbaled geophones with 25-m takeout spacing was employed to aid rapid data collection (Fig. 4).

A ski-mounted insulated hut (the *Thunder-Sled*) housed the recording equipment and the GI air gun (Fig. 4). The interior of the hut was divided into two rooms. The forward room was devoted to the GI air gun. Data recording instruments and the GI air-gun shot control were located in the rear room of the hut. Batteries, recharged by solar panels placed on the outer walls of the hut, supplied power for the recording and GI air-gun instrumentation. A propane heater fed by external tanks heated the recording room.

A single 210-in^3 GI air gun was suspended from a motorized winch. Compressed air for the air gun was stored in cylinders that were fed by a gasoline powered Bauer drive air compressor. A kerosene heater in the air-gun room and periodic injection of antifreeze kept the GI air-gun system from freezing.
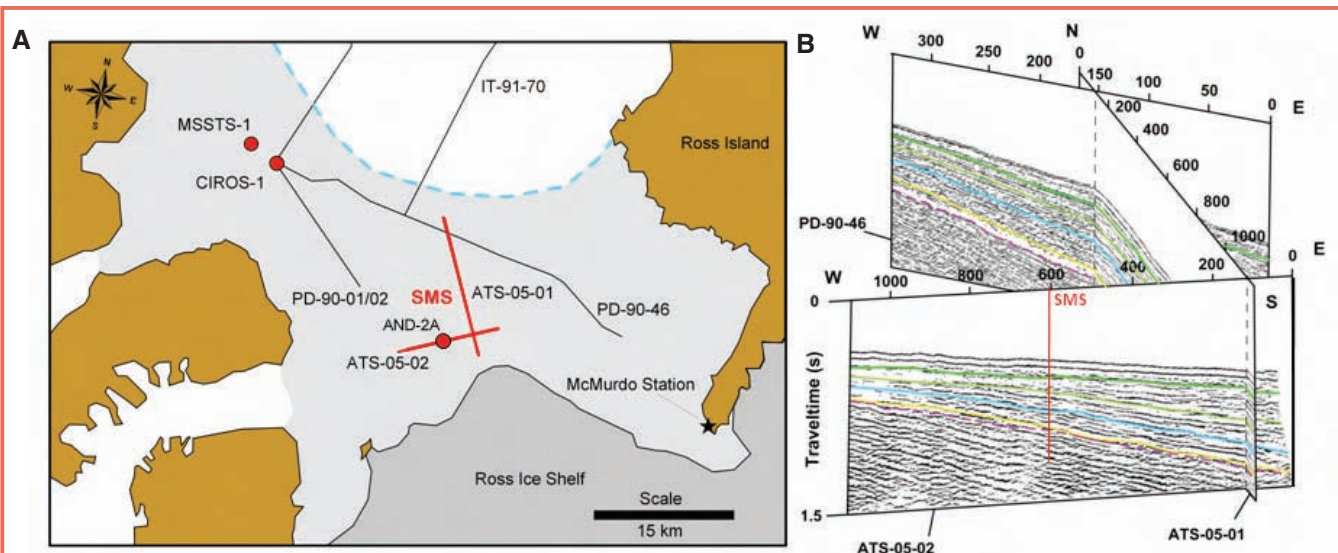
Figure 2. [A] Map of the 2005 SMS seismic survey location. The light black lines indicate existing marine seismic data (PD-90-46, PD-90-01/02, and IT-91-70), and the red lines show the location of the 2005 Southern McMurdo Sound (SMS) seismic survey (ATS-05-01 and ATS-05-02). Existing stratigraphic drill holes are labeled MSSTS-1, CIROS-1, and AND-2A in red (after Betterly et al., 2007). Dashed blue line shows the approximate extent of the 2005 ice breakout. [B] A fence diagram of PD-90-46 (single-channel marine profile), ATS-05-01, and ATS-05-02 (multichannel SMS 2005 seismic profiles) viewed from south to north. Horizontal values on ATS-05-01 and ATS-05-02 are Common MidPoint (CMP) locations. The spacing between CMP locations is 12.5 m. Horizontal locations on PD-90-46 are shot locations with spacing of 45 m. Each profile shows 1.5 s and 200 ms automatic gain control applied to these data. Colored lines overlie seismic reflectors that represent disconformities that record the advance and retreat of glaciers after the Harwood et al. (2004) interpretation.

The snow streamer consists of five cable sections with twelve takeouts per cable section. A single geophone was attached at each takeout every 25 m along the cable (Fig. 3B). The geophones are constructed using 30-Hz velocity sensors that are 360° roll gimbaled and have a 180° pitch tolerance. Each gimbaled geophone weighs approximately 1 kg. The cable sections have a central Kevlar stress member attached to a stainless steel cable connection. The cables are designed to remain flexible in extreme cold, and all connections are waterproof and designed to withstand a load of 13,000 N. Special sleds were built for each cable connection to reduce the amount of drag friction from the ice and snow surface and to protect the cable heads. The streamer was pulled

behind the source/recording hut, and a load cell was placed between the hut and the streamer to monitor load on the streamer (Fig. 3C).

The signal to noise ratio was increased during windy conditions by repeating air-gun shots (stacking) at each source location, then summing the shots. Seismic acquisition could be carried out in higher wind conditions if the wind blew inline, because the gimbaled geophones have a smaller profile in this direction, so wind-generated noise is minimal. Snow drifting was only a problem after major storms requiring the snow streamer to be dug out. Generally, the snow streamer could be removed from small snow drifts by
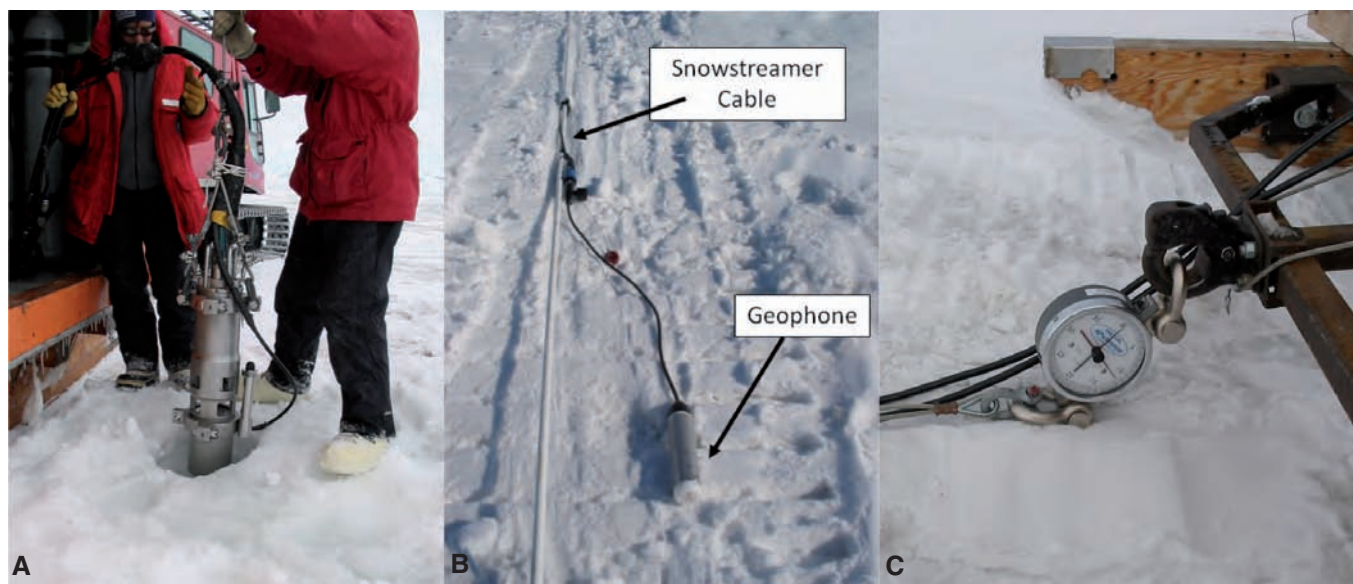

Figure 3. [A] Generator-Injector (GI) air gun being deployed through an auger hole in 6-m-thick sea ice; [B] Gimbaled geophone and the snow streamer cable; [C] Load cell attached to the back of the Thunder Sled and connected to a tow cable for the snow streamer (photos by R. Levy).
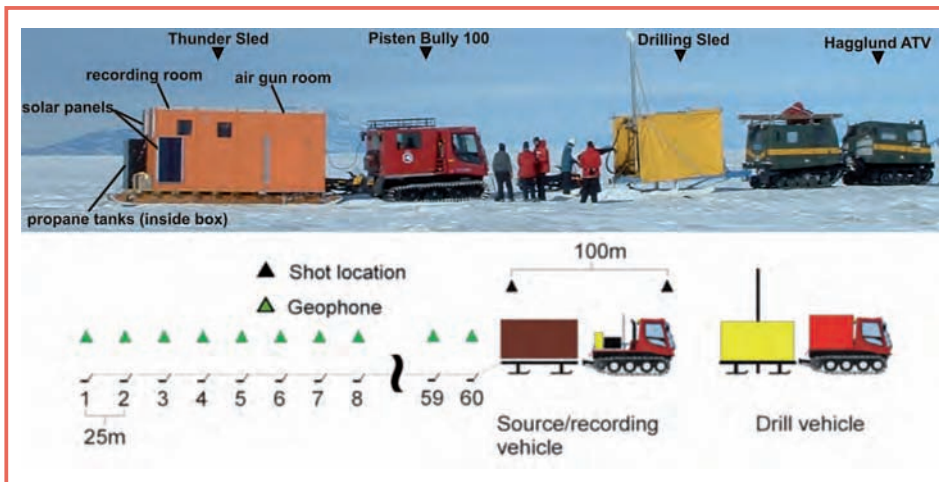
Figure 4. Images showing vehicles and sleds in operational position. The Thunder Sled consisted of a plywood hut mounted on a Komatik sled. The hut was separated into two rooms, one for the air-gun system and one to contain data recording equipment (photo by M. Buchanan). Left corner the diagram showing the setup of the over-sea-ice system during data acquisition. Black triangles represent shot locations; green triangles represent geophone locations. The source spacing was 100 m, and the receiver spacing was 25 m. The source-to-near-geophone interval was 25 m. Shot holes were prepared by the drill vehicle, and the 60-channel snow streamer with gimbaled geophones was towed behind the source/recording vehicle.

pulling it forward with a negligible force observed on the load cell.

The GI air gun provided good source coupling and minimized the source bubble effects and flexural mode problems seen in previous over-sea-ice experiments in polar regions. By extending the interpretations from nearby marine seismic surveys south to a region of thick multiyear sea ice, ANDRILL scientists were able to plan a safe location of the SMS Project drill site.

Additional Successful Surveys

During the austral summer 2007, a Vertical Seismic Profile (VSP) survey was conducted at the newly drilled SMS Project borehole. The SMS Project drill core recovered a thick succession of lower Miocene, middle Miocene, and Pliocene to Recent sedimentary rock (Florindo et al., 2008). The VSP survey used a GI air-gun source and demonstrated that high-quality borehole seismic data can be collected in a sea-ice environment. These data were collected using a three-component clamped geophone and a single near-offset source location. This is the first successful VSP survey conducted from a sea-ice platform using a GI air gun.

In addition, during the austral spring-summer 2007, ANDRILL collected approximately 20.5 km of high-quality seismic reflection data in Granite Harbor on the coast of southern Victoria Land. The Mackay Sea Valley (MSV; Fig. 1) is a deep trough likely formed beneath Granite Harbor by previous expansion of the Mackay Glacier. This seismic survey's intent was to image recent sediment layers that accumulated in the MSV after it had been eroded and last occupied by the ice sheet. The MSV seismic survey incorporated and refined techniques of over-sea-ice seismic data collection that had been used previously during the ANDRILL SMS seismic site survey. The MSV seismic survey was successful in locating a thin succession of low-amplitude reflections atop the higher-amplitude granite basement reflections in the deepest parts of the valley (Fig 5). The low-amplitude reflections are likely caused by layers of pelagic sediment. Future coring of these recent sediments could provide a high-resolution Quaternary climate record.

Future Plans

During the austral spring-summer 2008, an over-sea-ice multi-channel seismic reflection survey will be conducted in Offshore New Harbor (ONH; Fig. 1) to investigate the stratigraphic and tectonic history of westernmost Southern McMurdo Sound during the Greenhouse World (Eocene) into the start of the Icehouse World (Oligocene). This planned seismic survey will use over-sea-ice seismic methods employed successfully by ANDRILL's 2005 SMS and 2007 MSV surveys. A new seismic recording sled with a larger air compressor, larger air tanks, and improved air-gun winch system is being built to improve the speed and efficiency of data collection.
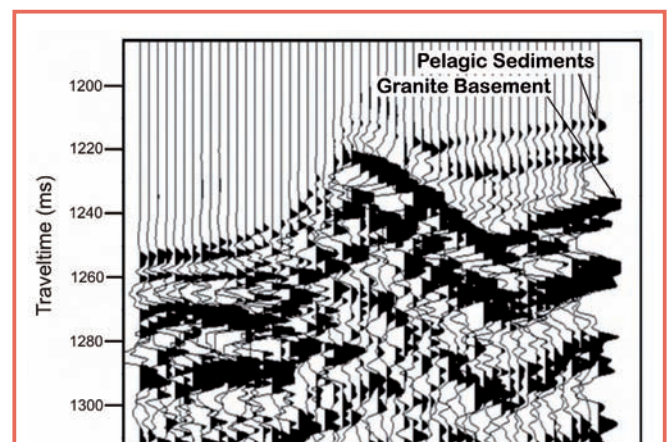
Acknowledgements

Figure 5. Unprocessed single-fold seismic reflection data from Mackay Sea Valley (MSV) seismic survey in Granite Harbor showing low-amplitude sediments overlying a high-amplitude granite basement. The high-amplitude reflection that appears to be a basement step could instead be caused by a terminal moraine. Trace spacing is 50 m.

References

ANDRILL International Science Proposal, 2003. *ANDRILL: Investigating Antarctica's Role in Cenozoic Global Environmental Change*. ANDRILL Contribution 2, University of Nebraska-Lincoln, Lincoln, Neb.

Bannister, S.C., and Naish, T.R., 2002. ANDRILL site investigations, New Harbour and McMurdo Ice Shelf, southern McMurdo Sound, Antarctica. *Institute of Geological & Nuclear Sciences Science Report,* 2002/01, 24 pp.

Barrett, P., Sarti, M., and Wise, S.W., Jr., 2000. Studies from the Cape Roberts Project, Ross Sea, Antarctica, Initial Report on CRP-3. *Terra Antart.*, 7(1/2), 209 pp.

Betterly, S.J., Speece, M.A., Levy, R.H., Harwood, D.M., and Henrys, S.A., 2007. A novel over-sea-ice seismic reflection survey in McMurdo Sound, Antarctica. *Terra Antart.*, 14(2):97–106.

Cobb, A.T., 1973. 'Vibroseis'® applications in the Arctic. *Proceedings from National Convention, Canadian Society of Exploration Geophysicists*, 115–140.

Cook, R.E., 1973. Experimental seismic methods in the Canadian Arctic. *Proceedings from National Convention, Canadian Society of Exploration Geophysicists*, 47–57.

Davy, B.W., and Alder, G., 1989. Seismic reflection surveys. *In* Barrett, P.J. (Ed.), *Antarctic Cenozoic history from the CIROS-1 drill hole, McMurdo Sound. Bulletin in the Miscellaneous Series of the New Zealand Department of Science and Industrial Research*, 245:15–21.

Falconer, T., Pyne, A., Olney, M., Curren, M., Levy, R., and the ANDRILL-MIS Science Team, 2007. Operations overview for the ANDRILL McMurdo Ice Shelf Project, Antartica. *In* Naish, T., Powell, R., and Levy, R. (Eds.), *Studies from the ANDRILL, McMurdo Ice Shelf Project, Antarctica Initial Science Report on AND-1B. Terra Antart.*, 14(3):131–140.

Florindo, F., Harwood, D., Levy, R., and SMS Project Science Team, 2008. ANDRILL's success during the 4th International Polar Year. *Sci. Drill.*, 6:29–31, doi: 10.2204/iodp.sd.6.03.2008.

Harwood, D., Levy, R., Cowie, J., Florindo, F., Naish, T., Powell, R., and Pyne, A., 2006. Deep drilling with the ANDRILL Program in Antarctica. *Sci. Drill.*, 3:43–45, doi:10.2204/iodp.sd.3.09.2006.

Harwood, D.M., Florindo, F., Levy, R.H., Fielding, C.R., Pekar, S.F., and Speece, M.A., 2004. *ANDRILL Southern McMurdo Sound Project Scientific Prospectus*. ANDRILL Contribution 5, University of Nebraska-Lincoln, Lincoln, Neb., 29 pp.

Horgan, H., and Bannister S., 2004. Explosive Source Seismic Experiments from a Sea-Ice Platform, McMurdo Sound, 2003. *Institute of Geological & Nuclear Sciences Science Report*, 2004/15.

McGinnis, L.D., Bowen, R.H., Erickson, J.M., Aldred, B.J., and Kreamer, J.L., 1985. East-West Antarctic boundary in McMurdo Sound. *Tectonophysics*, 14:341–356, doi:10.1016/0040-1951(85)90020-4.

Mertz, R.W., Brooks, L.D., and Lansley, M., 1981. Deepwater vibrator operations – Beaufort Sea, Alaska, 1979 winter season. *Geophysics*, 46:172–181, doi:10.1190/1.1441187.

Naish, T.R., Powell, R., Levy, R., Florindo, F., Harwood, D., Kuhn, G., Niessen, F., Talarico, F., and Wilson, G., 2007. A record of Antarctic climate and ice sheet history recovered. *EOS Trans., Am. Geophys. Union* 88:557–558, doi:10.1029/2007EO500001.

Rendleman, C.A., and Levin, F.K., 1990. Seismic exploration on a floating ice sheet. *Geophysics*, 55:402–409, doi:10.1190/1.1442849.

Authors

Marvin A. Speece, Geophysical Engineering Department, Montana Tech, 1300 West Park Street, Butte, Mont., 59701-8997, U.S.A., e-mail: mspeece@mtech.edu

Richard H. Levy and **David M. Harwood**, ANDRILL Science Management Office and Department of Geosciences, University of Nebraska-Lincoln, 126 Bessey Hall, Lincoln, Neb. 68588-0341, U.S.A.

Stephen F. Pekar, School of Earth and Environmental Sciences, Queens College, CUNY, 65-30 Kissena Boulevard, Flushing, N.Y., 11367, U.S.A.

Ross D. Powell, Department of Geology and Environmental Geosciences, Northern Illinois University, DeKalb, Ill., 60115, U.S.A.

Wireline Coring and Analysis under Pressure: Recent Use and Future Developments of the HYACINTH System

by Peter Schultheiss, Melanie Holland, and Gary Humphrey

Introduction

The pressure of the deep sea and of deep earth formations has subtle effects on all aspects of physics, chemistry, and biology. Core material recovered under pressure, using pressure cores, can be subjected to sophisticated laboratory analyses that are not feasible *in situ*. Though many fields of study might benefit from pressurized cores, most obviously, any investigation on gas- or gas-hydrate-rich formations on land or under the sea certainly requires pressure coring.

Downhole Pressure Coring and HYACINTH

Scientific investigations of marine gas hydrate formations have provided the impetus for all wireline pressure core development apart from proprietary oilfield technology, including the HYACINTH (HYACe In New Tests on Hydrate, 2001) system. The first scientific wireline pressure corer, the Pressure Coring Barrel, was developed by the Deep Sea Drilling Project to capture gas hydrate. It was used by Kvenvolden et al. (1983) in depressurization and gas collection experiments to quantify gas hydrate within cores. The Ocean Drilling Program (ODP) later developed the Pressure Core Sampler (PCS; Pettigrew, 1992; Graber et al., 2002), and the Pressure-Temperature Coring System (PTCS) was developed for Japan Oil, Gas and Metals National Corporation (JOGMEC, formerly Japanese National Oil Company, JNOC; Takahashi and Tsuji, 2005). Both of these systems were used almost exclusively for gas hydrate research. The HYACE (HYdrate Autoclave Coring Equipment, 1997) and the subse-

quent HYACINTH programs (Schultheiss et al., 2006; Schultheiss et al., 2008a), funded by the European Union, were also driven by the need for gas hydrate research.

The HYACINTH vision of scientific pressure coring encompassed not only coring tools but also an array of down-stream core processing equipment and capabilities. The two coring tools, the Fugro Pressure Corer (FPC) and the Fugro Rotary Pressure Corer (FRPC; previously HYACE Rotary Corer, HRC), were designed to recover high-quality cores in a complete range of sedimentary formations. The combined suite of equipment (the HYACINTH system) enables these cores to be acquired and transferred in their core liners from the pressure corers into chambers for non-destructive testing, sub-sampling, and storage as required.

The HYACINTH system has continually improved over the ten years since its inception. ODP and the Integrated Ocean Drilling Program (IODP) have played major roles in this development, allowing the tools to be initially tested (ODP Legs 194 and 201) and then used on both recent gas hydrate expeditions (ODP Leg 204, Hydrate Ridge, offshore Oregon; Tréhu et al., 2003; IODP Expedition 311, Cascadia Margin, offshore Vancouver Island, Canada; Riedel et al., 2006). Since that time, further improvements to the performance and capabilities of the coring and analysis assemblies have been made, and the system has allowed new scientific insights into the structure of natural marine gas hydrate deposits.

Recent HYACINTH Expeditions

Since the completion of IODP Expedition 311 in 2005, the HYACINTH system has been used on four major gas hydrate expeditions for quantification of gas hydrate and detailed measurements on gas-hydrate-bearing sediments. The need to assess the nature, distribution, **and concentration of gas** hydrate in the marine environment has multiple driving forces. Scientific interest in gas hydrate centers on carbon cycling and climate impact, but to the oil and gas industry hydrate is an irritating geohazard, and to national governments it is a potential resource ripe for exploitation. Political climate change has made national energy independence a high priority for governments, and in the last few years, the biggest financial input into marine gas-hydrate-related drilling expeditions has come from national governments and their associated national energy and geological organi-
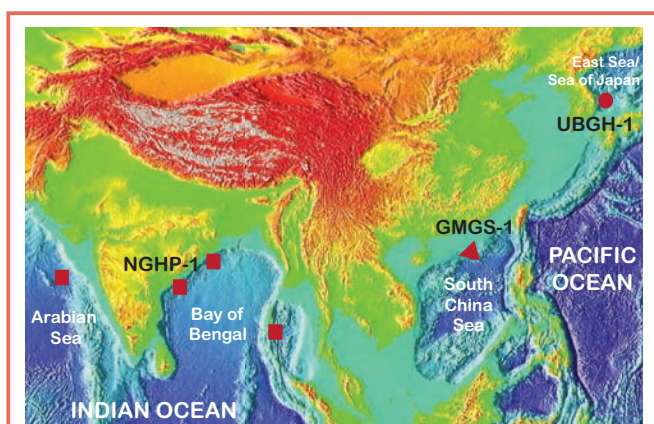

Figure 1. Map of South and Southeast Asia (based on http://www.ngdc.noaa.gov/mgg/image/2minrelief.html) showing the location of recent gas hydrate expeditions NGHP-1 (red squares), GMGS-1 (red triangle), and UBGH-1 (red circle).

zations. Of the four recent expeditions since IODP Leg 311 on which the HYACINTH coring and analysis system has been used, one was to define geohazards related to oil and gas production, and three were to quantify resources for the governments of India, China, and Korea.

India, 2006

The first Indian National Gas Hydrate Program drilling expedition (NGHP-1; Fig. 1) took place on the drillship *JOIDES Resolution* in the summer of 2006, led by the Indian Directorate General of Hydrocarbons (DGH) and the United States Geological Survey (USGS). It was designed to investigate the gas hydrate resource potential of sites around the Arabian Sea, the Bay of Bengal, and the Andaman Sea (Collett et al., 2006). This was an ambitious program, lasting 113 days, involving over a hundred scientists and technical staff from India, Europe, and the United States, and drilling thirty-nine locations at twenty-one distinct sites. It was a hugely successful program, collecting more gas-hydrate-bearing cores than any previous expedition and describing in detail at multiple scales one of the richest gas hydrate accumulations ever discovered (Collett et al., 2008).

As part of the coring program, forty-nine pressure cores were recovered under pressure and analyzed at sea and postcruise. These included IODP PCS cores as well as HYACINTH FPC and HRC/FRPC cores. The onboard pressure core analysis included routine core measurement of all pressure cores in the HYACINTH Pressure Core Analysis and Transfer System (PCATS). All nondestructive data was collected at *in situ* pressure. The analytical portion of the PCATS is designed to measure continuous profiles of P-wave velocity and gamma density at *in situ* pressure and temperature conditions on HYACINTH pressure cores, as well as collect high-resolution 2D X-ray images (Fig. 2). To perform these analyses, the PCATS extracts the lined cores from the HYACINTH corer autoclaves under pressure and moves them past the sensors. The PCATS was modified to accept PCS corer autoclaves. As the PCS core could not be extracted under pressure, only gamma density and X-ray images could be collected on these cores and at a reduced resolution.

The X-ray images collected from pressure cores taken in the Krishna-Godavari Basin showed hydrate structures with remarkable complexity and in unprecedented detail (Fig. 2A). Cores were rotated in the PCATS to understand their three-dimensional nature. Less dense (lighter) patches in the original X-ray (Figs. 2A, 2C) are dipping veins of gas hydrate when seen from a perpendicular view (Fig. 2D). The P-wave velocity and gamma density profiles also reflect this anisotropy. In the first data set (Fig. 2C), the profiles were taken perpendicular to (through) the major gas hydrate veins, and a slight lowering of density and a smooth increase in P-wave velocity is seen in the area of greatest gas hydrate concentration (Fig. 2C). In the second data set (Fig. 2D), the
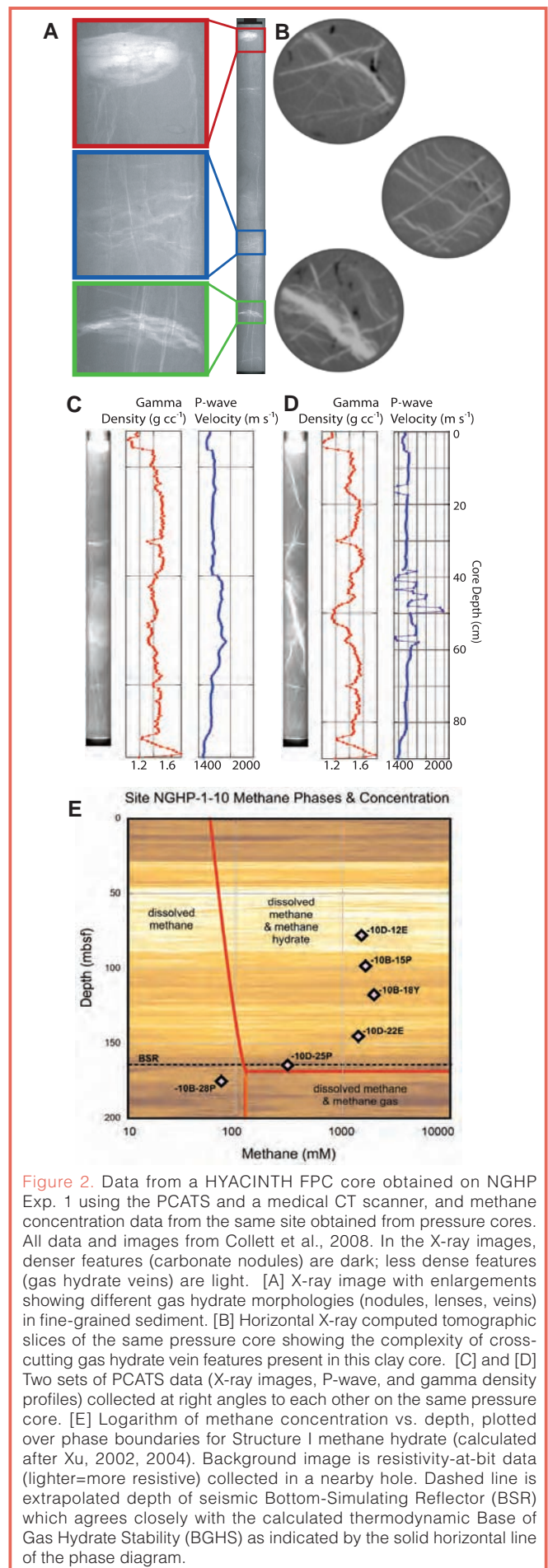
Figure 2. Data from a HYACINTH FPC core obtained on NGHP Exp. 1 using the PCATS and a medical CT scanner, and methane concentration data from the same site obtained from pressure cores. All data and images from Collett et al., 2008. In the X-ray images, denser features (carbonate nodules) are dark; less dense features (gas hydrate veins) are light. [A] X-ray image with enlargements showing different gas hydrate morphologies (nodules, lenses, veins) in fine-grained sediment. [B] Horizontal X-ray computed tomographic slices of the same pressure core showing the complexity of cross-cutting gas hydrate vein features present in this clay core. [C] and [D] Two sets of PCATS data (X-ray images, P-wave, and gamma density profiles) collected at right angles to each other on the same pressure core. [E] Logarithm of methane concentration vs. depth, plotted over phase boundaries for Structure I methane hydrate (calculated after Xu, 2002, 2004). Background image is resistivity-at-bit data (lighter=more resistive) collected in a nearby hole. Dashed line is extrapolated depth of seismic Bottom-Simulating Reflector (BSR) which agrees closely with the calculated thermodynamic Base of Gas Hydrate Stability (BGHS) as indicated by the solid horizontal line of the phase diagram.

profiles are taken parallel to (along) the major gas hydrate veins, showing low-density zones and a complex P-wave velocity profile. Some extreme values are artifacts caused by pulse interference effects from hydrate structures.

A decision was made to hold five of these cores for additional, more detailed shore-based investigations. The morphology of the gas hydrate within this clay-hosted deposit is worth extended study, not only to explain the mechanisms of gas hydrate growth in fine-grained sediments but also to predict the sediment behavior during gas hydrate dissociation. Models predicting the behavior of such gas-hydrate-bearing sediments during dissociation, whether for well-bore stability, geohazard assessment, or potential methane gas production, are certainly dependent on the small-scale spatial relationship in the sediment. X-ray computed tomography (CT) scans showed that the fine-grained sediments hosted a complex gas hydrate vein network (Fig. 2B). The pressure cores were individually transferred into the Instrumented Pressure Testing Chamber (IPTC; Yun et al., 2006) using the PCATS. Measurements of P-wave velocity, S-wave velocity, electrical resistance, and strength of the sediment were made at regular intervals along the three pressure cores. Cores were then sub-sampled under pressure with the HYACINTH PRESS system (Parkes et al., in press) or rapidly depressurized and placed in liquid nitrogen for further analyses at varous laboratories.

The rest of the pressure cores had been depressurized onboard the ship directly after PCATS analyses to determine

Figure 3. [A] Gas hydrate saturation from porewater freshening (blue circles) and from depressurization experiments and methane mass balance from pressure cores (red circles) at Site SH2 in the Shenhu area, South China Sea (Wu et al., in press). [B] Example of gas-hydrate-bearing sediment from 204 mbsf at Site SH2. Though the core has a gas hydrate saturation of approximately 30% by pore volume, no gas hydrate was visible to the naked eye. [C] A gas-hydrate-bearing pressure core is slowly depressurized to release methane. A rough compositional test is sometimes performed before gas chromatographic analysis.

the exact methane content and hence the gas hydrate saturation (Fig. 2E). Pressure cores are the "gold standard" for gas hydrate quantification and are used to calibrate other methods of gas hydrate detection. The slow, isothermal release of pressure from a pressure core allows gases to exsolve from pore fluids and allows gas hydrate to dissociate. Measuring the quantity of gas, its composition, and its evolution relative to time and pressure provides information on the quantity, composition, and surface area of gas hydrate (Kvenvolden et al., 1983; Dickens et al., 2000; Milkov et al., 2004). The fundamental number obtained through these experiments is the nominal concentration of methane in the pore fluids, assuming all methane is in solution. If this nominal concentration is greater than the calculated methane saturation, gas hydrate (or free gas, depending on the thermodynamic conditions) is assumed to be present, and the amount can be quantitatively calculated. Data that shows the sediment is under-saturated in methane is equally important, as careful pressure core analysis is the only technique that can confirm the absence of gas hydrate. Figure 2E shows pressure core methane data from the same site as the core shown in Figs. 2A–D. All pressure cores taken above the base of gas hydrate stability were oversaturated in methane, allowing calculation of the exact quantity of gas hydrate contained in the cores.

China, 2007

China's first gas hydrate drilling expedition, GMGS-1 (Fig. 1), was carried out by Fugro and Geotek for the Guangzhou Marine Geological Survey (GMGS), China Geological Survey (CGS), and the Ministry of Land and Resources of China. The expedition took place on the geotechnical drillship *SRV Bavenit*, which visited eight sites in the northern South China Sea (Zhang et al., 2007; Yang et al., 2008; Wu et al., in press) from April to June 2007. The project goal—to determine the gas hydrate distribution at as many sites as possible in the allotted time—required maximum flexibility in the drilling program. The strategy was to use pressure cores (FPC and FRPC) and conventional wireline piston cores to ground-truth wireline logs, and after confidence was developed in the downhole log interpretation, some locations were surveyed by downhole log alone.

Gas hydrate was detected in a thick layer (10–25 m) just above the base of gas hydrate stability at three of the five sites cored. PCATS pressure core analysis provided ground-truth for gas hydrate saturation, as well as gamma density, P-wave velocity, and X-ray images at *in situ* pressure. Gas hydrate occupied pores between silty clay sediment grains, in direct contrast to the hydrate-bearing clays cored off India, which contained hydrate at similar overall saturations but in distinct veins and layers. While surprising, this conclusion is based on the extremely high gas hydrate saturations (20%–40% of pore volume), the nature of the matrix (variably silty clay), the elevated P-wave velocities (over 2000 m s^{-1}) without change in the gamma density, and the smooth, pre-
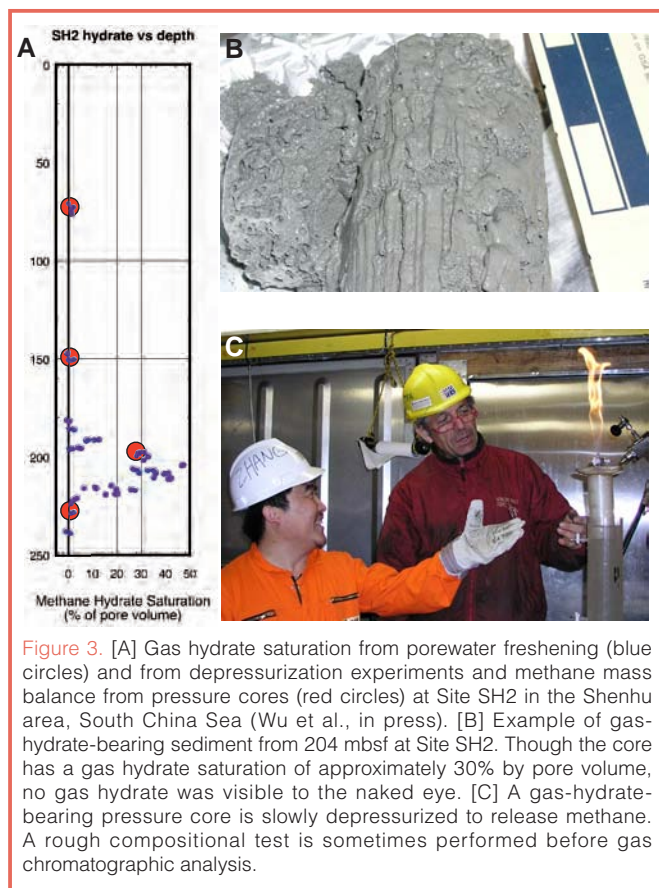
dictable increases in downhole sonic velocity and electrical resistivity.

The distribution of gas hydrate in the Shenhu region, within the sediment column and at the grain scale, is unusually simple and uniform. Its presentation in a relatively homogenous layer, directly above the base of gas hydrate stability, is the type of distribution predicted from simple models of gas hydrate formation (Hyndman and Davis, 1992; Xu and Ruppel, 1999). However, a clear field example of such a gas hydrate distribution has not previously been reported. Similarly, the homogeneous, pore-filling, small-scale hydrate distribution found at Shenhu is the type of distribution typically used when modeling gas hydrate formation and dissociation in sediments of all grain sizes. Both of these characteristics would allow the gas-hydrate-bearing sediments in the Shenhu deposit to be used to test the assumptions and predictions, at various scales, of some gas hydrate models.

Korea, 2007

Ulleung Basin Gas Hydrate Expedition 1 (UBGH1) was South Korea's first large-scale gas hydrate exploration and drilling expedition in the East Sea (Fig. 1; Park et al., 2008). It took place from September to November 2007, aboard the multipurpose offshore support vessel *REM Etive*, which was converted to a drilling ship by Fugro Seacore using the heave-compensated R100 portable drill rig. The Korean National Oil Company (KNOC) and Korean Gas Corporation (KOGAS), advised by the Korean Gas Hydrate R&D Organization and the Korean Institute of Geoscience and Mineral Resources (KIGAM), contracted Fugro, Schlumberger, and Geotek to investigate five seismically identified locations for gas hydrate in the Ulleung basin (Stoian et al., 2008). After the previous expeditions, pressure core analysis was recognized as the key dataset to which all others could be referenced (Schultheiss et al., 2008b).

Gas hydrate was detected at all three sites cored in the clay matrix as veins and layers, and as pore-filling material within silty/sandy layers. Both types of gas hydrate habit were observed in FPC and FRPC pressure cores via the PCATS datasets (gamma density, P-wave velocity, X-ray images), using a PCATS newly equipped with automated rotational and translational capability. The shipboard PCATS data showed that a number of cores contained a particularly dense network of gas hydrate veins (Fig. 4A). These cores were not depressurized onboard, but instead were transferred under pressure to HYACINTH storage chambers and saved for detailed post-cruise analysis.

At one site, a 130-m-thick gas-hydrate-bearing sedimentary interval of interbedded sands and clay was penetrated. This is one of the thickest gas-hydrate-bearing intervals to be documented worldwide. The gas hydrate saturation from analysis of pressure cores, which average over a one-meter sample, was 11%–27% gas hydrate by pore volume in this
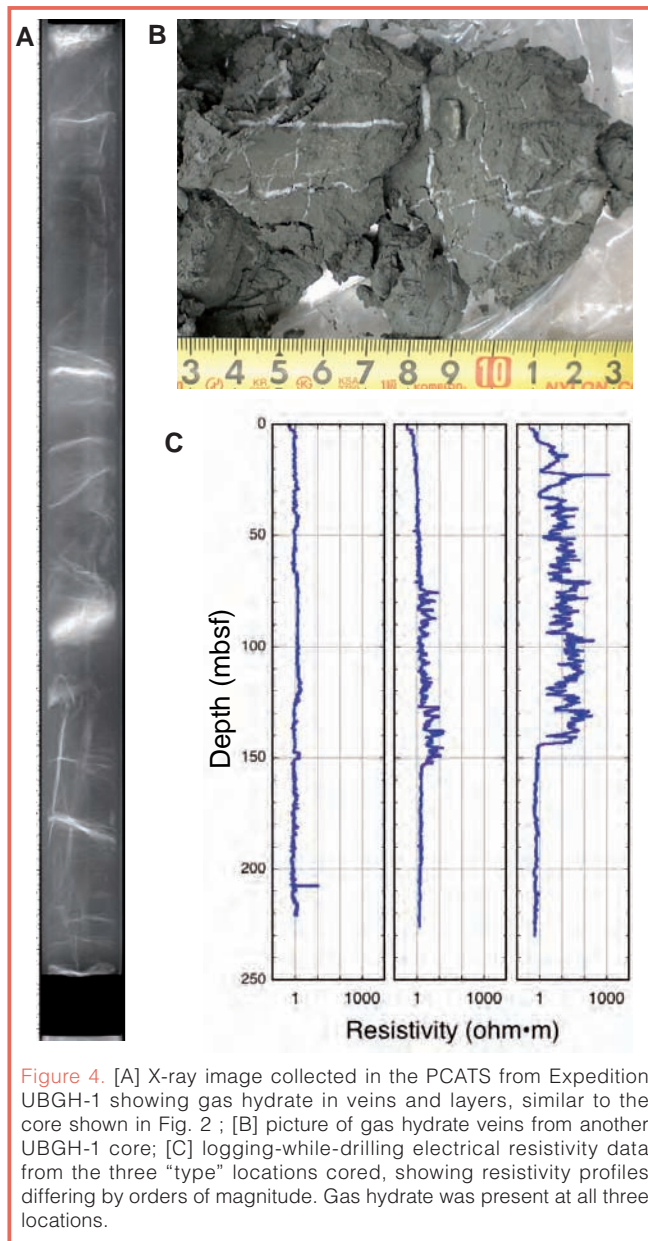
Figure 4. [A] X-ray image collected in the PCATS from Expedition UBGH-1 showing gas hydrate in veins and layers, similar to the core shown in Fig. 2 ; [B] picture of gas hydrate veins from another UBGH-1 core; [C] logging-while-drilling electrical resistivity data from the three "type" locations cored, showing resistivity profiles differing by orders of magnitude. Gas hydrate was present at all three locations.

interval. Because much of the gas hydrate was in grain-displacing veins and layers, there was no obvious quantitative relationship between the electrical resistivity logs and the average gas hydrate saturation, though the overall magnitudes were correlated (Fig. 4C).

X-ray CT scanning of the saved pressure cores confirmed the PCATS data, showing a complex fracture structure within the sediment that was filled with gas hydrate. This information aided in the selection of locations for further geophysical testing inside cores relative to the sedimentological and gas hydrate structures. These specific locations were tested with the IPTC, using the direct-contact probes to measure P-wave velocity, S-wave velocity, electrical resistivity, and strength. The combined translational and rotational precision of the PCATS and the radial precision of the IPTC allowed probes to be inserted into the cores with millimeter accuracy. The preliminary data indicated that physical properties varied on a sub-centimeter-scale in these

pressure cores containing thin hydrate veins (Park et al., 2009).

While five of these cores were depressurized to determine hydrate saturation during physical measurements ("mini-production tests"), some of the cores were preserved for further gas hydrate studies. Two of the cores that were tested were rapidly depressurized and portions stored in liquid nitrogen for further testing. In addition, the most lavishly-veined core was not tested invasively and remains stored under pressure, awaiting equipment to be designed for further pressurized analyses.

Future HYACINTH Developments

When a new technique appears, or an old technique is applied in a new location, new insights follow. The recent HYACINTH deployments have provided such new insights into the nature and morphology of natural gas hydrate (Holland et al., 2008). To continue these ground-breaking studies, we are making technological improvements to the HYACINTH system and hope to deploy it in exciting and diverse formations, on land and under the sea.

Over their development period, both the FPC and FRPC have been incrementally modified to improve their success at retaining pressure and the quality of the cut core. Over the last two years success rates for both tools has been 70%–80%. The success of such sophisticated tools is markedly improved when operated in a stable drill string. Experimentation with systems used routinely in geotechnical drilling, such as seabed frames in which to clamp the drill string, has shown that both the success rate and core quality improve relative to those taken in an unclamped string.

Like all equipment in a state of continuing development, the HYACINTH tools currently have some intrinsic limitations and inconsistencies, which are being addressed over time as funding and opportunities allow. The diameter of the core recovered by the two corers is 57 mm for the FPC and 51 mm for the FRPC, and developments have been planned to increase the diameter of the FRPC core to match that of the FPC for increased compatibility in downstream analyses. An increase in the length of the recovered cores (currently one meter) is also planned to ensure recovery of the target formations and to maximize the use of valuable ship time.

The ability to manipulate cores, take sub-samples, and make measurements—all at *in situ* pressures—were major objectives of the HYACINTH project. Like the coring tools themselves, the PCATS has been improved over the past few years and has major new improvements planned in the next few years. Non-destructive measurements of pressure cores in the PCATS have been vitally important as an immediate survey of the core, to determine if a successful core has been retrieved and to look for obvious signs of the presence of gas hydrate. PCATS measurements have also provided primary data on sediment-hydrate properties to ground-truth larger-scale measuremnts. The main analytical improvement that has been made to the PCATS system is the core manipulation capabilities, that now include fully automated translational and rotational control (±0.5 mm and ±0.5° of accuracy, respectively). A combination of precise rotational capability with high-resolution X-ray imaging provides three-dimensional X-ray visualization through the core that enables complex structural features to be examined in detail. This capability has been used to provide remarkable images, showing the complexity of gas hydrate vein networks that can exist in fine-grained sediments, as well as crucial clues to hydrate vein origin and growth mechanisms. In the future, CT software integration could enable PCATS to collect and display X-ray CT data along with the current high-resolution gamma density and P-wave velocity profiles.

Planned improvements to the PCATS infrastructure in the near future include lengthening the system to accept core up to 3.5 m long and active temperature control. In addition, a versatile cutter arrangement to subsection long

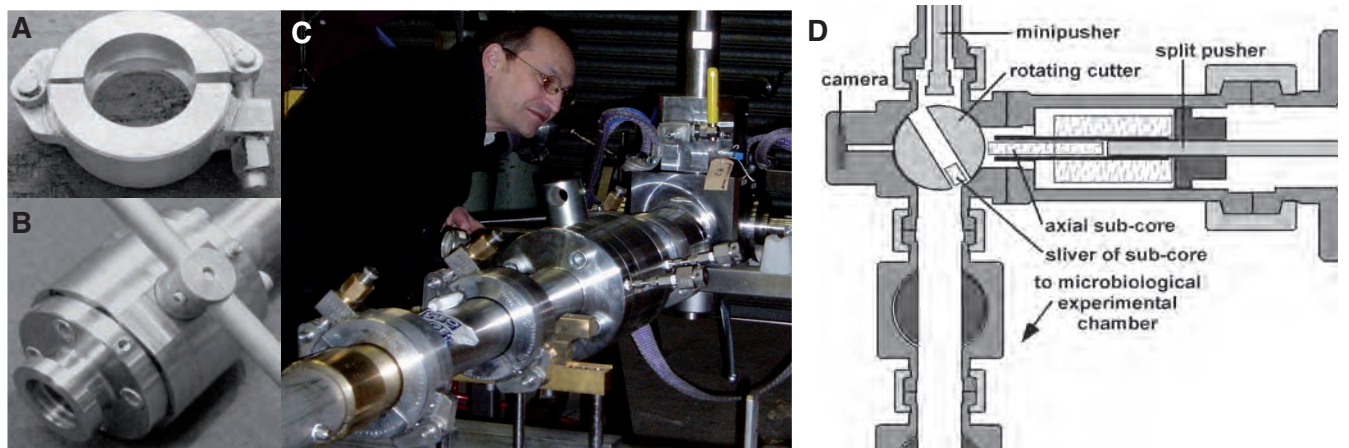Figure 5. Interfacing third-party equipment to the HYACINTH PCATS. [A] Quick-clamp; [B] ball valve (65 mm internal diameter) and mating flange; [C] the DeepIsoBug, showing ball valves and quick-clamps in use ; [D] diagram of the complex subcoring and sampling mechanism at the heart of the DeepIsoBug. All manipulations are carried out under hyperbaric pressure equivalent to *in situ* hydrostatic pressure.

cores into custom lengths will allow further analysis or storage, as is most appropriate. Parts of a core might be depressurized on board ship, while other parts of the same core could be stored under pressure for shore-based studies. This increased flexibility will enable all cores to be more fully assessed and will further increase the value of every pressure core recovered.

PCATS was envisaged and designed as the midpoint, not the endpoint, of a full pressure coring and pressure core analysis system. Upstream compatibility to new coring tool developments and downstream compatibility to third-party equipment is paramount to its future evolution. The specifications for the HYACINTH mating flange, clamps, and ball valves used in the PCATS (Fig. 5) are publicly available, and any investigator may design "PCATS-compatible" pressurized equipment. Independent research scientists have already developed pressurized equipment that has been used with the PCATS and stored HYACINTH cores, including the previously mentioned IPTC and the DeepIsoBug (Schultheiss et al., 2006; Parkes et al., in press). The DeepIsoBug, designed to take aseptic slices of a subcore for use in pressurized microbial culturing, has prototyped some extremely complex core sampling mechanisms under pressure (Fig. 5D). There are also developments underway for other PCATS-compatible test apparatus to enable more sophisticated geotechnical measurements on pressure core samples.

The ODP and the IODP have been fundamental to the development of the HYACINTH tools and infrastructure. Since its last use for IODP on Exp. 311, the system has continued to be used and improved on commercially funded expeditions. With the restart of *JOIDES Resolution* drilling, the scientific community can reap the benefits of these commercial improvements in pressure coring and analysis, and will be able to realize its initial investment in these pressure coring and pressure core analysis systems.

Acknowledgements

The authors would like to thank all of the crews, technical staff, and scientists who sailed on ODP Legs 194, 201, 204, and IODP Exp. 311, for their patience as the HYACINTH system found its feet. We would also like to thank the literally hundreds of people involved in the Indian, Chinese, and Korean gas hydrate expeditions, especially the funding agencies (noted in the text) that made the work possible.

References

Collett, T.S., Riedel, M., Boswell, R., Cochran, J.R., Kumar, P., Sethi, A.K., Sathe, A.V., and NGHP Expedition-01 Scientific Party, 2006. International team completes landmark gas hydrate expedition in the offshore of India. *Fire in the Ice* (U.S. DOE–NETL newsletter) Fall 2006, 1–4.

Collett, T., Riedel, M., Cochran, J., Boswell, R., Presley, J., Kumar, P., Sathe, A., Sethi, A., Lall, M., Sibal, V., and the NGHP Expedition 01 Scientists, 2008. *Indian National Gas Hydrate Program Expedition 01 Initial Reports*, Indian Directorate General of Hydrocarbons, New Delhi, India.

Dickens, G.R., Wallace, P.J., Paull, C.K., and Borowski, W.S., 2000. Detection of methane gas hydrate in the pressure core sampler (PCS): volume-pressure-time relations during controlled degassing experiments. *In* Paull, C.K., Matsumoto, R., Wallace, P.J., and Dillon, W.P. (Eds.), *Proc. ODP, Sci. Results, 164*, College Station, Texas (Ocean Drilling Program), 113–126.

Holland, M., Schultheiss, P., Roberts, J., and Druce, M., 2008. Observed gas hydrate morphologies in marine sediments. *Proc. 6th Intl. Conf. Gas Hydrates (ICGH 2008)*, Vancouver, British Columbia, Canada, 6–10 July 2008.

Hyndman, R.D., and Davis, E.E., 1992. A mechanism for the formation of methane hydrate and seafloor bottom-simulating reflectors by vertical fluid expulsion. *J. Geophys. Res.*, 97:7025–7041, doi:10.1029/91JB03061.

Graber, K.K., Pollard, E., Jonasson, B. and Schulte, E., 2002. Overview of ODP engineering tools and hardware. *ODP Tech. Note* 31, College Station, Texas (Ocean Drilling Program).

Kvenvolden, K.A., Barnard, L.A., and Cameron, D.H., 1983. Pressure core barrel: application to the study of gas hydrates, Deep Sea Drilling Project Site 533, Leg 76. *In* Sheridan, R.E., Gradstein, F.M., et al., *Init. Repts. DSDP 76*, Washington, DC (U.S. Govt. Printing Office), 367–375.

Milkov, A.V., Dickens, G.R., Claypool, G.E., Lee, Y-J., Borowski, W.S., Torres, M.E., Xu, W., Tomaru, H., Tréhu, A.M., and Schultheiss, P., 2004. Coexistence of gas hydrate, free gas, and brine within the regional gas hydrate stability zone at Hydrate Ridge (Oregon margin): evidence from prolonged degassing of a pressurized core. *Earth Planet. Sci. Lett.*, 222:829–843., doi:10.1016/j.epsl.2004.03.028.

Park, K.-P., Bahk, J.-J., Kwon, Y., Kim, G.Y., Riedel, M., Holland, M., Schultheiss, P., Rose, K., and the UBGH-1 Scientific Party, 2008. Korean National Program expedition confirms rich gas hydrate deposits in the Ulleung basin, East Sea. *Fire in the Ice* (U.S/ DOE–NETL newsletter) Spring 2008, 6–9.

Park, K.-P., Bahk, J.-J., Holland, M., Yun, T.-S., Schultheiss, P.J., Santamarina, C., 2009. Improved pressure core analysis provides detailed look at Korean cores. *Fire in the Ice* (U.S. DOE-NETL Newsletter), Winter 2009.

Parkes, R.J., Amann, H., Holland, M., Martin, D., Schultheiss, P.J., Anders, E., Wang, X., and Dotchev, K., 2008. Technology for high-pressure sampling and analysis of deep sea sediments, associated gas hydrates and deep biosphere processes. *In* Collett, T. (Ed.), *AAPG Special Volume on Gas Hydrates*, in press.

Pettigrew, T.L., 1992. Design and operation of a wireline pressure core sampler. *ODP Tech. Note 17*, College Station, Texas (Ocean Drilling Program).

Riedel, M., Collett, T.S., Malone, M.J., and the Expedition 311 Scientists, 2006. *Proc. IODP, Exp. Repts., 311*, College Station, Texas (Ocean Drilling Program).

Schultheiss, P.J., Francis, T. J.G., Holland, M., Roberts, J.A., Amann, H., Thjunjoto, Parkes, R.J., Martin, D., Rothfuss, M., Tuynder, F., and Jackson, P.D., 2006. Pressure coring, logging and sub-sampling with the HYACINTH system.

In Rothwell, G. (Ed.), *New Techniques in Sediment Core Analysis, Geol. Soc. London, Spec. Pub.*, 267:151–163.

Schultheiss, P.J., Holland, M.E., and Humphrey, G.D., 2008a. Borehole pressure coring and laboratory pressure core analysis for gas hydrate investigations, OTC 19601. *Proc. Offshore Technology Conference*, Houston, Texas, 5–8 May 2008.

Schultheiss, P., Holland, M., Roberts, J., and Humphrey, G., 2008b. Pressure core analysis as the keystone of a gas hydrate investigation. *Proc. 6th Intl. Conf. Gas Hydrates (ICGH 2008)*, Vancouver, British Columbia, Canada, 6–10 July 2008.

Stoian, I., Park, K.-P., Yoo, D.-G., Haacke, R.R., Hyndman, R.D., Riedel, M., and Spence, G.D., 2008. Seismic reflection blank zones in the Ulleung Basin, offshore Korea, associated with high concentrations of gas hydrate. *Proc. 6th Intl. Conf. Gas Hydrates (ICGH 2008)*, Vancouver, British Columbia, Canada, 6–10 July 2008.

Takahashi, H., and Tsuji, Y., 2005. Multi-well exploration program in 2004 for natural hydrate in the Nankai trough, offshore Japan, OTC 17162. *Proc. Offshore Technology Conference*, Houston, Texas, 2–5 May 2005.

Tréhu, A.M, Bohrmann, G., Rack, F.R., Torres, M.E., et al., 2003. *Proc. ODP, Init. Repts., 204.* [CD-ROM]. Available from: Ocean Drilling Program, Texas A&M University, College Station, Texas 77845-9547, U.S.A.

Wu, N., Yang, S., Zhang, H., Liang, J., Schultheiss, P., Holland, M., Wang, H., Wu, D., Su, X., Fu, S., and Zhu, Y., 2008. Gas hydrate system of Shenhu Area, Northern South China Sea: Preliminary geochemical results. *J. Asian Earth Sci.*, in press.

Xu, W., 2002. Phase balance and dynamic equilibrium during formation and dissociation of methane gas hydrate. *Proc. 4th Intl. Conf. Gas Hydrates*, 19023:199–200, Yokohama, Japan.

Xu, W., 2004. Modeling dynamic marine gas hydrate systems. *Am. Mineralogist*, 89: 1271–1279.

Xu, W., and Ruppel, C., 1999. Predicting the occurrence, distribution and evolution of methane gas hydrates in porous sediments. *J. Geophys. Res.*, 104:5081–5096, doi:10.1029/1998 JB900092.

Yang, S., Zhang, H., Wu, N., Su, X., Schultheiss, P., Holland, M., Zhang, G., Liang, J., Lu, J., and Rose, K., 2008. High concentration hydrate in disseminated forms obtained in Shenhu area, North Slope of South China Sea. Proc. 6th Intl. Conf. Gas Hydrates (ICGH 2008), Vancouver, British Columbia, Canada, 6–10 July 2008.

Yun, T.S., Narsilio, G., Santamarina, J.C., and Ruppel, C., 2006. Instrumented pressure testing chamber for characterizing sediment cores recovered at *in situ* hydrostatic pressure. *Mar. Geol.*, 229:285–293, doi:10.1016/j.margeo.2006. 03.012.

Zhang, H., Yang, S., Wu, N., Su, X., Holland, M., Schultheiss, P., Rose, K., Butler, H., Humphrey, G., and the GMGS-1 Science Team, 2007. Successful and surprising results for China's first gas hydrate drilling expedition. *Fire in the Ice* (U.S. DOE–NETL newsletter) Fall 2007, 6–9.

ZoBell, C.E., and Morita, R.Y., 1957. Barophilic bacteria in some deep-sea sediments. *J. Bacteriol.*, 73:563–568.

Authors

Peter Schultheiss, Geotek Ltd., 3 Faraday Close, Daventry, Northants, NN11 8RD, UK.
Melanie Holland, Geotek Ltd., 3 Faraday Close, Daventry, Northants, NN11 8RD, UK, e-mail:melanie@geotek.co.uk.
Gary Humphrey, Fugro GeoConsulting, Inc., 6100 Hillcroft Avenue, Houston, Texas, 77081, U.S.A.

Related Web Links

http://www.netl.doe.gov/technologies/oil-gas/publications/Hydrates/Newsletter/HMNewsFall06.pdf
https://circle.ubc.ca/handle/2429/1201
http://www-odp.tamu.edu/publications/tnotes/tn31/INDEX.HTM
http://www.netl.doe.gov/technologies/oil-gas/publications/Hydrates/Newsletter/HMNewsSpring08.pdf
https://circle.ubc.ca/handle/2429/1200
https://circle.ubc.ca/handle/2429/1162
https://circle.ubc.ca/handle/2429/1178
http://www.netl.doe.gov/technologies/oil-gas/publications/Hydrates/Newsletter/HMNewsFall07.pdf
http://www.ngdc.noaa.gov/mgg/image/2minrelief.html

Photo Credits

Fig. 3: N. Wu, GMGS. (Currently at GIEC, Guangzhou Institute of Energy Conversion)
Fig. 4: J. -H. Chun, KIGAM
Fig. 5: P. Schultheiss

Scientific Collaboration on Past Speciation Conditions in Lake Ohrid–SCOPSCO Workshop Report

by Bernd Wagner, Thomas Wilke, Sebastian Krastel-Gudegast, Andon Grazhdani, Klaus Reicherter, Sasho Trajanovski, and Giovanni Zanchetta
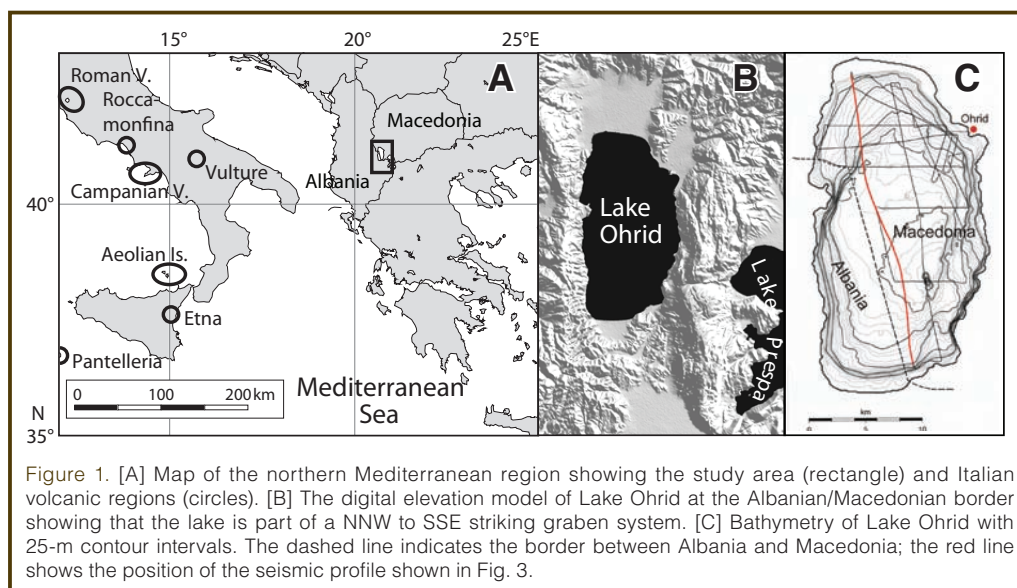
Transboundary Lake Ohrid between Albania and Macedonia (SE Europe, Fig. 1) is considered to be the oldest continuously existing lake in Europe with a likely age of three to five million years. The lake has a surface area of 360 km^2 and is 289 m deep. An extraordinarily high degree of endemism, including more than 210 described endemic species (Fig. 2), makes the lake a unique aquatic ecosystem of worldwide importance. Due to its old age, Lake Ohrid is one of the very few lakes in the world representing a hot spot of evolution and a potential evolutionary reservoir enabling the survival of relict species (Albrecht and Wilke, 2008). Its importance was emphasized when the lake was declared a UNESCO World Heritage Site in 1979.

The continuous existence since the Tertiary makes Lake Ohrid an excellent archive of environmental changes in the northern Mediterranean region. Because of its geographic position and its presumed age, Lake Ohrid represents an important link between climatic and environmental records from the Mediterranean Sea and the adjacent continents. In the eastern Mediterranean Sea, most records focus on the Late Pleistocene and Holocene history (Geraga et al., 2005), and only few cover several glacial-interglacial cycles (Schmiedl et al., 1998). Similarly, most terrestrial records from this region are restricted to the Late Pleistocene and Holocene (Denèfle et al., 2000; Sadori and Narcisi, 2001). Longer continuous records covering more than the last glacial-interglacial cycle are relatively sparse (Wijmstra, 1969; Tzedakis et al., 1997). Extant sedimentary records from Lake Ohrid were recovered during field campaigns in 1973 (Roelofs and Kilham, 1983) and more recently between 2001 and 2007 (Belmecheri et al., 2007; Matzinger et al., 2007; Wagner et al., 2008a, 2008b). These records cover (with some hiatuses) the past glacial-interglacial cycle and reveal that Lake Ohrid is a valuable archive of volcanic ash dispersal and climate change in the northern Mediterranean region. However, with respect to the extraordinarily high en-

demism in the lake, these records are too short to provide information about the age and origin of the lake and to unravel the mechanisms controlling the evolutionary development. Molecular clock analyses of mitochondrial DNA genes from several endemic species flocks (i.e., groups of closely related species) indicate that Lake Ohrid is probably two to three million years old (Albrecht and Wilke, 2008). Moreover, concurrent genetic breaks in several invertebrate groups indicate that major geological and/or environmental events must have shaped the evolutionary history of endemic faunal elements in Lake Ohrid (Albrecht and Wilke, 2008).

Different site surveys between 2004 and 2008 (Wagner et al., 2008b) focused on a detailed seismic investigation of the sedimentological inventory of the lake and on the recovery of sediment sequences spanning the last glacial-interglacial cycle. The results of these site surveys emphasized the potential of Lake Ohrid for deep drilling. Such a drilling will allow us to:

- understand the impact of major geological/environmental events on general evolutionary patterns and on generating an extraordinary degree of endemic biodiversity as a matter of global significance,

- obtain a continuous record containing information on tectonic and volcanic activities and climate changes in the northern Mediterranean region, and

Figure 1. [A] Map of the northern Mediterranean region showing the study area (rectangle) and Italian volcanic regions (circles). [B] The digital elevation model of Lake Ohrid at the Albanian/Macedonian border showing that the lake is part of a NNW to SSE striking graben system. [C] Bathymetry of Lake Ohrid with 25-m contour intervals. The dashed line indicates the border between Albania and Macedonia; the red line shows the position of the seismic profile shown in Fig. 3.
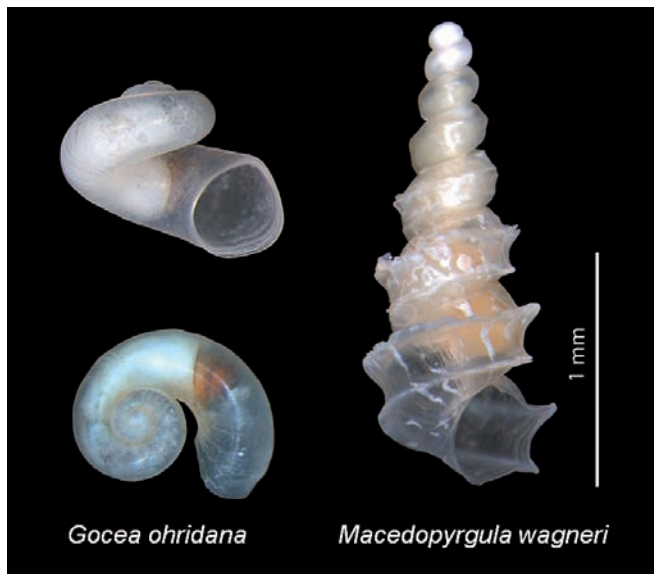
Figure 2. Photographs from two representatives of the more than 210 endemic species of Lake Ohrid.

- obtain more precise information about age and origin of the lake and, thus, meet key issues of International Continental Scientific Drilling Program (ICDP).

Under the auspices of the ICDP, on 13–17 October 2008 a workshop was held on the **S**cientific **C**ollaboration **O**n **P**ast **S**peciation **C**onditions in Lake **O**hrid (SCOPSCO) in the city of Ohrid, Republic of Macedonia. Its intent was to review the existing datasets and interpretations as well as discussions on objectives and intended achievements, required laboratory analyses and techniques, scientific collaboration and responsibilities, drill sites and operations, logistics, legal issues, and funding. Altogether, thirty-four scientists from eleven nations (Albania, France, Germany, Italy, Macedonia,

Netherlands, Poland, Sweden, Switzerland, U.K., and U.S.A.) participated in the workshop. The agenda included the presentation of posters and talks on the first day, the formation of breakout groups and a half-day excursion on the second day, and the presentation and discussion of the results and goals defined by the breakout groups, as well as a discussion of future steps towards deep drilling, on the third day.

Overall, **nineteen talks provided a general introduction** into the SCOPSCO project, the history of the region and the Hydrobiological Institute in Ohrid, and an overview on existing geological, recent biological, tectonic, and sedimentological datasets. In addition, five posters focusing on tectonic and biological aspects were presented. After the presentation of talks and posters on the first day, three breakout groups were formed in order to define the specific aims and drill sites of a future deep drilling campaign. The three breakout groups focused on **the following topics:** (1) speciation and endemism in Lake Ohrid, (2) seismic and neotectonic issues in Lake Ohrid and its vicinity, **and** (3) sedimentological and tephrostratigraphical questions to be addressed within the scope of the SCOPSCO project.

The breakout group on speciation and endemism in Lake Ohrid defined two to three drill sites close to recent subaquatic springs in the lake where a high degree of endemism can be observed. The seismic and neotectonic breakout group defined several drilling target sites on the basis of more than 500 km of seismic profiles across the lake (Figs. 1 and 3). **Drilling less than about 200 m into the** sediments **at these sites will allow for a better understanding** of the sediment input into the lake, the formation and chronology of foresets and slides (**particularly in the southern** part of the lake), **and the fault development mainly along the** western and eastern sides of the lake. **One drill site was** defined **for sedimentological** and tephrostratigraphical issues, including the reconstruction of the past environmental conditions at Lake Ohrid throughout its existence. This main drill site is located in the central, almost deepest part of the lake, where a sediment fill of about 700 m (Fig. 3) promises to contain the complete history of the lake back to its origin.

Possible overlaps, particularly between sites for studying neotectonic activities and those providing information to speciation and endemism around the
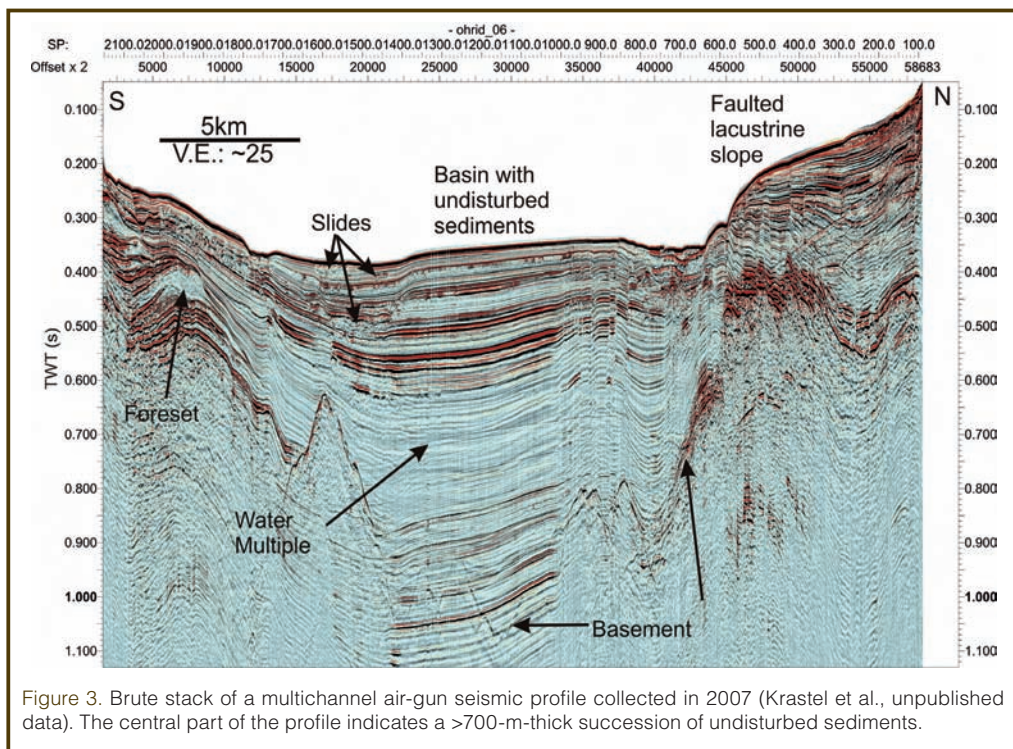

Figure 3. Brute stack of a multichannel air-gun seismic profile collected in 2007 (Krastel et al., unpublished data). The central part of the profile indicates a >700-m-thick succession of undisturbed sediments.

springs, will reduce the number of total target sites to about five or six. For all sites, downhole logging and core logging issues were discussed and defined.

The excursion in the afternoon of the second day led to the Galicica Mountains, which separate lakes Ohrid and Prespa, and later to the southeastern part of Lake Ohrid to visit St. Naum springs, which form a major part of the water supply to the lake. The third day of the workshop focused on future steps towards an ICDP deep drilling campaign, with respect to logistic and legal issues, funding within the scope of national and international programs, and support by local ministries and institutes. Finally, the schedule for submission of a full proposal was established.

In summary, the SCOPSCO workshop provided a reliable platform to discuss the present state of knowledge and future steps towards a deep drilling campaign. A full proposal for an ICDP drilling campaign will be submitted in 2009.

Acknowledgements

References

Albrecht, C., and Wilke, T., 2008. Ancient Lake Ohrid: biodiversity and evolution. *Hydrobiologia*, 615:103–140, doi:10.1007/s10750-008-9558-y.

Belmecheri, S., von Grafenstein, U., Bordon, A., Andersen, N., Lézine, A.M., Mazaud, A., and Grenier, C., 2007. Last Glacial-interglacial cycle palaeoclimatology and palaeoecology reconstruction in the southern Balkans: an ostracode stable isotope record from Lake Ohrid (Albania). *Geophys. Res. Abstr.*, 9:09622.

Denèfle, M., Lézine, A.M., Fouache, E., and Dufaure, J.J., 2000. A 12,000 year pollen record from Lake Maliq, Albania. *Quat. Res.*, 54:423–432, doi:10.1006/qres.2000.2179.

Geraga, M., Tsaila-Monopolis, S., Ioaim, C., Papatheodorou, G., and Ferentinos, G., 2005. Short-term climate changes in the southern Aegean Sea over the last 48,000 years. *Palaeogeogr. Palaeoclimatol. Palaeoecol.*, 220:311–332, doi:10.1016/j.palaeo.2005.01.010.

Matzinger, A., Schmid, M., Veljanoska-Sarafiloska, E., Patceva, S., Guseka, D., Wagner, B., Sturm, M., Müller, B., and Wüest, A., 2007. Assessment of early eutrophication in ancient lakes – A case study of Lake Ohrid. *Limnol. Oceanogr.*, 52:338–353.

Roelofs, A.K., and Kilham, P., 1983. The diatom stratigraphy and paleoecology of Lake Ohrid, Yugoslavia. *Palaeogeogr. Palaeoclimatol. Palaeoecol.*, 42:225–245, doi:10.1016/0031-0182(83)90024-X.

Sadori, L., and Narcisi, B., 2001. The postglacial record of environmental history from Lago di Pergusa, Sicily. *The Holocene*, 11:655–670, doi:10.1191/09596830195681.

Schmiedl, G., Hemleben, C., Keller, J., and Segl, M., 1998. Impact of climatic changes on the benthic foraminiferal fauna in the Ionian Sea during the last 330,000 years. *Paleoceanography*, 13:447–458, doi:10.1029/98PA01864.

Tzedakis, P.C., Andrieu, V., de Beaulieu, J.-L., Crowhurst, S., Follieri, M., Hooghiemstra, H., Magri, D., Reille, M., Sadori, L., Shackleton, N.J., and Wijmstra, T.A., 1997. Comparison of terrestrial and marine records of changing climate of the last 500,000 years. *Earth Planet. Sci. Lett.*, 150:171–176, doi:10.1016/S0012-821X(97)00078-2.

Wagner, B., Lotter, A.F., Nowaczyk, N., Reed, J.M., Schwalb, A., Sulpizio, R., Valsecchi, V., Wessels, M., and Zanchetta, G., 2008a. A 40,000-year record of environmental change from ancient Lake Ohrid (Albania and Macedonia). *J. Paleolimnol.*, (in press), doi: 10.1007/s10933-008-9234-2.

Wagner, B., Reicherter, K., Daut, G., Wessels, M., Matzinger, A., Schwalb, A., Spirkovski, Z., and Sanxhaku, M., 2008b. The potential of Lake Ohrid for long-term palaeoenvironmental reconstructions. *Palaeogeogr. Palaeoclimatol. Palaeoecol.*, 259:341–356, doi:10.1016/j.palaeo.2007.10.015.

Wijmstra, T.A., 1969. Palynology of the first 30 m of a 120 m deep section in northern Greece. *Act. Bot. Neerl.*, 18:511–527.

Authors

Bernd Wagner, Institute of Geology and Mineralogy, University of Cologne, Zülpicher Str. 49a, D-50674 Köln, Germany, e-mail: wagnerb@uni-koeln.de.

Thomas Wilke, Animal Ecology and Systematics, Justus Liebig University Giessen, Heinrich-Buff-Ring 26-32, D-35392 Giessen, Germany.

Sebastian Krastel-Gudegast, Leibniz Institute of Marine Sciences (IFM-GEOMAR), Wischhofstr. 1-3, D-24148 Kiel, Germany.

Andon Grazhdani, Universiteti Politeknik, Fakulteti i Gjeologjise dhe Minierave, Tiranė, Albania.

Klaus Reicherter, Lehr- und Forschungsgebiet Neotektonik und Georisiken, RWTH Aachen University, Lochnerstr. 4-20, D-52056 Aachen, Germany.

Sasho Trajanovski, Hydrobiological Institute Ohrid, Naum Ohridski 50, 6000 Ohrid, Republic of Macedonia.

Giovanni Zanchetta, Dipartimento di Scienze della Terra, University of Pisa, Via S. Maria 56, I-56126 Pisa, Italy.

Related Web Links

http://www.geologie.uni-koeln.de/lake_ohrid.html
http://ohrid.icdp-online.org

Photo Credits

Fig. 1: Wagner et al., 2008b
Fig. 2: photo by T. Wilke

The Magma-Hydrothermal System at Mutnovsky Volcano, Kamchatka Peninsula, Russia

by John Eichelberger, Alexey Kiryukhin, and Adam Simon

Introduction

What is the relationship between the kinds of volcanoes that ring the Pacific plate and nearby hydrothermal systems? A typical geometry for stratovolcanoes and dome complexes is summit fumaroles and hydrothermal manifestations on and beyond their flanks. Analogous subsurface mineralization is porphyry copper deposits flanked by shallow Cu-As-Au acid-sulfate deposits and base metal veins. Possible reasons for this association are (1) upward and outward flow of magmatic gas and heat from the volcano's conduit and magma reservoir, mixing with meteoric water; (2) dikes extending from or feeding towards the volcano that extend laterally well beyond the surface edifice, heating a broad region; or (3) peripheral hot intrusions that are remnants of previous volcanic episodes, unrelated to current volcanism.

These hypotheses are testable through a Mutnovsky Scientific Drilling Project (MSDP) that was discussed in a workshop during the last week of September 2006 at a key example, the Mutnovsky Volcano of Kamchatka. Hypothesis (1) was regarded as the most likely. It is also the most attractive since it could lead to a new understanding of the magma-hydrothermal connection and motivate global geothermal exploration of andesitic arc volcanoes.

Geology and Volcanic Activity of Mutnovsky Volcano

Mutnovsky Volcano on Russia's Kamchatka Peninsula (Fig. 1) is exemplary of associated hydrothermal and volcanic regimes. The volcano has gone through four stages spanning late Pleistocene through Holocene time. Each stage probably reflects the evolution of a small shallow magma reservoir, and the transition from one stage to the next has involved a shift of the eruptive center and perhaps the active reservoir by as much as 1 km. All stages except for the current incompletely developed stage have produced magmas ranging from basalt to dacite (Selyangin, 1993). Mutnovsky IV is characterized by basaltic andesites. Mutnovsky III ended its eruptive cycle with a Holocene eruption of dacitic pyroclastic flows and emplacement of a dacite dome within its crater (Fig. 2). This crater has been enlarged by explosion, collapse, and/or erosion and is now occupied by a crater glacier, possibly the main recharge source of the hydrothermal system. The breach in Mutnovsky III crater, cut by a river, exposes a magnificent dike swarm (Fig. 3).

The crater of Mutnovsky III is the scene of intense fumarolic activity, modestly superheated and arranged in a ring, apparently defining the conduit margin of the late dacite dome. A powerful phreatic explosion in 2000 at the edge of the adjoined Mutnovsky IV crater reopened a large pre-existing sub-crater. This event appears to have been caused
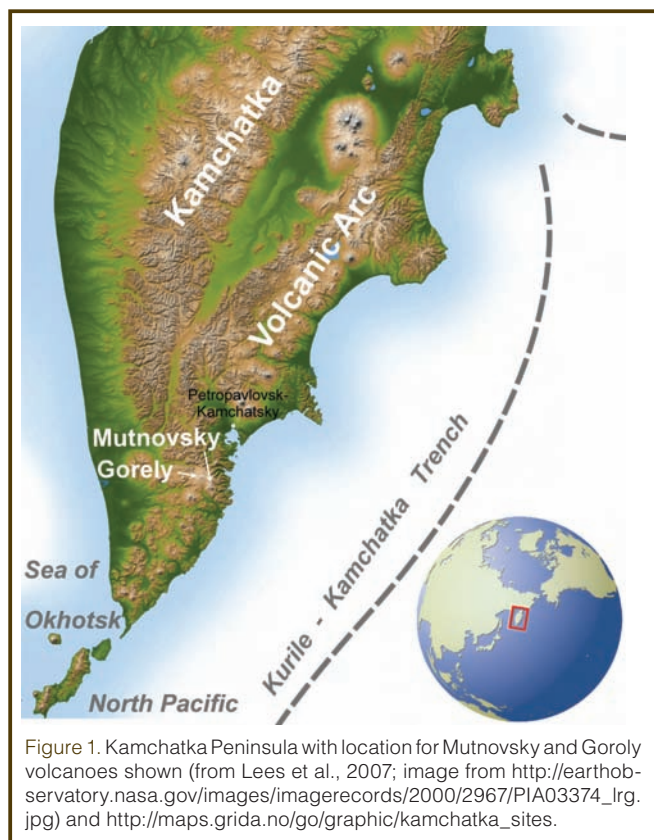

Figure 1. Kamchatka Peninsula with location for Mutnovsky and Goroly volcanoes shown (from Lees et al., 2007; image from http://earthob-servatory.nasa.gov/images/imagerecords/2000/2967/PIA03374_lrg.jpg) and http://maps.grida.no/go/graphic/kamchatka_sites.
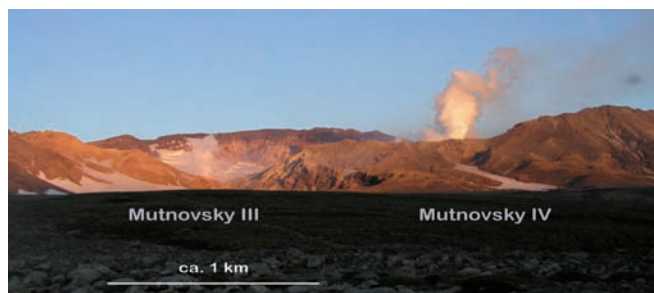

Figure 2. Mutnovsky Volcano from the west. The Crater Glacier and the hydrothermal plume of Mutnovsky III crater is visible through the breach formed by the Volcannaya River in Dangerous Ravine left of center. The larger plume from the Active Crater of Mutnovsky IV rises to the right. Width of the field of view is approximately 3 km (photo by J. Eichelberger).

by a dike propagating upward and intersecting the hydrothermal system centered beneath Mutnovsky IV. A second power-ful explosion occurred in 2007, excavating a new sub-crater on the floor of the **active crater of** Mutnovsky IV.

Mutnovsky's geothermal field (Dachny) was discovered in 1960 and described in detail by Vakin et al. (1976). The **active crater (Mutnovsky IV)** has fumaroles as hot as $620^{\circ}C$, emit**ting a continuous SO_2-rich plume** (92.8 wt% steam, 3.3wt% CO_2, 2.9 wt% SO_2, 0.6 wt% H_2S, 0.3 wt% HCl, 0.1 wt% HF and H_2). Mutnovsky craters' combined thermal (**>1000 MWt**
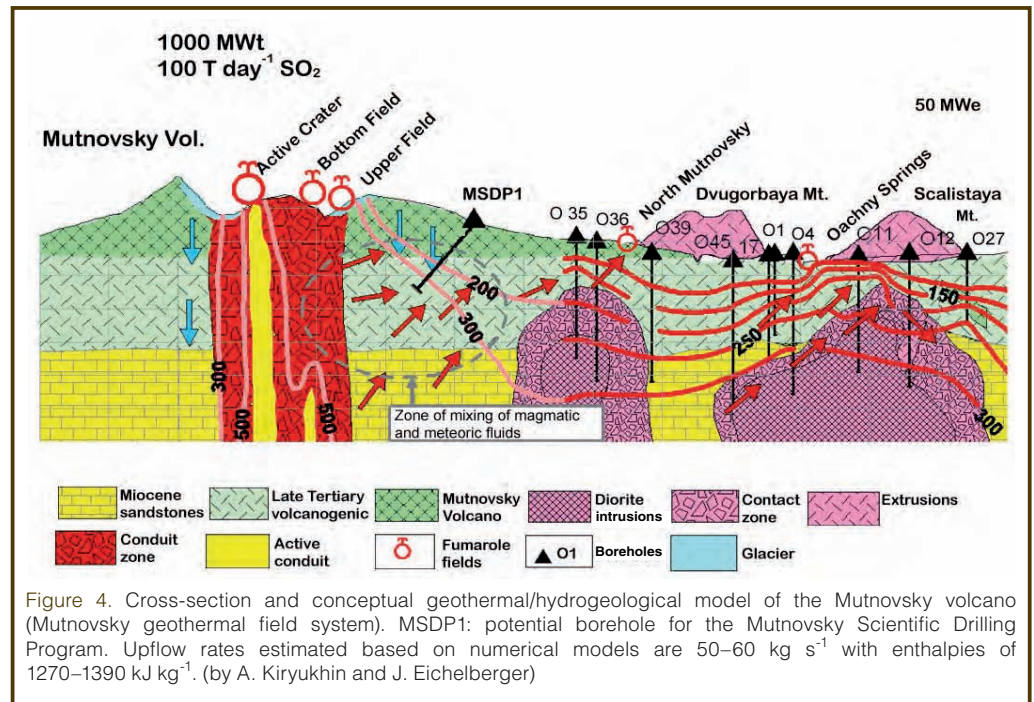

Figure 4. Cross-section and conceptual geothermal/hydrogeological model of the Mutnovsky volcano (Mutnovsky geothermal field system). MSDP1: potential borehole for the Mutnovsky Scientific Drilling Program. Upflow rates estimated based on numerical models are 50–60 kg s^{-1} with enthalpies of 1270–1390 kJ kg^{-1}. (by A. Kiryukhin and J. Eichelberger)

with temperatures above $600^{\circ}C$) **and gas emission** (~100 T d^{-1} SO_2; Trukhin, 2003**) imply shallow magma de**gassing (Wallace et al., 2003) and cooling at a rate on the order of 1 m^3 s^{-1}, a rate comparable to recent dome lava discharge rates of Mount St. **Helens. This is exceptional for a** volcano in repose and would seem to require robust magma convection within Mutnovsky's conduit. Moreover, the magmatic contribution is an underestimate because the hydrothermal system is apparently scrubbing gas output, an important issue in volcano monitoring. Scrubbing has given rise to an extraordinarily diverse population of *Sulfolobus*, a single-celled Archaea micro-organism. The opportunity to define the pressure and temperature limits of such microbiological activity as well as constrain its rate of evolution in a primordial environment is an exciting one, with implications for the origin of life on Earth and existence of life elsewhere in the **solar system.**

Seismic modeling of Mutnovsky IV volcano's magma chamber, performed recently by Utkin et al. (2005), yielded the following estimations of chamber parameters: elevation-1.7 km (approximately 3 km depth), radius 1.5 km, temperature $900^{\circ}C$–$1250^{\circ}C$. Heat content of the chamber and adjacent host rocks is estimated to be 3×10^{19} J. Fumaroles of the volcano are grouped as the **Upper Field (UF) and** Bottom Field (BF) of Mutnovsky III Crater and the Active Crater (AC) of Mutnovsky IV (Fig. 4).

In the laboratory, volcanic gases sampled **with evacuated** bottles were analyzed for SO_2 and H_2S. **Condensates were** analyzed **for HF, HCl, and HBr, and** δD and $\delta^{18}O$ values were determined in water from condensates. On a δD-$\delta^{18}O$ plot, all sampling points are close to a classic mixing line between magmatic water and local meteoric waters (Fig. 5). However, correlations between isotopic and chemical compositions

Figure 3. Dike swarm exposed in the wall of Mutnovsky III crater. Height of field of view is approximately 500 m (photo by J. Eichelberger).

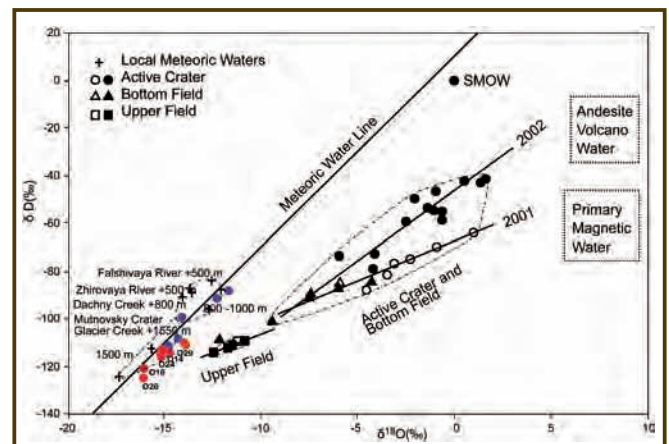Figure 5. Integrated δD vs $\delta^{18}O$ data of the Mutnovsky geothermal field (red circles - production wells, blue circles - meteoric waters; Kiryukhin et al., 1998; 2002) and Mutnovsky crater fumaroles (Zelensky et al., 2002).

divide all fumaroles into two independent hydrothermal systems.

The Mutnovsky Geothermal Field

The main and the most powerful hydrothermal system discharges at the active crater and the BF. Gases of this system originate from mixing of magmatic 800°C fluid with low temperature (100°C–150°C) hydrothermal steam. The source of the steam, according to its isotopic composition, may be meteoric waters from 900 m elevation. Another powerful hydrothermal system discharges as the upper fumarolic field (UF) with rather high temperature (300°C) meteoric steam along with a very low content of acids. The steam mixes with cold meteoric water from 1500 m elevation, probably from the adjacent crater glacier. Complementary to the fumarole volatiles, an isotopic geochemistry study has been performed on the trace metals in the fumaroles. The solutions in the boilers have compositions that appear to be unique in the world due to extremely high contents of Cl, Cr, Ni, Co, Ti, V, and B (Bortnikova et al., 2007). These elements are extracted from magma and wall rocks by acid magmatic gases and then concentrated in zones of secondary boiling. Thus, a modern ore-forming zone exists in the region of brine formation.

Exploration work began in 1978, including delineation of surface manifestations, temperatures, soil gas surveys, resistivity surveys, T-gradient drilling, and drilling of eighty-nine exploration wells. Flow tests from production wells, conducted during the 1983–1987 time period, and modeling confirmed the potential for 50 MWe production. Hence, in 1999 a pilot 12 MWe power plant was put into operation, followed in 2002 by the Mutnovsky 50 MWe power plant, located about 8 km NNE of the Mutnovsky II Crater. Mutnovsky's geothermal power plant provides one-third of the nearby city of Petropavlovsk's electric power

Conceptual Model of the Mutnovsky Magma-Hydrothermal System

At Mutnovsky there are two strong arguments for a direct connection between geothermal production and active magma beneath the volcano. First, the main production zone in the Mutnovsky field is a dyke-like plane of high permeability that if projected towards the volcano intersects the active conduit at shallow depth. Second, there is a component of the producing fluid, defined in terms of O and H isotopic composition, for which the only known equivalent is the crater glacier. The glacier apparently acts as the main source of meteoric water recharge area for the fluids producing by exploitation wells. Meteoric recharge is accelerated by melting of the glacier due to high heat flows in the crater (Fig. 4).

Thermal input to the production zone may alternatively come from other magmatic bodies accumulated in the North Mutnovsky volcano-tectonic zone. Some of the wells bottom in diorite intrusives that could represent a local heat source. It is not clear at present whether or not such bodies are (1) directly connected to the magmatic system of the active Mutnovsky volcano, (2) isolated remnants of magma intruded into the plane of hydro-magma-fracturing created by Mutnovsky volcano, or (3) as some have argued, much older intrusions related to a predecessor magmatic system unrelated to the current volcanic activity.

Mutnovsky Scientific Drilling Project Workshop 2006

Thirty-nine presenting scientists from Russia and six countries abroad, and many additional Russian participants for a total of about seventy, met in Petropavlovsk-Kamchatsky in September 2006 to consider scientific drilling at Mutnovsky. The meeting was held at the Institute for Volcanology and Seismology (IVS), Academy of Science of the Russian Far East.

The project concept, as introduced at the start of the meeting, was to drill and sample the magma-hydrothermal system at a point intermediate between the active craters and the geothermal production field, and to conduct hydraulic and chemical tests to assess their connectivity. With a system geometry characterized by lateral transition from magmatic vapor to dilute hydrothermal fluid at <2 km depth, Mutnovsky is an attractive drilling target for understanding magma-hydrothermal interactions. The presentations and discussions included a number of past and current scientific drilling projects such as deepening of commercially drilled wells for scientific purposes. Further deliberations highlighted the research on several wells that have been drilled to depths exceeding 2000 m and to temperatures exceeding 300°C.

Through the efforts of Russian scientists and the local development company, a large body of data already exists for the Mutnovsky system concerning fluid composition and conditions in the geothermal and volcanic systems. Some interesting pressure excursions have been associated with regional earthquakes, suggesting that the entire system may be a sensitive strainmeter. The three fumarole fields within the crater were defined as related through dilution of magmatic gas by meteoric water. Fumaroles depositing pyrite and arsenopyrite explain the remarkable chemistry (for example, the highest fumarolic Cr concentrations ever recorded). Mutnovsky's fumaroles are an epithermal ore-depositing system in action and have been termed "a unique natural chemical reactor" where thirty-five previously unknown hydrothermal minerals have been discovered. In counterpoint, some scientists view the volcano as a parasitic chimney on a more powerful and older Mutnovsky hydrothermal system. It should also be noted that the diverse microbiological population of extremophiles is an object of extensive international research.

The workshop moved to the Mutnovsky Power Plant for two days of tours and discussions. The highlight of the meeting was the visit to Mutnovsky's craters. Under the leadership of Adam Simon, proposals for this pre-drilling phase of the project are being submitted to the U.S. National Science Foundation.

Proposed Surface and Holes of Opportunity Investigations

There are a number of surface investigations that will contribute to testing the single system hypothesis and help to guide and complement later dedicated scientific drilling. Thermal horizons, both magmatic and aqueous, have very low electrical resistivity in comparison with host rocks, and this resistivity provides a basis for using surface electromagnetic methods for their spatial definition. Magneto-telluric soundings can be used to illuminate the magma-hydrothermal system by imaging conductivity distribution. Self-potential (SP) anomalies are directly related to subsurface heat and fluid movements; thus, SP mapping and modeling are strong tools to investigate the structure of a volcanic body and geothermal reservoir. In studying the Mutnovsky geothermal field, an SP mapping survey will be conducted widely in and around the Mutnovsky volcano.

In the area around the volcano there are no seismic stations. The nearest one is near Gorely Volcano at a distance of about 12 km to the northwest. In this situation, it is impossible to define seismic activity at Mutnovsky Volcano on a satisfactory level. One of the main tasks for future investigations in this area is acquisition of sufficient local seismic and

geodetic observations in order to differentiate between production-caused and natural events and to assess the connectedness of the volcano and geothermal system (Fig. 6). If there is a hydraulic connection between the volcano and the geothermal field due to migration of magma, fluids, or both, the 4-D pattern of deformation and seismicity should detect it.

The project also proposes to establish and monitor a micro-gravity network and a continuous-gravity network at Mutnovsky, both of which will require GPS elevation control. The aim of the micro-gravity and ground deformation network is to quantify any sub-surface mass movements occurring as a result of magma movements, degassing episodes, hydrothermal activity and geothermal exploitation. In particular, microgravity data may be able to differentiate between deformation caused by migration of fluids and that caused by migration of magma.

Investigation of aqueous geochemistry of the system will be expanded so that analysis of surface and borehole fluids from the north flank of Mutnovsky and the production field span the same range of elements and isotopes as the thoroughly studied crater fumarole fields. These data will permit a much better assessment of Mutnovsky Volcano's contribution to the geothermal system than is possible now.

At this time there is just one well, where pressure monitoring with a capillary tubing system has been conducted from 1995 until September 2006. Intriguing pressure excursions have been recorded during and just prior to regional earthquakes. The hydrothermal system appears to function as a sensitive strainmeter. This is consistent with many recent studies citing seismicity at volcanoes triggered by distant earthquakes, and speculating that earthquakes could trigger eruption. The utility of pressure sensors in multiple boreholes in assessing connectivity of the system is obvious, and it may even be possible to capture the fluid pressure signal in the near and far fields from phreatic explosions such as occurred in 2000 and 2007.

A considerable amount of core has already been acquired in the course of exploration and development of the Mutnovsky geothermal field. Core parameters are planned to be measured: density, porosity, gas permeability,
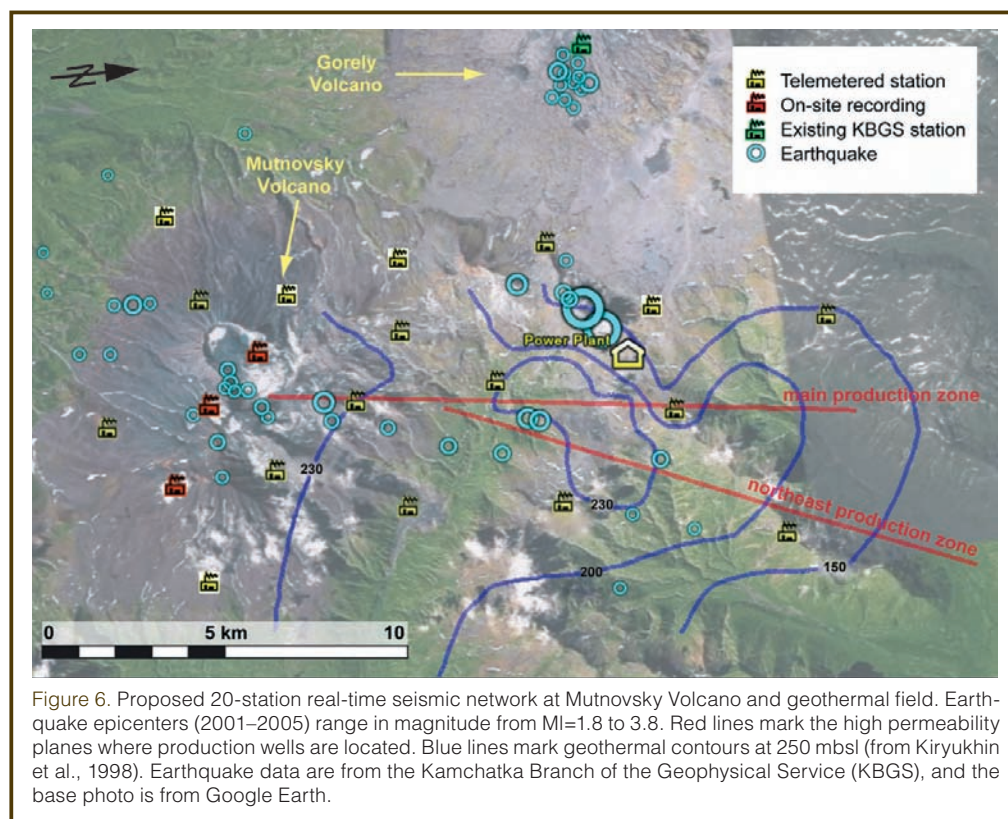

Figure 6. Proposed 20-station real-time seismic network at Mutnovsky Volcano and geothermal field. Earthquake epicenters (2001–2005) range in magnitude from Ml=1.8 to 3.8. Red lines mark the high permeability planes where production wells are located. Blue lines mark geothermal contours at 250 mbsl (from Kiryukhin et al., 1998). Earthquake data are from the Kamchatka Branch of the Geophysical Service (KBGS), and the base photo is from Google Earth.

pore space structure, microfracture network, sonic velocities, geomechanical characteristics (compression and tensile strength, elastic modulus), thermal and magnetic properties, and then interpreted according to the rocks' petrography. These subsurface properties will be used to create improved geophysical and surface deformation models. Chemical investigations of available core and surface samples will also reveal the internal geochemical stratigraphy of Mutnovsky Volcano. This work will involve unit-by-unit, high-quality geochemical analyses of drill core recovered by the project. The analyses of major and trace elements by X-ray fluorescence spectroscopy will also serve to identify hydrothermal alteration processes and the extent of alteration of the original magmas. These data will define the magma evolution of the Mutnovsky systems and its relationship to mineralization.

A goal of hydrothermal petrology of core will be to understand the permeability controls and chemical evolution of high-temperature, magmatically driven hydrothermal systems, mechanisms for focusing ore-formation, and energy use of Mutnovsky-type geothermal resources. The gas and heat output of the volcano can be viewed as providing a measure of the amount of magma undergoing decompression and cooling, respectively, per unit time. Taking the rough estimate of Mutnovsky's fumarolic SO_2 output of ~100 T d^{-1} and applying a value of solubility of S in basaltic andesite of 400 ppm (Wallace et al., 2003) yields a result that about 1 m^3 s^{-1} of magma must be decompressed to maintain this discharge rate. Cooling this amount of magma would satisfy the ~1000 MWe thermal budget as well. This is not insignificant, being equivalent to the rate of extrusion of dome lava in 2007 at Mount St. Helens volcano, yet Mutnovsky is not erupting. The only obvious explanation for this behavior is that magma is vigorously convecting within the conduit that is undergoing decompression, but the degassed and cooled magma is flowing back down the conduit rather than erupting. An ascent rate of 1 cm s^{-1}, (equivalent to that commonly inferred for lava eruptions) over a cross-sectional conduit area of 10 m2 would supply the observed SO_2 discharge. When combined with new data on geochemistry of Mutnovsky magma and melt volatiles as a function of time, coupled gas/heat/mass flux observations will provide an unprecedented definition of the source term for the Mutnovsky magma-hydrothermal system.

Drilling Investigations

If the hypothesis of a direct magma-hydrothermal connection at Mutnovsky is correct, then our objective will become to penetrate and sample the transition zone. Such a borehole will become a key observation midpoint and sample port in a ~10-km-long fracture-hosted system, with active magma at one end and geothermal production at the other. The magmatic end will be monitored at the surface within Mutnovsky III and active craters, and the geothermal end will be monitored at depth through existing wells. In addition

to obtaining direct information on the current chemical and physical state of the system, it will be possible to use time-dependent behavior to determine the hydraulic characteristics of the entire system.

The plan for drilling will be developed in parallel with progress in the surface investigations; however, some aspects of drilling can be considered now. It seems clear that drilling should penetrate as far beneath the Mutnovsky edifice and as close to the active conduit as possible. The borehole will therefore need to be directionally drilled. Its path should take it across the projection of the plane of geothermal production. The science team will continue discussions with the local geothermal company concerning the extent to which geothermal and scientific objectives can be combined and hence costs shared (for example, whether this could be a geothermal well that will be deepened for the scientific objectives). An important question is how close the well or wells can be sited to the volcano. If drilling conditions are favorable and data indicate that the active conduit is within reach, a subsequent stage of the project will be proposed aimed at intersecting, quenching at depth, and sampling magma. This is an objective embraced by the decadal white paper of ICDP (Harms et al, 2007) and would provide an unprecedented "ground truth" in volcanology, both in terms of the internal structure and conditions of volcanoes and the state and composition of unerupted magma. It will also be envisaged that MSDP will support continuation of the International Volcanological Field School based on Mutnovsky and founded in 2003 by the Kamchatka State University and University of Alaska Fairbanks.

Summary

The MSDP proposes a comprehensive geophysical and geochemical research program with stages wherein drilling will play an increasingly important role. Immediate priorities are magneto-telluric, seismic, geodetic, and gravity surveys to define the extent and behavior of the magma-hydrothermal system. The geothermal development company is currently drilling new 2000-m wells. This firm and the scientific drilling consortium formed at the workshop have agreed to collaborate in order to maximize scientific gain from drilled wells.

Based on results from this first phase, MSDP will drill a more proximal portion of the system that is hotter and more enriched in magmatic components than subsurface fluids previously sampled. Physical properties measurements on core will be used to refine initial geophysical models, particularly rheological properties relevant to inversion of measured surface displacements. Tracer and hydraulic tests will be used to assess overall connectivity of the system, from crater to production zone. Natural events, the numerous strong regional earthquakes and occasional eruptions, will also provide pressure perturbation tests. Finally, if feasibility can be demonstrated, we hope that the project will attempt to

penetrate Mutnovsky's active conduit. The goal of reaching magma in a decadal time frame is one endorsed by the International Continental Scientific Drilling Program White Paper (Harms et al., 2007).

We anticipate important results in the following areas:

1. The relationship of hydrothermal activity to active volcanism, with implications for future geothermal exploration of circum-Pacific and other supra-subduction zone volcanoes.
2. The relationship of active ore deposition to fluid regimes, transitioning from high-temperature acid magmatic to moderate-temperature neutral hydrothermal.
3. The extent and evolution of life in a sulfur-rich environment spanning a large temperature and pressure range
4. New constraints on the volatile budget of arc volcanoes; in particular, an assessment of subsurface "losses" to hydrothermal systems relevant to use of SO_2 emission as a monitoring and eruption-predictive tool.
5. The deep structure of arc volcanoes and the nature of unerupted magma.
6. Engagement of students from a number of countries in international, resource-oriented research.

Acknowledgements

References

Bortnikova, S.B., Sharapov, V.N., and Bessanova, E.P., 2007. Hydro-geochemical composition of springs at the Donnoe Fumarole Field, Mutnovsky Volcano (Southern Kamchatka) and problems of their relation with supercritical magmatic fluids. *Dokl. Earth Sci.*, 413A(3):410–414, doi:10.1134/S1028334X07030208.

Harms, U., Koeberl, C., and Zoback, M.D., 2007. *Continental Scientific Drilling: A Decade of Progress and Challenges for the Future*. Berlin (Springer), 366 pp.

Kiryukhin, A. V., Korneev, V.A., and Polyakov, A.Yu., 2006. On a possible relationship between strong earthquakes and anomalous pressure variations in a two-phase geothermal reservoir. *Volcanology and Seismology Journal*, 6:3–11 (in Russian).

Kiryukhin, A.V., Leonov, V.L., Slovtsov, I.B., Delemen, I.F., Puzankov, M.Yu., Polyakov, A.Yu., Ivanysko, G.O., Bataeva, O.P., and Zelenskii, M.E., 2005. Modeling the utilization of area Dachnyi of the Mutnovskii geothermal field in connection with the supply of heat-transfer agent to the 50 MW Mutnovskii Geologic Power Station. *Vulkanologiya i Seismologiya*, 5:19–44. Russian

Kiryukhin, A.V., Takahashi, M., Polyakov, A.Yu., Lesnykh, M.D., and Bataeva, O.P., 1998. Origin of water in the Mutnovsky geo-thermal field: an oxygen (^{18}O) and hydrogen (D) study. *Volcanology and Seismology Journal*, 4–5:54–62 (in Russian).

Lees, J.M., VanDecar, J., Gordeev, E., Ozerov, A., Brandon, M., Park, J., and Levin, V., 2007. Three-dimensional images of the Kamchatka-Pacific plate cusp. *In* Eichelberger, J., Gordeev, E., Kasahara, M., Izbekov, P., and Lees, J. (Eds.), *Volcanism and Subduction: The Kamchatka Region, Geophysical Monograph Series 172, American Geophysical Union*: 65–75.

Selyangin, O.B., 1993. New about Mutnovsky volcano. *Vulkanologiya i Seismologiya*, 1:17–35 (in Russian).

Trukhin, Y.P., 2003. *Geochemistry of the Active Geothermal Processes and Geotechnologies Applications*. Moscow (Nauka Publ.), 376 pp. (in Russian).

Utkin, I.S., Fedotov, S.A., Delemen, I.F., and Utkina, L.I., 2005. Dynamics of the development of flowing magmatic chambers on Mutnovsko-Gorelovsky group of volcanoes, their thermal fields and underground heat capacity. *Volcanology and Seismology Journal*, 5:1-30 (in Russian).

Vakin, E.A., Kirsanov, I.T., and Kirsanova, T.P., 1976. Hot areas and thermal springs of the Mutnovskii volcanic region. *Gidroterm. Sist. Term. Polya Kamchatski*: 85–114 (in Russian).

Wallace, P.J., Carn, A.S., Rose, I.W., Bluth, J.S.G., and Gerlach, T., 2003. Integrating petrologic and remote sensing perspectives on magmatic volatiles and volcanic degassing. *EOS, Trans. Am. Geophys. Union*, 84(42):441–447, doi:10.1029/2003EO420001.

Zelensky, M.E., Ovsyannikov, A.A., Gavrilenko, G.M., and Senyukov, S.L., 2002. Eruption of Mutnovskii Volcano, Kamchatka, March 17, 2000. *Volcanology and Seismology Journal*, 6:25–28 (in Russian).

Authors

John Eichelberger, University of Alaska Fairbanks, Department of Geology and Geophysics, Reichardt Building, Alaska, U.S.A. [Current Address: Volcano Hazards Program, U.S. Geological Survey, 12201 Sunrise Valley Drive, MS 904, Reston, Va., 20192, U.S.A., e-mail: jeichelberger@usgs.gov.]

Alexey Kiryukhin, Institute of Volcanology and Seismology, 9 Piip Boulevard, Petropavlovsk-Kamchatsky, 683006, Russia.

Adam Simon, Department of Geoscience, University of Nevada–Las Vegas, 4505 South Maryland Parkway, Las Vegas, Nev., 89154-4010, U.S.A.

Related Web Links

http://kamchatka.icdp-online.org
http://earthobservatory.nasa.gov/images/imagerecords/2000/2967/PIA03374_lrg.jpg
http://maps.grida.no/go/graphic/kamcatka_sites

Photo Credits

Figs. 2 and 3: J. Eichelberger

MOLE: A Multidisciplinary Observatory and Laboratory of Experiments in Central Italy

by Massimo Cocco, Paola Montone, Massimiliano R. Barchi, Georg Dresen, and Mark D. Zoback

Introduction

The structure and mechanics of active Low Angle Normal Faults (LANFs) have for decades been posing questions—in particular, if low angle normal faults accommodate crustal extension, and if they generate large magnitude earthquakes, or if they move aseismically. To shed new light on these challenging questions, MOLE intends to drill (down to 4–5 km) an active LANF in the Umbria-Marche sector of the northern Apennines (Fig. 1) and to establish a deep borehole observatory. The target site offers a unique opportunity to reach a LANF at drillable seismogenic depth to unravel the "low angle normal fault mechanical paradox" (Wernicke, 1995; Axen, 2007).

In order to discuss the scientific background and plan the MOLE project, sixty-two scientists from various research fields attended an international workshop in Spoleto, Italy, on 5–8 May 2008. The workshop focused on the following goals that need to be achieved: (I) to collect new observational data at depth for constraining the fault zone structure; (II) to perform laboratory experiments with gouge and fault zone materials to understand frictional properties and weakening mechanisms; (III) to record microearthquakes at distance comparable to the source radius, and (IV) to obtain stress and strain measurements and geochemical data in and near the fault zone at depth to understand the mechanics of earthquakes and faulting.

Scientific Background – the LANF Paradox

The question whether or not moderate-to-large magnitude earthquakes can nucleate on LANFs and contribute to accommodate extension of continental crust is widely debated in the literature (Wernicke, 1995 and references therein; Axen, 2007). Indeed, from a theoretical point of view, in an extensional tectonic setting characterized by a vertical principal stress σ_1, no slip is expected on faults dipping less than 30° with a friction coefficient ranging between 0.6 and 0.85 (Byerlee, 1978). In boreholes at depth in the vicinity of many high-angle, normal faults around the world, direct stress measurements are consistent with both theory and laboratory-derived coefficients of friction (Zoback, 2007). Nevertheless, observed slip on LANFs implies the reactivation of severely misoriented low angle structures (Sibson, 1985) occurring either because of anomalously weak frictional conditions ($\mu_s \ll 0.6$) or because of abrupt rotation of principal stress directions. If the orientation of principal stresses rotates in the direct vicinity of a LANF, it can be determined by stress measurements in a borehole through the fault zone (Zoback, 2007). High fluid pressure may be causing slip on a LANF, which means that the fault zone itself must be overpressured with respect to the rocks in the adjacent hanging wall and footwall.

Seismological observations indicate that no moderate-to-large magnitude earthquakes have been documented on LANFs based on well-constrained focal mechanisms (Collettini and Sibson, 2001; Jackson and White, 1989). On the contrary, geological evidence of active low-angle normal faulting has been documented in numerous field-based structural studies and also interpreted on seismic reflection profiles. Therefore, the role of LANFs and their contribution to seismic risk are still controversial. Despite recent studies which provided observational evidence and physical interpretations (Axen, 1999; Collettini and Holdsworth, 2004; Floyd et al., 2001; Hayman et al.,
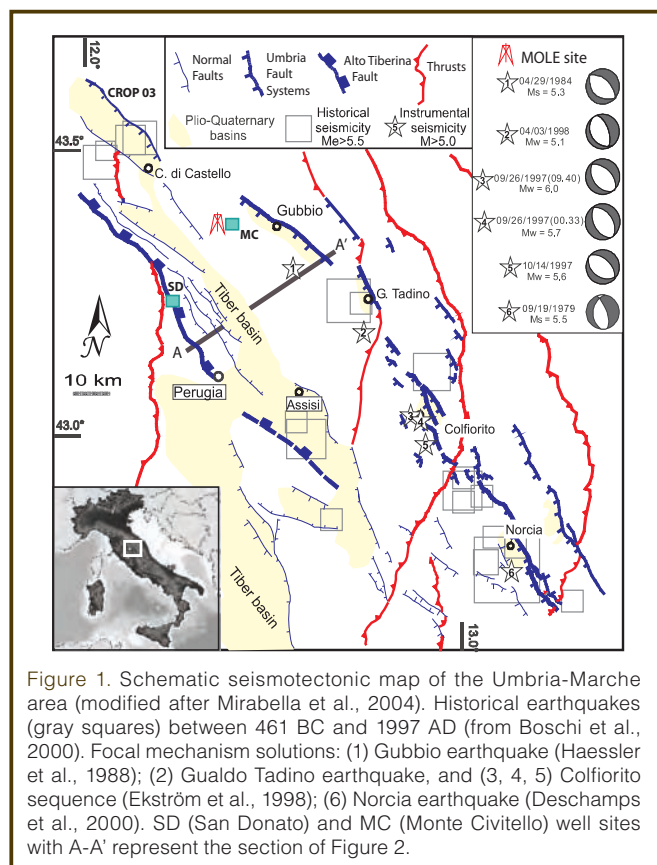

Figure 1. Schematic seismotectonic map of the Umbria-Marche area (modified after Mirabella et al., 2004). Historical earthquakes (gray squares) between 461 BC and 1997 AD (from Boschi et al., 2000). Focal mechanism solutions: (1) Gubbio earthquake (Haessler et al., 1988); (2) Gualdo Tadino earthquake, and (3, 4, 5) Colfiorito sequence (Ekström et al., 1998); (6) Norcia earthquake (Deschamps et al., 2000). SD (San Donato) and MC (Monte Civitello) well sites with A-A' represent the section of Figure 2.

2003; Holdsworth, 2004; Sorel, 2000), more experimental data and *in situ* studies are needed to shed light on these important unanswered issues.

Geology and Seismicity of the Project Area

The MOLE project aims to integrate several already existing/planned monitoring and research projects designed to create a multidisciplinary test site in the target area of the High Tiber Valley in the northern Apennines of Central Italy (Fig. 1). In this sector of the Apennines, the upper crust is made up of four main lithological units, each about 1.5–2 km thick. From bottom to top these are a phyllitic basement (not exposed at the surface), Upper Triassic evaporites (alternated anhydrites and dolostones), Jurassic to Oligocene multilayered carbonates, and a cover of Miocene and Pliocene synorogenic deposits (Figs. 2 and 3). The present-day tectonic setting derives from the superposition of two main tectonic phases, compressional structures related to arc-shaped folds and thrusts (Late Miocene) and extensional structures related to NW-SE trending normal faults (Late Pliocene-Quaternary). The easternmost and more recent NW-SE extensional structures have been named as the Umbria Fault System (Fig. 1). These SW-dipping normal faults represent the prominent extensional structures of the region, controlling the onset and evolution of neo-autochthonous continental intra-mountain basins located on the hanging wall of the subsiding areas.

Several moderate-magnitude earthquakes struck the study area in the past (Fig. 1). This seismicity is clearly associated with Quaternary faults. The most recent earthquakes are the 1979 Norcia M_s=5.5, the 1984 Gubbio M_s=5.3, the 1988 Gualdo Tadino M_w=5.1 events, and the 1997–98 Colfiorito earthquake sequence 5.2<M_w<6.0 (Amato and Cocco, 2000). However, all these earthquakes ruptured SW-dipping normal faults antithetic to the Alto Tiberina Fault (Fig. 2).

Figure 3. Stratigraphic sketch of the Monte Civitello (MC) and San Donato (SD) deep wells (see Fig. 1 for location). S_{hmin} orientation from breakout data performed in the wells. Beside each is a rose plot with the S_{hmin} orientation, standard deviation, the breakout's number and length, and the quality assigned to the result (modified from Mariucci et al., 2008).

The Alto Tiberina Fault (ATF) is a NE-dipping LANF cutting the upper crust in Central Italy, a region characterized by active extension and moderate-magnitude seismicity (Fig. 1). The subsurface geometry of the ATF (Fig. 2) has been depicted along a deep seismic, nearly vertical reflection transect (CROP03; Pialli et al., 1998), further constrained by a set of seismic reflection profiles (Mirabella et al., 2004) and calibrated by deep boreholes (e.g., San Donato and Perugia 2 wells). All these data define in detail a portion of the ATF (N150° trending) which is at least 55–60 km long. In cross-section, the ATF is characterized by a staircase trajectory with a mean dip of 15°–20° recognizable in the seismic profiles down to a depth of about 12 km (Fig. 2). Seismo-tectonic data and preliminary geodetic investigations (D'Agostino et al., 2008) demonstrate that the ATF is presently active and accommodates crustal extension. Moreover, the absence of historical earthquakes doubtlessly associated with the ATF and the presence of a source of over-pressurized fluids located
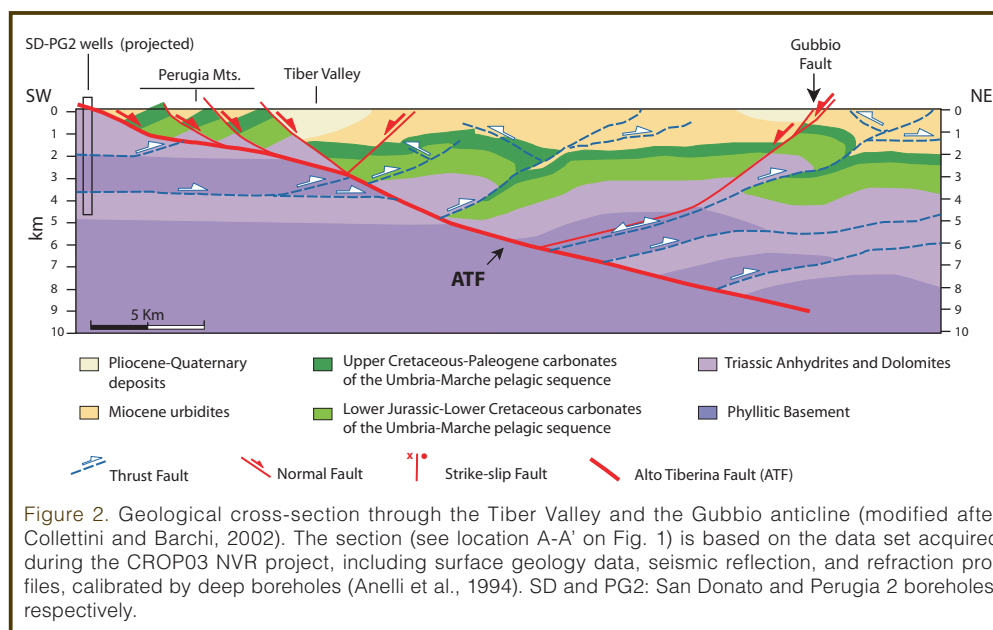

Figure 2. Geological cross-section through the Tiber Valley and the Gubbio anticline (modified after Collettini and Barchi, 2002). The section (see location A-A' on Fig. 1) is based on the data set acquired during the CROP03 NVR project, including surface geology data, seismic reflection, and refraction profiles, calibrated by deep boreholes (Anelli et al., 1994). SD and PG2: San Donato and Perugia 2 boreholes, respectively.
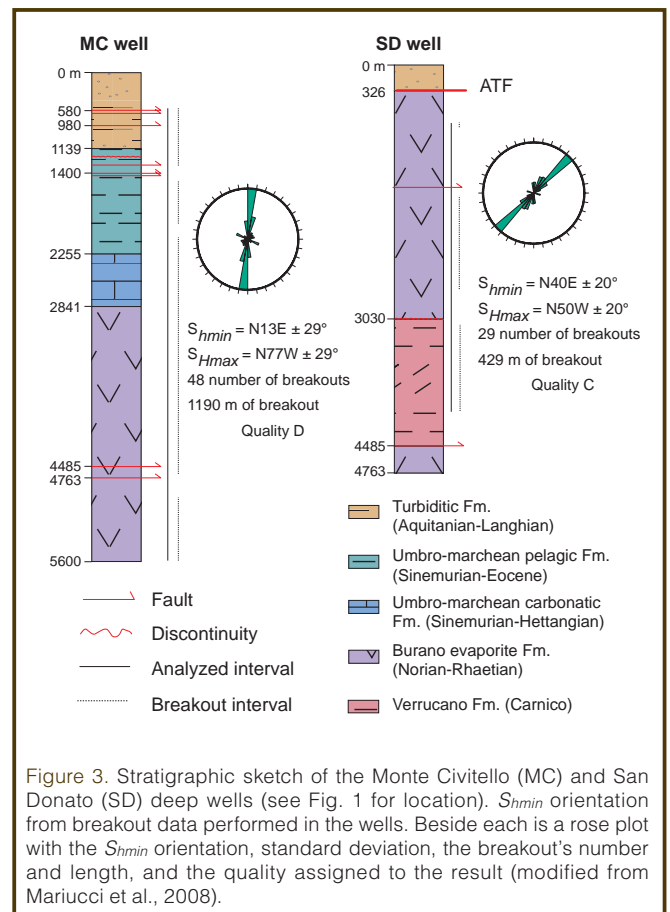
in the fault hanging wall (Chiodini et al., 2004) suggest that the fault most likely moves through a combination of seismic/aseismic slip and creep with repeating microearthquakes (Collettini, 2002). The ATF detaches an active hanging wall block from an aseismic footwall. In the hanging wall block, seismic reflection profiles and seismological data reveal the presence of moderately-to steeply-inclined minor faults soling into the detachment. While there is no instrumental evidence of moderate-magnitude earthquakes located on the ATF, it is important to note that microseismicity has been associated with the ATF (Boncio et al., 1998; Chiaraluce et al., 2007), thus confirming that it is an active LANF. A temporary dense local seismic network deployed in the study area for eight months allowed the recording of nearly 2000 (M<3.2) earthquakes (Piccinini et al., 2003). The
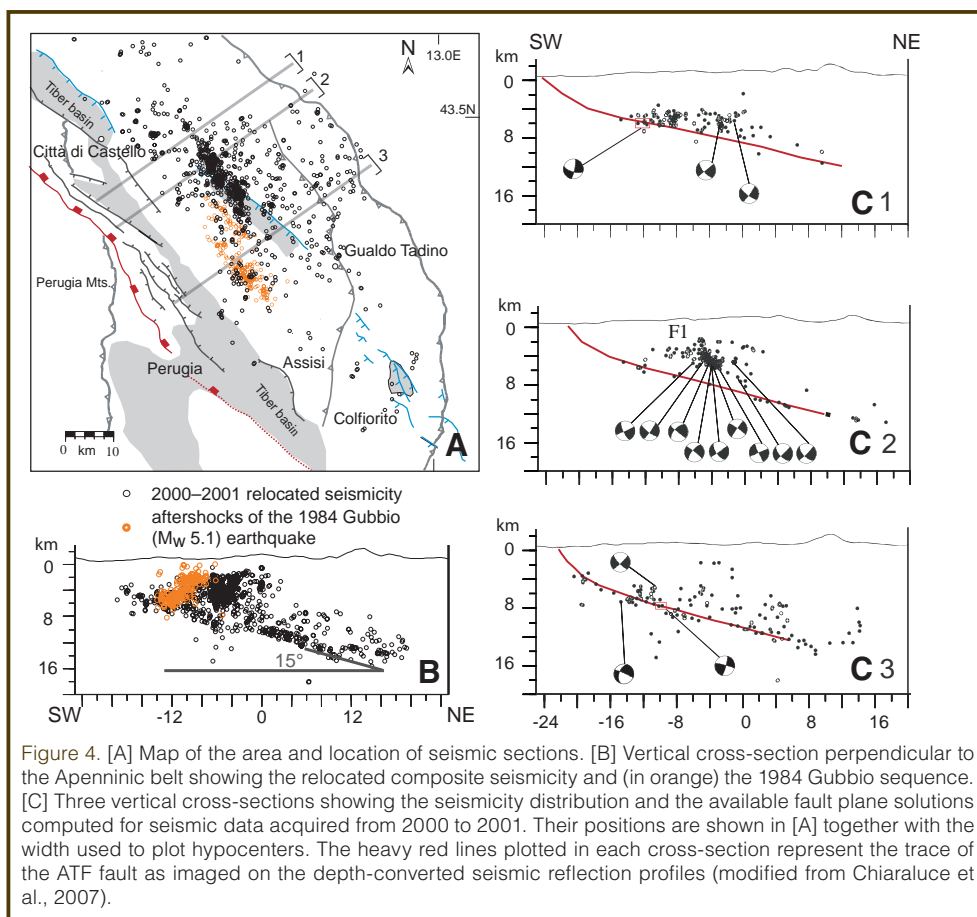

Figure 4. [A] Map of the area and location of seismic sections. [B] Vertical cross-section perpendicular to the Apenninic belt showing the relocated composite seismicity and (in orange) the 1984 Gubbio sequence. [C] Three vertical cross-sections showing the seismicity distribution and the available fault plane solutions computed for seismic data acquired from 2000 to 2001. Their positions are shown in [A] together with the width used to plot hypocenters. The heavy red lines plotted in each cross-section represent the trace of the ATF fault as imaged on the depth-converted seismic reflection profiles (modified from Chiaraluce et al., 2007).

integration of geological observations and seismicity data, together with the interpretation of seismic reflection profiles, led to a clear identification of a 60-km-long portion of the E-dipping low angle normal ATF (Fig. 4). The analysis of this multidisciplinary data set shows that in the last 2 Ma this structure has accumulated 2 km of displacement.

The computed focal mechanisms of microearthquakes (Chiaraluce et al., 2007) are in agreement with the geometry of the faults (Fig. 4). The latter are nicely highlighted by the earthquake distributions that appear in seismic reflection profiles in accord with a stress field characterized by a nearly vertical σ_1 and a NE-trending σ_3, perpendicular to the strike of the ATF, which has also been inferred from regional stress data (Mariucci et al., 2008; Montone et al., 2004). This microseismicity is uniformly distributed over the ATF plane, and the earthquake distribution in the down-dip direction reveals a fault zone thickness ranging from 500 m to 1000 m. Repeating earthquakes occur in very small slip patches whose dimensions are of the order of 10–100 m (Chiaraluce et al., 2007).

Collettini and Holdsworth (2004) brought up the hypothesis that the ATF at depth consists of a phyllosilicate-rich fault core. This relies on analogy with the Zuccale Fault, an older, presently inactive, ATF-like structure cropping out west of the Alto Tiberina fault on the island of Elba. This hypothesis is consistent with the proposed aseismic behavior of a misoriented fault in which microseismicity might be generated by local, short-lived build-ups in fluid pressure during regional scale degassing of the deep crust and the mantle, associated with regional tectonic extension (Chiodini et al., 2004). However, their theory must be corroborated by *in situ* observations and experimental evidence.

Workshop Program and Results

During the MOLE workshop participants from eight countries discussed drilling deep (4–5 km) into the Alto Tiberina Fault. During the first day other deep fault drilling projects were presented, followed by a session on the seismotectonics, geology, seismology, geodesy, and geochemistry of the target area during the second day. Another session focused on laboratory experiments on rock friction and rock mechanics using fault zone materials. The third day was dedicated to outlining preliminary studies, investigations during the drilling phase, and research after drilling. The potential drill site (Fig. 5) and some major normal faults of the region were visited during a half-day field trip. During the last afternoon, the key scientific and technical issues associated with the deployment of the deep borehole and the long-term multidisciplinary observatory at depth were summarized, and a scientific rationale for the MOLE deep drilling project was drafted. An unusually large set of geological and geophysical data is available, including detailed geological mapping, seismic reflection profiles, deep boreholes data, seismicity data, GPS measurements, and
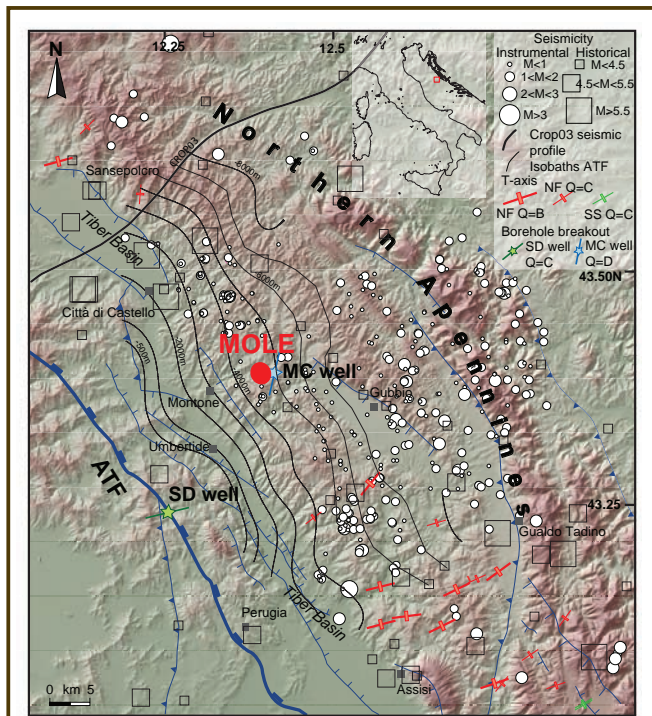
Figure 5. Digital Elevation Model around the planned MOLE borehole (red circle) showing the seismicity (instrumental from Chiaraluce et al., 2007 and historical from Boschi et al., 2000), T-axes from focal mechanisms (Montone et al., 2004), breakout data (Mariucci et al., 2008) and Alto Tiberina Fault isobaths (Mirabella, 2002).

more. These data support the fact that the ATF is an active LANF. The workshop participants concluded that the potential ATF drilling site is ideal for setting up a unique laboratory to investigate the mechanics and the seismogenic potential of active LANFs. However, prior to drilling it will be necessary to improve hypocenter determination and collect site survey data in new seismic and geodetic campaigns, including high resolution seismic reflection data to better image and constrain depth of the target.

An interesting opportunity that emerged during the workshop was the re-opening of Monte Civitello well, which was closed many years ago by AGIP company through the injection of several plugs. The ATF was not identified during the drilling of Monte Civitello well probably because the drilling was stopped just above it. We are presently evaluating the possibility of re-opening Monte Civitello in order to install a deep array of seismometers and possibly to monitor geofluids at an expected maximum depth of nearly 2000 m.

Another key conclusion from the workshop was to start drilling with a 2-km-deep pilot hole very close to the final MOLE borehole. This will allow for further detailed observations at depth to refine existing crustal structure models and to implement monitoring activities with particular attention to deep geo-fluids. Moreover, this will provide new data through borehole logging and sampling that will help to set up a permanent observatory at depth and improve planning for the deep hole.

Summary

One of the main conclusions of the workshop was that drilling through the Alto Tiberina Fault will provide information on crustal stress and fluid pressures. It will also allow us to do the following: (I) sample fault zone materials to measure their physical properties; (II) install down-hole seismometers, strainmeters, and fluid chemistry recorders to measure seismicity, strain rate, and transmigration of fluids; and (III) better understand the fault zone structure of a normal fault dipping at ~15°–20°, of which the seismogenic potential is unknown. Taken together, these studies will directly address many of the key questions related to the LANF paradox with particular regard to the understanding of the local stress field within the fault zone and the role of fluids in this process.

While the main goals of the MOLE project are to improve the understanding of the mechanical and physico-chemical behavior of LANFs, the impact of the project is certainly broader. The collected data and direct observations will provide a step toward more realistic models of earthquake nucleation and strain localization within fault zones. Laboratory experiments on rock friction with real and fresh fault zone materials can provide important constraints on fault friction and dynamic fault weakening processes. In general, MOLE will become a natural laboratory for monitoring and modeling the geophysical and geochemical processes controlling normal faulting in an active tectonic setting.

References

Amato, A., and Cocco, M., 2000. Special Issue: The Umbria-Marche, Central Italy, Seismic Sequence of 1997-1998. *J. Seismol.*, 4: 5–598.

Anelli, L., Gorza, M., Pieri, M., and Riva, M., 1994. Subsurface well data in the Northern Apennines. *Mem. Soc. Geol. It.*, 48: 461–471.

Axen, G.J., 1999. Low-angle normal fault earthquakes and triggering. *Geophys. Res. Lett.*, 26: 3693–3696, doi:10.1029/1999GL005405.

Axen, G.J., 2007. Research Focus: Significance of large-displacement, low-angle normal faults. *Geology*, 35(3): 287-288.

Boncio, P., Ponziani, F., Brozzetti, F., Barchi, M., Lavecchia, G., and Pialli, G., 1998. Seismicity and extensional tectonics in the Northern Umbria-Marche Apennines. *Mem. Soc. Geol. It.*, 52: 539–555.

Boschi, E., Guidoboni, E., Ferrari, G., Mariotti, D., Valensise, G., and Gasperini, P., 2000. *Catalogue of Strong Italian Earthquakes*. *Annali di Geofisica*, 43(4), 268 pp., with database on CD-ROM.

Byerlee, J.D., 1978. Friction of rocks. *Pure Appl. Geophys.*, 116: 615–629, doi:10.1007/BF00876528.

Chiaraluce, L., Chiarabba, C., Collettini, C., Piccinini, D., and Cocco, M., 2007. Architecture and mechanics of an active low angle normal fault: the Alto Tiberina fault (northern Apennines, Italy) case study. *J. Geophys. Res.*, 112: B10310, doi:10.1029/2007JB005015.

Chiodini, G., Cardellini, C., Amato, A., Boschi, E., Caliro, S., Frondini, F., and Ventura, G., 2004. Carbon dioxide Earth degassing and seismogenesis in central and southern Italy. *Geophys. Res. Lett.*, 31: L07615, doi:10.1029/ 2004GL019480.

Collettini, C., 2002. Hypothesis for the mechanics and seismic behaviour of low-angle normal faults: the example of the Altotiberina fault Northern Apennines. *Ann. Geophys.*, 45(5): 683–698.

Collettini, C., and Barchi, M.R., 2002. A low angle normal fault in the Umbria region (Central Italy): a mechanical model for the related microseismicity. *Tectonophysics*, 359: 97–115.

Collettini, C., and Holdsworth, R.E., 2004. Fault zone weakening processes along low-angle normal faults: insights from the Zuccale Fault, Isle of Elba, Italy. *J. Geol. Soc.*, 161: 1039–1051, doi:10.1144/0016-764903-179.

Collettini, C., and Sibson, R.H., 2001. Normal faults normal friction? *Geology*, 29(10): 927–930, doi:10.1130/0091-7613 (2001)029<0927:NFNF>2.0.CO;2.

D'Agostino, N., Mantenuto, S., D'Anastasio, E., Avallone, A., Barchi, M., Collettini, C., Radicioni, F., Stoppini, A., and Fastellini, G., 2008. Contemporary crustal extension in the Umbria–Marche Apennines from regional CGPS networks and comparison between geodetic and seismic deformation. *Tectonophysics*, in press, doi:10.1016/j.tecto.2008.09.033.

Deschamps, A., Courboulex, F., Gaffet, S., Lomax, A., Virieux, J., Amato, A., Azzara, A., Castello, B., Chiarabba, C., Cimini, G.B., Cocco, M., Di Bona, M., Marghereti, L., Mele, F., Selvaggi, G., Chiaraluce, L., Piccinini, D., and Ripepe M., 2000. Spatio-temporal distribution of seismic activity during the Umbria-Marche crisis, 1997. *J. Seismol., Special Issue*, 4:377–386, doi:10.1023/A:1026568419411.

Ekström, G., Morelli, A., Boschi. E., and Dziewonski, A.M., 1998. Moment tensor analysis of the central Italy earthquake sequence of September-October 1997. *Geophys. Res. Lett.*, 25:1971–1974.

Floyd, J.S., Mutter, J.C., Goodliffe, A.M., and Taylor, B., 2001. Evidence for fault weakness and fluid flow within active low-angle normal fault. *Nature*, 411:779–783, doi:10.1038/35081040.

Haessler, H., Gaulon, R., Rivera, L., Console, R., Frogneux, M., Gasparini, G., Martel, L., Patau, G., Siciliano, M., and Cisternas, A., 1988. The Perugia (Italy) earthquake of 29 April 1984: a microearthquake survey. *Bull. Seismol. Soc. Am.*, 78:1948–1964.

Hayman, N.W., Knott, J.R., Cowan, D.S., Nemser, E., and Sarna-Wojcicki, A.M., 2003. Quaternary low-angle slip on detachment faults in Death Valley, California. *Geology*, 31: 343–346.

Holdsworth, R.E., 2004. Weak faults-rotten cores. *Science*, 303:181–182, doi:10.1126/science.1092491.

Jackson, J.A., and White, N.J., 1989. Normal faulting in the upper continental crust: Observations from regions of active extension. *J. Struct. Geol.*, 11:15–36, doi:10.1016/ 0191-8141(89)90033-3.

Mariucci, M.T., Montone, P., and Pierdominici, S., 2008. Active stress field in central Italy: a revision of deep well data in the Umbria region. *Ann. Geophys.*, 51, 2/3, in press.

Mirabella, F., 2002. Seismogenesis of the Umbria- Marche region (Central Italy): Geometry and kinematics of the active faults and mechanical behaviour of the involved rocks. Ph.D. thesis, University of Perugia, Perugia, Italy, 121 pp.

Mirabella, F., Ciaccio, M.G., Barchi, M.R., and Merlini, S., 2004. The Gubbio normal fault (Central Italy): geometry, displacement distribution and tectonic evolution. *J. Struct. Geol.*, 26:2233-2249, doi:10.1016/j.jsg.2004.06.009.

Montone, P., Mariucci, M.T., Pondrelli, S., and Amato, A., 2004. An improved stress map for Italy and surrounding regions (central Mediterranean). *J. Geophys. Res.*, 109:B10410, doi:10.1029/2003JB002703.

Pialli, G., Barchi, M., and Minelli, G., 1998. Results of the CROP03 deep seismic reflection profile. *Mem. Soc. Geol. It.*, 52, 654 pp.

Piccinini, D., Cattaneo, M., Chiarabba, C., Chiaraluce, L., De Martin, M., Di Bona, M., Moretti, M., Selvaggi, G., Augliera, P., Spallarossa, D., Ferretti, G., Michelini, A., Govoni, A., Di Bartolomeo, P., Romanelli, M., and Fabbri, J., 2003. A microseismicity study in a low seismicity area of Italy: the Città di Castello 2000-2001 experiment. *Ann. Geophys.*, 46(6): 1315–1324.

Sibson, R.H., 1985. A note on fault reactivation. *J. Struct. Geol.*, 7:751–754, doi:10.1016/0191-8141(85)90150-6.

Sorel, D., 2000. A Pleistocene and still-active detachment fault and the origin of the Corinth-Patras rift, Greece. *Geology*, 28:83–86, doi:10.1130/0091-7613(2000)28<83:APASDF>2.0.CO;2.

Wernicke, B., 1995. Low-angle normal faults and seismicity: A review. *J. Geophys. Res.*, 100:20159–20174, doi:10.1029/95JB01911.

Zoback, M.D., 2007. *Reservoir Geomechanics*, Cambridge, UK (Cambridge University Press), 449 pp.

Authors

Massimo Cocco and Paola Montone, Istituto Nazionale di Geofisica e Vulcanologia (INGV), Via di Vigna Murata, 605–00143, Rome, Italy, e-mail: cocco@ingv.it.

Massimiliano R. Barchi, University of Perugia, Dipartimento di Scienze della Terra, Piazza dell'Università, 1, 06100 Perugia, Italy.

Georg Dresen, GeoForschungsZentrum Potsdam (GFZ), Telegrafenberg 14473, Potsdam, Germany.

Mark D. Zoback, Stanford University, Department of Geophysics, Mitchell Building 347, Stanford, Calif. , 94305-4606, U.S.A.

Related Web Link

http://mole.icdp-online.org

European Geosciences Union General Assembly

19–24 April 2009, Vienna, Austria

IODP/ECORD Booth No. 54–55 will be opened Monday to Friday, 20–24 April 2009 as a meeting point for the scientific drilling community. A joint ICDP–IODP Townhall meeting will also be held on Thursday, 23 April 2009, Room 1.

Detailed information will be regularly posted on the ECORD web site at: http://www.ecord.org/pi/egu09.html. Contact: ema@jussieu.ipgp.fr.

Beyond 2013—The Future of European Scientific Drilling Research

A session "Beyond 2013—The Future of European Scientific Drilling Research" will be held at the EGU General Assembly 2009 in Vienna, Austria. The session, convened by G. Camoin and R. Stein, will be followed by a two-day workshop April 24–25 specifically addressing the future of European scientific drilling research. Its main objectives are to define and document the European interests in IODP beyond 2013, and to prepare for the IODP renewal conference INVEST (p. 66, this volume). More details at: http://www.essac.ecord.org/index.php?mod=workshop&page=euroforum.

Session: *23 April 2009, Vienna*
Workshop: *24–25 April 2009*
At the University of Vienna, Geocenter

NERC UK IODP Directed Program: Two-Day Conference

18–19 May 2009, Royal Society, London, U.K.

The aim of this conference is to highlight important scientific achievements from the current IODP phase, and to solicit contributions and challenges that will take Ocean Research Drilling forward post-2013, when the existing IODP program ends. It is envisaged that the two-day conference will cover a range of scientific themes from the evolution of the planet through climate change and the deep biosphere. We also hope to showcase post-graduate, PhD and post-doctorate research, which has made use of the extensive wealth of data collected during the varied IODP expeditions. A session of the conference will be an open discussion on the future IODP program beyond 2013.

Information on the event will be available at the UKIODP website (www.ukiodp.bgs.ac.uk). For enquiries please contact the UKIODP Science Coordinator at ukiodp@bgs.ac.uk.

Continental Scientific Drilling Workshop

4–5 June 2009, Denver, Colorado
Application Deadline: 15 April 2009

A forward-looking workshop will identify areas where significant scientific advances in the understanding of continental or whole Earth processes and history require samples or data that can only be obtained by continental drilling or coupled continental-ocean drilling. The workshop will also stress developing collaborations with parallel communities, such as those that participate in IRIS, IODP, NCAR, MARGINS, and EarthScope. The aim of the workshop will be to produce a brief document, with supplementary information, that will inform the geologic community, support planning of future funding,

and supply a template for future continental scientific drilling. This workshop is the first step in developing a general science plan for continental drilling. Topics to be addressed range broadly: global climate and environmental change at all time scales, geodynamics of faults and hotspots, magmatic and volcanic processes, impacts, natural resources, the deep biosphere, and the facilities necessary to optimize return on investment in drilling projects. The organizers hope that other topics will emerge during the planning process or at the workshop itself.

The organizers seek participation of a diverse group of active investigators. International applications are welcome. For further information, to apply to participate, or for others, please contact Tony Walton at twalton@ku.edu or call at 1-785-864-2726. Related web links at DOSECC (http://www.dosecc.org) or the University of Kansas (http://www.geo.ku.edu/).

4th International Symposium in Okinawa, Japan

29 June–3 July 2009, Okinawa, Japan

Seven other sponsors are also supporting this event.

The 4th International Symposium on "Chemosynthesis-Based Ecosystems" will be held on 29 June–3 July 2009 in Okinawa, Japan. This symposium highlights the recent achievements in the field of unique ecosystems driven by chemosynthesis rather than photosynthesis. Major topics include biogeography, biodiversity, evolution, symbiosis, ecology, physiology, geochemistry, microbiology, and research technology & methods. Venue is the Bankoku Shinryokan (http://www.shinryokan.com) in Nago City, Okinawa, Japan, which is set next to beautiful sandy beaches. Coral reefs and subtropical forests with exotic wildlife surround the venue. For updated information, visit the website: http://www.jamstec.go.jp/xbr/4th_CBE/. Contact: Yoshihiro Fujiwara or Yoshiko Takeoka, E-mail: 4th_CBE_office@jamstec.go.jp.

ECORD Summer School

31 August–11 September 2009, Bremen, Germany

ECORD Summer School on "Geodynamics of mid-ocean ridges" will be held at the Center for Marine Environmental Sciences (MARUM), University of Bremen. Lecture topics range from mantle melting to tectonic exhumation of mantle to hydrothermal/microbial interactions. Participants will be introduced to a full range of IODP related topics from general introduction to the program to writing IODP proposals. In The Virtual Ship, ocean drilling cores from the Mid-Atlantic Ridge stored at the IODP Bremen Core Repository (BCR) will be used to teach "shipboard" methodologies applied on the drilling vessels of the program. These include core curation, visual core description, physical properties measurements, and petrographic observations. Also, planned is a field trip to a Devonian submarine volcanic province. A registration form will be circulated in spring 2009. For further information, see http://www.glomar.uni-bremen.de/ECORD_Summer_School_2009.html.

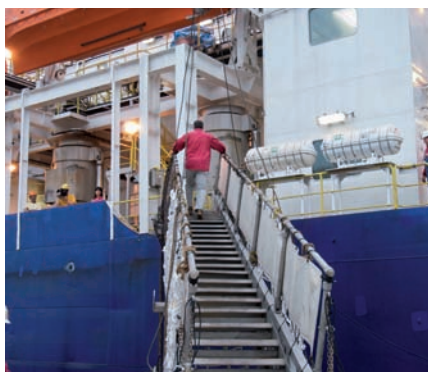Photo Credit: Wolfgang Bach, MARUM, Bremen University, Germany

Conference Call: IODP New Ventures in Exploring Scientific Targets–INVEST

23–25 September 2009, Bremen, Germany

The IODP conference, INVEST, is planned as a large, multidisciplinary, international, scientific meeting to

Now stepping forward to future scientific drilling program.

define the scientific research goals of the second phase of IODP scheduled to begin in late 2013. INVEST will take place at the University of Bremen in Germany on 23–25 September 2009. The meeting, open to all interested scientists and students, provides the principal opportunity for science community members from everywhere to influence the future of scientific ocean drilling. The goal of INVEST is to build the framework for the next tier of success in scientific ocean drilling. Input from a broad swath of scientists actively working in or having a future interest in IODP is solicited. INVEST will seek to sum-marize the state of knowledge across interdisciplinary geoscience themes, identify emerging science, new re-search initiatives, and implementation strategies. Also, identifying technological and fiscal needs will be pur-sued.

For more information on INVEST steering committee and meeting program, please see www.marum.de/en/iodp-invest.html. or www.iodp.org. Registration opens 4 April 2009. Travel support programs are being organized by all current IODP members.

ICDP Training 2009 Goes to the Projects

The Operational Support Group of ICDP is in preparation for two train-ing sessions for 2009. The first one is in cooperation with and hosted by the Swedish Deep Drilling Program (SDDP). The SDDP working group is planning a drilling program for four world-class deep boreholes over a

ten-year period. Accordingly, an adapted training program in Sweden in early summer 2009 will comprise the modules *Planning of Scientific Drilling Projects* and *Writing of an ICDP Proposal* in addition to the basic module *Fundamentals of Scientific Drilling*. A second training program in fall 2009 will be held in conjunction with the envisaged Campi Flegrei Drilling Project in southern Italy and will address high-temperature drilling issues in addition to the basic element on fundamentals of drilling. A limited number of places in these courses is open to scientists from ICDP member countries with preference for those involved in planned ICDP projects. Further information: http://www.sddp.se and http://www.icdp-online.org.

GESEP: German Scientific Earth Probing Consortium

German funding agencies and institutes invested significantly in infrastructure and know-how for scientific drilling for many decades. But, until now there was only limited coordination for exchange or joint use of facilities and industry cooperation. To overcome this weakness the "Deutsche Forschungsgemeinschaft" (DFG) has supported the formation of GESEP, an alliance founded by university and non-university earth science institutes. Its major goal is focusing interests of researchers and engineers in scientific drilling. GESEP opens with a short course for postgraduates (Earth Drilling School) in Potsdam on 18–19 March 2009. Current plans are to establish GESEP as a knowledge center on scientific drilling. First milestones envisaged are establishment of a core repository for continental drill cores and related samples to complement the Bremen Core Repository, plus design and set-up of a related data bank and information platform. GESEP will also act as a contact to ensure that long-term partnerships are generated for adaptation of energy service industry tools and methods for scientific drilling and monitoring tools. GESEP will organize

meetings, provide a contact point for questions on scientific drilling and coordinate public relations and outreach. Advanced training courses and schools will be based on various expertise in participating institutes. URL: http://www.gesep.org.

New Drill Site on the Ross Ice Shelf

ANDRILL

The ANtarctic geological DRILLing (ANDRILL) Program is developing new drill sites for the Coulman High (CH) Project in the western Ross Sea (http://www.andrill.org/science/ch). The CH Project will target an early Miocene and Paleogene section to address evolution and stability of the cryosphere; warm climate periods in the Early Tertiary; orbital variability controls on climate; and tectonics within the West Antarctic Rift System. Drill sites are on the CH at the former C-19 giant iceberg calving site (Fig. 1) located on a seismic profile completed at the Ross Ice Shelf edge in 2003, now covered by the advancing ice shelf. The stratigraphic record here would extend the Miocene and younger data obtained from ANDRILL sites MIS and SMS (*Sci. Drill.,* 2006, 3:43–45; *Sci. Drill.,* 2008, 6:29–31) and recover underlying sediments representing the Early Tertiary greenhouse world. Technical challenges include drilling
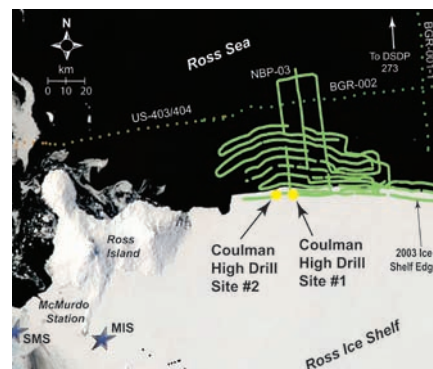

Fig. 1. Coulman High Drilling Project site location map. Proposed drill sites (yellow dots) are 125 km from McMurdo Station. Prior successful ANDRILL drill sites SMS and MIS are shown (stars).

into the seabed while the ice is moving north at more than two meter per day and maintaining an open hole through the nearly 250-m-thick ice shelf. A U.S. proposal is under review, and proposals for New Zealand and Europe are under development. ANDRILL (www.andrill.org) is currently seeking international partners in developing a multinational collaboration for this exciting new effort. For more information please contact the ANDRILL Science Management Office at ch@andrill.org.

Modernized *JOIDES Resolution* is Tested and Ready for IODP Science Operations

IODP INTEGRATED OCEAN DRILLING PROGRAM

The *JOIDES Resolution*— a 20-year workhorse on behalf of scientific ocean drilling— sailed away from a Singapore shipyard on 25 January after a complete transformation to modernize and upgrade the ship. To get the *JR* into the shape she's in now has taken years of diligent effort by a talented team of project managers, dozens of IODP-USIO staffers, thousands of skilled shipyard laborers (averaging roughly 350 per day), and more.

The renovation, funded mostly by the U.S. National Science Foundation (NSF) and partly by Overseas Drilling Limited, includes state-of-the-art upgrades to the ship's science laboratories and facilities, all-new, expanded and refined accommodations, refurbishment and renewal of ship equipment and infrastructure, advanced safety and environment safeguards, and augmented logging and drilling capabilities.

An external scientific assessment team boarded the ship in Guam on 7 February. Sea trials took place at Ontong Java Plateau, ODP Site 807, and transit to Honolulu followed, making the ship ready again for IODP expeditions in early March. The *JR* is now poised to help IODP continue to push the edge of science. A multimedia overview of the "new" *JR*, including daily reports, is available online from http://oceanleadership.org/node/2000.

In early March 2009, the *JR* will set sail from Honolulu for the equatorial Pacific for the first of two nine-week expeditions. The second expedition will follow immediately, commencing in May 2009, and both are grouped into one science program. This science program, known as the Pacific Equatorial Age Transect, will investigate how the equatorial Pacific is intricately linked to major changes in the global climate system. http://iodp.tamu.edu/science-ops/expeditions/equatorial_pacific.html.

Restored *JOIDES Resolution* ready for sailing. (Departing from Singapore)

Schedules

	ESO Operations *	Platform	Dates	Port of Origin
1	313 - New Jersey Shallow Shelf	MSP	May 2009–Aug. 2009	TBD
2	325 - Great Barrier Reef	MSP	Sep. 2009–Dec. 2009	TBD
	**USIO Operations **	**Platform**	**Dates**	**Port of Origin**
3	320 - Pacific Equatorial Age Transect	*JOIDES Resolution*	05 Mar. 2009–05 May2009	Honolulu, Hawaii, U.S.A.
4	321 - Pacific Equatorial Age Transect/ Juan de Fuca Cementing Operations	*JOIDES Resolution*	05 May 2009–05 Jul. 2009	Honolulu, Hawaii, U.S.A.
5	323 - Bering Sea	*JOIDES Resolution*	05 Jul. 2009–04 Sep. 2009	Victoria, Canada
6	324 - Shatsky Rise	*JOIDES Resolution*	04 Sep.2009–04 Nov.2009	Yokohama, Japan
7	317 - Canterbury Basin	*JOIDES Resolution*	04 Nov. 2009–04 Jan. 2010	Townsville, Australia
8	318 - Wilkes Land	*JOIDES Resolution*	04 Jan. 2009–09 Mar. 2010	Wellington, New Zealand
	CDEX Operations *	**Platform**	**Dates**	**Port of Origin**
9	319 - NanTroSEIZE Stage 2: Riser/Riserless Observatory 1— Sediment Inputs	*Chikyu*	05 May 2009–31 Aug. 2009	TBD
10	322 - NanTroSEIZE Stage 2: Subduction Input NanTroSEIZE—Riserless Observatory Casing	*Chikyu*	01 Sep. 2009–10 Oct. 2009	TBD

MSP = Mission Specific Platform   TBD = to be determined

* Exact dates in this time frame dependent upon final platform tender.

** Sailing dates may change slightly. Staffing updates for all expeditions to be issued soon.

*** CDEX schedule subject to OTF and SAS approval.

	ICDP Projects	Drilling Dates	Location
1	Iceland Deep Drilling Project	Jun. 2008–2010	Krafla, Iceland
2	Lake El'gygytgyn Drilling Project	Oct. 2009–May 2010	Chukotka, Russia
3	New Jersey Shallow Shelf**	May 2009–Aug. 2009	Offshore New Jersey, U.S.A.
4	Lake Van	Jul. 2010–Sep. 2010	Anatolia, Turkey

**IODP-ICDP joint project

Exact dates in this time frame dependent upon final platform tender.